Regional Climate Modeling over Ontario using the WRF model

Zhongqi Yu

A THESIS SUBMITTED TO
THE FACULTY OF GRADUATE STUDIES
IN PARTIAL FULFILLMENT OF THE REQUIREMENTS
FOR THE DEGREE OF
MASTER OF SCIENCE

GRADUATE PROGRAM IN EARTH AND SPACE SCIENCE

YORK UNIVERSITY

TORONTO, ONTARIO

August 2013

Abstract

Global climate models (GCMs) are widely used to study climate change. Due to their coarse resolutions, GCMs cannot resolve some microscale and mesoscale processes such as topographical effects. Dynamic downscaling simulations using Regional Climate Models (RCMs) are often required to provide higher spatial- and temporal-resolution climate variabilities in specific regions. Uncertainties in dynamic downscaling simulations due to errors in the atmospheric state and models need to be understood first in the present climate simulations. Then the reliability for future projections can be inferred.

This research contains three parts. The first part gives an assessment of temperature and precipitation over Ontario based on the North American Regional Climate Change Assessment Program (NARCCAP) RCM simulation data. In part two, five 8-year downscaling simulations using the Weather Research and Forecasting (WRF) model driven by five NARCCAP model data over Ontario are studied. Each of these simulation results and their mean are analyzed to address the dynamic downscaling effect on temperature and precipitation and their variabilities. Lastly in the third part, a 14-member perturbed ensemble simulation using the WRF model was conducted. The ensemble means of temperature and precipitation are evaluated and the uncertainties in regional climate modeling are discussed.

The temperature and precipitation in seven NARCCAP RCM simulations from 1979 to 2004 are compared to the observations over Ontario. The observed annual area mean temperature has a remarkable rising trend in the late 1990s after decades of fluctuation. It is mainly due to a significant rise of winter area mean temperature during that period. This rising trend has been

revealed in all seven models. For the annual area mean precipitation, the observed values fluctuate during this period, and the NARCCAP RCM model simulations show larger discrepancies.

One focus of this thesis is to assess the impact of increased model resolution on regional climate simulations. Five NARCCAP RCM (MM5I, RCM3, HRM3, CRCM and WRFG) simulation data with 50-km horizontal resolution are downscaled to 10-km horizontal grid over Ontario to provide initial and boundary conditions for the WRF downscaling simulations in the period from 1991 to 1998. The model results show that the high resolution has great impact on regional climate simulations.

Three sets of ensembles, the seven-member NARCCAP RCM simulations, the five-member WRF downscaling simulations, and a 14-member perturbed ensemble simulations using WRF model with the stochastic kinetic energy backscatter scheme are analyzed to assess the performance of the ensemble approach in regional climate simulations. The ensemble mean temperature and precipitation are compared to reanalysis data and the observations. The root mean square errors (RMSE) and the correlations are calculated. The results show that the ensemble method improves the accuracy of simulations, for both temperature and precipitation.

Acknowledgements

I would like to thank Yongsheng Chen from York University for supporting my work on this thesis. His warm-heart, inspiration and perfect teaching give me great power to overcome difficulties and handle a lot of problems. Thank you to Professor Gordon Huang and John Liu, for providing me with very valuable suggestions on this research and their supports. Special thanks to Prof. Gordon Huang for providing partial financial support to this study. Thank you to Dr. Yun Qian for sharing the WRF model configurations and to ComputeCanada for providing computing resources on its supercomputers. Thank you to Jianyu Liang, Nan Miao, Sopan Kurkute and Geoffrey James Bell for helping me during my study. And thanks to my family, while I was trying to finish my thesis.

Table of Contents

Contents

List of Figures

List of Tables

Chapter 1: Introduction

1.1 Climate Change

Climate change is a change in average weather conditions over periods ranging from decades to millions of years. A lot of factors contribute to climate change, including solar radiation, continental drift, volcano eruptions, changes in Earth's orbit, oceanic circulations and human activities. Climate change is one of the greatest concerns in the 21st century. The insured losses from extreme weather and climate events have increased greatly during recent decades (Munich Re, 2002). More and more people now believe that anthropogenic greenhouse gas emissions have caused the global warming (IPCC, 2007). In recent decades, our climate has been changing much more rapidly than any other period in history. Extreme weather phenomena, such as storms, blizzards, floods, droughts and heat waves, appeared more frequently during recent decades. The increasing frequency and intensity of extreme weather and climate events are great threats to humans and other components of the ecosystems. The decline in Arctic and Antarctic sea ice, both in its extent and thickness, is also the evidence of global warming. The global land precipitation (excluding Antarctica) has increased by about 9mm over the 20th century, which is thought to be related to the El Niño–Southern Oscillation (ENSO), the Arctic and Antarctic oscillation (AO and AAO) (New et al., 2001). Global warming accelerates the vegetation growth, which results in vegetation stress, loss of plants and desertification in some regions. It also

devastates some of the rainforests in tropical areas, affecting the local ecosystems. Under global warming, the northern hemisphere is warmer in recent decades than any other period during the last 1000 years. In addition, the World Health Organization estimated that many human diseases are related to climate fluctuations in temperature and precipitation. The warming trend over recent decades led to more morbidity and mortality in many areas around the world (Patz et al., 2005). Therefore, these facts in climate change indeed have great impacts on humans' living conditions and qualities, and affect our ecosystems.

In Canada, the climate is also changing significantly during recent decades. Zhang et al. (2000) and Cao et al. (2009) found that the climate in southern Canada including Ontario turned into a wetter and warmer pattern during the 20th century. From 1900 to 2003, the numbers of cold nights, cold days and frost days decreased, while warm nights, warm days and summer days occurred more frequently across the country. Canada also has more precipitating days, however with reduced intensity. The annual amount of snowfalls declined significantly during the second half of the 20th century due to the warming (Vincent and Mekis, 2010).

1.2 Regional Climate Simulations

Given its great impacts, the climate change deserves thorough studies. The characteristics of global climate changes in historic, current and future periods have been studied extensively. General circulation models(GCMs), describing physical processes among the oceans, the atmosphere and the land surface, are practical and advanced in simulating global climate systems. They are capable of simulating global scale climate change and variabilities. A GCM usually has

a horizontal resolution of 200 to 600 km, which is too coarse to resolve many subgrid scale physical processes, such as cloud-related processes. Instead, these unresolved processes are parameterized. Parameterization is one source of uncertainties in GCM simulations of climate change. In addition, uncertainties in various mechanisms in models concerning, for example, water vapor, radiation, clouds, ocean circulation, ice, and snow albedo, also deviate the simulation results. For these reasons, different GCMs may generate different responses to the same forcing. Since the mesoscale processes are not explicitly represented in GCMs, one remedy is to choose regional climate modeling approach with higher resolution.

A regional climate model is to some extent similar to a global climate model, except it has higher resolutions than a global climate model. Hence regional climate models usually resolve more details than global climate models. In particular, a high-resolution regional climate model can describe regional topography, land-sea contrasts and vegetation characteristics with more accuracy than global climate models (Giorgi and Marinucci, 1996; Stahl et al., 2011). It can also describe more accurately the upscale influence of regional forcings on large scale climate change (McCarthy et al., 2011). Regional climate models are primarily and widely used tools to provide detailed descriptions of different processes in climate change at high resolutions (Pal et al., 2007; Rougier et al., 2009). Typically, GCM simulation results with coarser resolution provide initial and lateral boundary conditions (ICs and BCs) to drive RCMs, including wind, temperature, water vapor, and surface pressure. Although there are still deficiencies in RCMs, they have been shown to improve the climate simulations in specific regions.

To investigate climate characteristics in historic, current and future periods, regional climate

models are developed for simulating climate change in specific regions around the world, including North America, Asia, Africa and some other areas (e.g., Qian and Leung, 2007; Alexandru et al., 2007; Jenkins, 1997). In the 4th IPCC Assessment Report (IPCC, 2007), some results at regional-scale via downscaling of large-scale GCMs, and results of RCM simulations at higher resolution (30 to 100 km) are presented. In particular, one of the climate-study programs, the North American Regional Climate Change Assessment Program (NARCCAP), has produced relatively high-resolution climate change simulations over North America. It ran a set of regional climate models at a spatial resolution of 50 km driven by reanalysis data and multiple atmosphere-ocean general circulation models (AOGCMs) over North America. This project, endorsed by the World Climate Research Program (WCRP), is a part of COordinated Regional Downscaling EXperiment (CORDEX). The multi-model approach can address the uncertainties in future climate projections on the regional scale. It can help us understand RCM behaviours better and identify issues that need to be improved in future model development.

1.3 Downscaling

The purpose of downscaling is to obtain high-resolution details in climate as accurately as possible over a region of interest. Various downscaling methods had been developed to downscale global climate model results, such as dynamic downscaling, statistical downscaling, physically based subgrid modelling (e.g., Ghan et al., 2002; Leung et al., 2003; Qian et al., 2010). Dynamic downscaling is expected to have the largest impact on simulating precipitation and surface hydrology in regions with complex orography (Leung et al., 2004). This is because that the improved representation of topographic effects in climate models may lead to improvements

in detailed seasonal climate simulations (Roads, 2004). Dynamic downscaling using RCMs has become a popular approach in regional climate simulations.

Relatively fewer observational and modeling studies of regional climate change over Ontario have been done. Zhang et al. (2000) found that the climate in southern Canada has been continuously becoming wetter and warmer during the 20th century. From 1900–1998, the annual mean temperature has increased by 0.5 to 1.5K in southern Canada. Cao and Ma (2009) found an upward trend of the occurrence frequency of summer severe-rainfall events over Ontario. In collaboration with the Ontario Ministry of the Environment, Huang et al. (2010, 2011, 2012) used the Providing REgional Climates for Impact Studies (PRECIS) model to conduct multiple climate downscaling studies over Ontario at a horizontal resolution from 10-km to 25-km , including probabilistic projections. Qiu and Zhu (2012) developed 45-km-resolution probabilistic climate projections for mean conditions over Ontario from multiple regional and global climate models. Gula and Peltier (2011) tried to improve regional climate modeling over Ontario by including a lake model for the Great Lakes. They used the Weather Research and Forecasting (WRF) model with a high-resolution of 10 km driven by the National Center for Atmospheric Research (NCAR) Community Climate System Model (CCSM) outputs.

1.4 Regional climate simulations using WRF

The WRF model was originally designed as a multiscale numerical weather prediction system for high resolution applications in both atmospheric research and operational forecasting, collaborated among the National Center for Atmospheric Research (NCAR), the National Oceanic and Atmospheric Administration (represented by the National Centers for

Environmental Prediction (NCEP) and the former Forecast Systems Laboratory (FSL)), the Air Force Weather Agency (AFWA), the Naval Research Laboratory, the University of Oklahoma, and the Federal Aviation Administration (FAA) in the United States. The WRF model is now widely used for simulations across scales from meters to thousands of kilometers. With regional climate simulation becoming more prevalent, the WRF model has been adapted and used extensively in recent years for high-resolution regional climate simulations (Leung et al., 2006). It is a non-hydrostatic model with multiple choices for physics schemes, including microphysics, convective parameterization, planetary boundary layer (PBL), land surface models (LSM), and longwave and shortwave radiation. Some of above physics schemes are crucial for climate simulations. For example, WRF contains advanced representations of cloud microphysics and land-surface processes so that it is capable of simulating complex interactions between precipitation and land surface characteristics (such as the snow cover and the soil moisture). Different parameterizations, dynamics, boundary and initial conditions, domains and some nesting options in the WRF model have been tested in the context of regional climate modeling, making the WRF model a reliable and useful tool for regional climate study. For example, Leung et al. (2009) used WRF to conduct a regional climate simulation over the western US to study the heavy precipitation and flooding induced by the atmospheric rivers in the western United States. Bukovsky et al. (2009) used WRF as a nested regional climate model to study the sensitivity of U.S. warm-season precipitation to variations in model setup. Downscaling RCM experiments using WRF have suggested that grid nudging can improve the accuracy of generating regional climate information (Lo et al., 2008; Bowden et. al., 2012).

1.5 Ensembles

Evaluating regional climate model uncertainties has received more attentions in recent years. One way to estimate the uncertainties is to use ensemble simulations. Statistically, the mean of a set of ensembles, has a smaller error than the average error of any individual ensemble member (Murphy, 1988). When the ensemble systems capture the true uncertainties, the sample statistics can provide useful information in climate simulation uncertainties.

Two kinds of ensemble generation techniques have been widely used, i.e., the multimodel ensemble (e.g., Meehl et al., 2007) and perturbed initial condition and boundary condition ensemble (e.g., Kjellstrom et al., 2011). Specifically, the multimodel ensemble employs several different models or a single model with different settings of physics schemes to conduct ensemble simulations. Doblas-Reyes et al. (2000) demonstrated that the multimodel ensemble approach has higher forecast skills than a single model ensemble. Kharin and Zwiers (2001) mentioned that in the Tropics, the ensemble mean produced the most skillful forecasts. Chien et al. (2006) showed the ensemble mean has smaller errors than any single ensemble member in simulating several meteorological variables, such as temperature, precipitation and wind. On the other hand, the perturbed initial condition and boundary condition ensemble uses one RCM, with different initial and boundary conditions downscaled from different GCM or RCM simulations or reanalysis data. In principle, nonlinearities in the climate system may amplify small perturbations in initial and boundary conditions to different final climate states.

The ensemble spread represented by the sample standard deviation (Std) is to measure the differences among the ensemble members. It can provide an estimate of the uncertainties in the forecasts. Large ensemble spreads indicate large ensemble uncertainties, while small ensemble spreads correspond to small uncertainties. The ensemble spread can also give a reliable estimation of the ensemble mean, by quantifying the correlation between the ensemble spread and the deterministic simulation error (e.g., Grimit and Mass, 2007; Murphy, 1988; Baker, 1991; Buizza, 1997). Whitaker and Loughe (1998) mentioned that the ensemble spread is probably the most useful predictor when the studied climatological variables are significantly larger or smaller compared with their climatological mean values.

This research used the WRF model at 10-km resolution to simulate the climate change over Ontario from 1991 to 1998. The results, particularly 2-m temperature and precipitation were compared with the NCEP Climate Forecast System Reanalysis (CFSR) data, station observations, and NARCCAP RCM simulations for the same period. The dynamic downscaling effects in regional climate simulations are discussed. The ensemble simulations using WRF were conducted. The ensemble mean and ensemble spread were analyzed and compared with the driving NARCCAP model, reanalysis data and the observations.

Chapter2: Methodology

2.1 Data and analysis methods

The data used in this research include seven regional climate model results from NARCCAP shown below in Table 2.1. All of these data are gridded model outputs. These simulations were driven by the National Center for Environmental Prediction and Department of Energy (NCEP-DOE) reanalysis II data in the time period from 1979 to 2004. The model results have a 50-km horizontal resolution, except WRFG (45-km resolution).

Table 2. 1: Brief description of seven regional climate model datasets used in this research

Regional Climate Model	Full Name	Group	Boundary condition
CRCM	Canadian Regional Climate Model	OURANOS	NCEP-DOE Reanalysis II
ECP2	Experimental Climate Prediction Center Regional Spectral Model, updated configuration	UC San Diego/Scripps	
ECPC	Experimental Climate Prediction Center Regional Spectral Model, original configuration	UC San Diego/Scripps	
HRM3 (PRECIS)	Hadley Regional Model 3/ Providing REgional Climates for Impact Studies	Hadley Centre	
MM5I	MM5-PSU/NCAR mesoscale model	Iowa State University	
RCM3	Regional Climate Model version 3	UC Santa Cruz	
WRFG	Weather Research & Forecasting model, updated Grell configuration	Pacific Northwest Nat'l Lab	

The global monthly surface air temperature and precipitation in the NCEP-DOE Reanalysis II is used for doing EOF analysis and analyzing the extreme winters. The data have a resolution of $2.5° \times 2.5°$.

The station observations of 2-m temperature (including daily maximum and minimum temperature) and precipitation are obtained from the Environment Canada (http://www.weatheroffice.gc.ca/canada_e.html). In this study, eight stations were chosen across Ontario from west to east (Ottawa, Toronto, Windsor, Sudbury, Timmins, Wawa, Sioux Lookout

and Kenora), as shown in Figure 2.1.

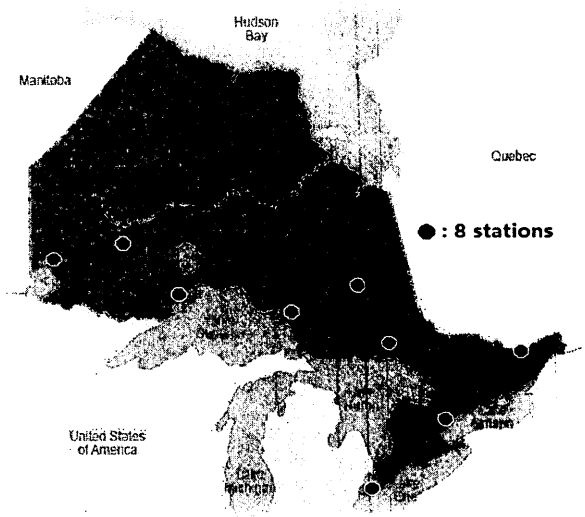

Figure 2.1: Distribution of selected 8 meteorological stations

The NCEP Climate Forecast System Reanalysis (CFSR) monthly surface air temperature and precipitation products from January 1979 to December 2004, with a 38km resolution covering the entire globe, were used for verification. The CFSR data was interpolated onto the 8 chosen station locations and compared with the station observations to validate the consistency of two datasets. Thus, the WRF simulation results can be compared with the gridded CFSR data.

Comparisons of temperature and precipitation were made between model interpolated data and corresponding station observations, using monthly, seasonally and annually averaged data. The maximum and minimum temperatures were compared with both observations and CFSR data.

Standardization (normalization) was applied to the observations and model data in the discussion of climate variations. Specifically, to obtain the standardized time series s(t), the time-mean value $\bar{s}$ is subtracted from the original time series S(t). It is then divided by its standard deviation σ_s (Zhang et al., 2008; Chu et al., 2008).

$$S(t) = \frac{s(t)-\bar{s}}{\sigma_s}. \tag{2.1.1}$$

Hence the standardized data is nondimentional. It can depict the high and low values more clearly. Nine-point moving average (using least square method) was applied to filter out high-frequency variations (Gorry 1990; Mobley and Preisendorfer, 1985). The least square method was also used to obtain the trend of all time series.

In addition, the periodicities of the temperature and precipitation anomalies were detected using spectral analysis methods. After calculating the power spectra of a time series, Hanning filter was used to filter out high frequency signals. It was also necessary to determine the corresponding noise level using a noise significance test. According to Torrence and Compo (1998) and Wei (1999), the critical value of autocorrelation coefficient at the 95% confidence level is

$$r_0 = \frac{-1+1.645\sqrt{n-2}}{n-1}, \tag{2.1.2}$$

where n is the sample size.

The time series is persistent, if the lag-1 autocorrelation coefficient r(1)>0.1. In this case, the red noise test is used to test its significance. Otherwise, when the series is not persistent (i.e.

r(1)≤0.1), the white noise test will be applied. In this research, the lag-1 autocorrelation coefficients of the temperature and the precipitation data are all smaller than 0.1, thus white noise test is used. If a peak in the power spectrum is higher than its white noise level, the peak is significant and it can be assumed to be a true feature with a certain percent confidence (95% in this case). Otherwise, the peak signal is not acceptable and it should be neglected.

The empirical orthogonal function analysis (EOF) was applied to find the spatial distributions and temporal variation of the temperature and precipitation anomalies. The EOF analysis attempts to find a relatively small number of independent variables that describe as much original information as possible. Compared with other representation methods used to decompose signals including Fourier transforms, wavelets, and Laplace transforms, the EOF analysis does not require a predetermined form. It decomposes a set of regional data into a series of orthogonal basis functions. These functions have correlations with the regional characteristics and reveal whether these characteristics have any influence on the spatial and temporal tendencies of the data. The EOF method converges very fast, so that the main information of the studied variables can be depicted in several modes. The EOF method has been widely applied to analyze meteorological and climatological data since 1950s (e.g., Storch and Zwiers, 2002; Hannachi et al., 2009; Zeng et al., 2006).

Let us assume that matrix S is a time evolving anomaly field, each row of S represents a spatial pattern at a fix time. The covariance matrix is $R = S^t * S$, the eigenvalues and eigenvectors of R can be obtained:

$$RC = CA. \tag{2.1.3}$$

Here A is a diagonal matrix containing the eigenvalues λ_i of R in a descending order ($\lambda_i > \lambda_{i+1}$). The eigenvalue λ_i corresponds to one eigenvector C_i (i.e., the i^{th} column of C), every eigenvector can be considered as a map. The eigenvectors are called the EOFs. EOF1, for example, is the eigenvector with the largest eigenvalue. EOF2 is the one with the second largest eigenvalue, and so on.

The eigenvector matrix C has one property that $C^tC = CC^t = I$, where I is the identity matrix. So all the EOFs are uncorrelated over space. To see how EOFs evolve over time, the time series F is projected on each EOF basis to obtain the principal component time series $\overrightarrow{a_j} = F\overrightarrow{c_j}$.The principal component time series are also orthogonal (uncorrelated over time). Therefore, the spatial distribution and temporal variation of each EOF can be found.

2.2 Dynamic downscaling using the WRF model

Dynamic downscaling simulations over an 8-year period (1991-1998) using the WRF model version 3 were conducted. The WRF model domain covered Ontario and the adjacent area (Fig. 2.2). The model domain had a 10km resolution with dimensions of 300 ×300 grid points horizontally and 28 vertical levels. Five NARCCAP RCM data (WRFG, MM5I, HRM3, RCM3 and CRCM) were interpolated to provide ICs and BCs to the WRF model. Since the WRF model does not predict the sea-surface temperature (SST) and the sea ice, these two variables are updated every 6 hours using the data from the Atmospheric Model Intercomparison Project (AMIP) conducted by the Program for Climate Model Diagnosis and Intercomparison (PCMDI).

AMIP SST and sea ice data are used by the NARCCAP RCMs for their simulations as well. The soil temperature and soil moisture in two layers (0-10cm and 10-200 cm) were extracted from the NCEP-DOE reanalysis II. The domain lateral boundaries had 15 points, gradually transitioning from the driving NARCCAP RCM data to the WRF interior values. The model simulation results are saved every 6h for the whole domain. Some variables such as the daily maximum and minimum temperatures were diagnosed at every time step but saved every 24h.

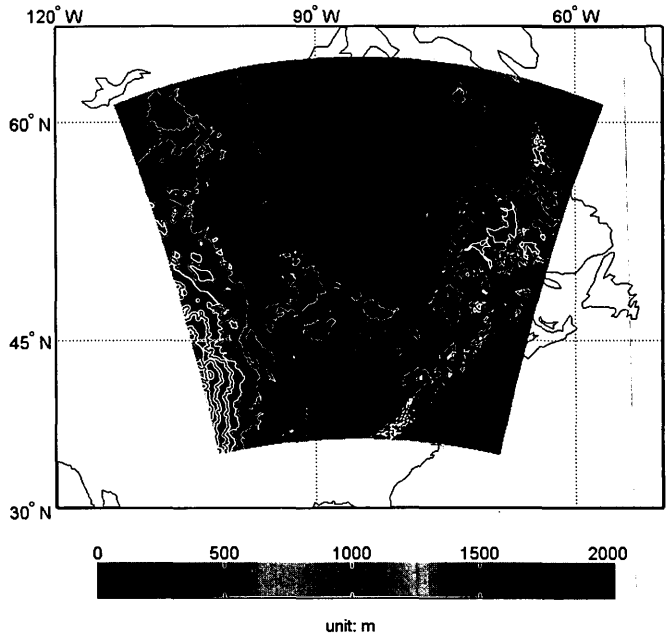

Figure 2. 2: The WRF model domain with 10-km resolution in this study. The topography is contoured and shaded (Unit: m).

In this study, the microphysics and convection parameterization schemes used were the WRF Single-Moment (WSM) 5-class scheme (Hong et al., 2004) and Grell-Devenyi ensemble scheme (Grell and Devenyi, 2002). The WSM5 microphysics scheme explicitly simulates rain, snow,

water vapor, cloud water and cloud ice. The Grell-Devenyi scheme is a multi-closure, multi-parameter, ensemble method with typically 144 sub-grid members. The land-surface model used was the Noah (NCEP, Oregon State University, Air Force, and Hydrologic Research Lab) Land-surface model. It is a four-layer model with fractional snow cover and frozen soilphysics.The planetary boundary layer (PBL) parameterization scheme used was the YSU (Yonsei University) scheme (Hong and Pan, 1996). This scheme includes counter gradient terms to represent heat and moisture fluxes. Atmospheric shortwave and longwave radiations are computed by the Community Atmospheric Model (CAM) shortwave and longwave schemes (Collins et al., 2004).

Since NARCCAP MM5I did not provide the sea level pressure and the surface pressure which are required for initializing the WRF model, they were calculated using the hypsometric equation (Eq. 2.2.1):

$$Z_2 - Z_1 = \frac{R_d T_v}{g_0} ln \frac{p_1}{p_2}, \tag{2.2.1}$$

where Z is the geopotential height, indices 1 and 2 represent two levels, R_d is the dry air gas constant, g_0 is the globally average gravity, T_v is average virtual temperature between these two levels, p is the pressure corresponding to Z. Thus,

The sea level pressure is:

$$p_{slp} = p_{1000hPa} * e^{\frac{Z_{1000hPa} * g_0}{R_d * T_v}}, \tag{2.2.2}$$

And the surface pressure is:

$$p_s = p_{slp} * e^{-\frac{Z_s * g_0}{R_d * T_v}}. \tag{2.2.3}$$

NARCCAP RCMs only provide geopotential height, specific humidity, temperature, zonal (U) and meridional (V) components of wind at pressure levels above the ground. To initialize the WRF model, vertical interpolations and extrapolations were carried out to fill the data at underground grid points, following the NCEP scheme. The Shuell pressure reduction method was applied to extrapolate the temperature and height under the ground. The principle for the extrapolation is to assume a moist lapse rate under the ground and to use the hypsometric equation to get the temperature and height underground. More details can be found in Collins' (1983). In addition, the specific humidity, and horizontal winds are assumed to be uniform below the first model pressure level above the ground.

When all the simulations were completed, similar analyses of temperature and precipitation were performed and compared to previous NARCCAP results. The correlations and root mean square errors between the model data and the CFSR data were calculated.

The significance test for the RMSE followed Wei (1999). If the total variance is unknown, the significance test taken into usage is the F-test, where the test statistic coefficient is defined as below:

$$F = \frac{\frac{n_1}{n_1-1}s_1^2}{\frac{n_2}{n_2-1}s_2^2}. \qquad (2.2.4)$$

Here, (s_1,n_1) and (s_2,n_2) are the sample RMSEs and sample sizes.

The test statistic F follows the F distribution, with the degrees of freedom that $\gamma_1=n_1-1$, $\gamma_2=n_2-1$. Suppose that the null hypothesis is given that the two RMSEs are not significantly different

(s_1=s_2). Then for a given confidence level α and the calculated F following Eq. 2.2.4, the hypothesis is rejected if $F \geq F_{\alpha/2}$, so that the two RMSEs are significantly different.

The significant test for the correlations given below followed Wei (1999):

$$t = r\sqrt{\frac{n-2}{1-r^2}}, \tag{2.2.5}$$

where t is the significance value, n is the number of elements, r is the correlation.

After stating the hypotheses, we need to find the critical values in the Pearson's table. Then we compute the test value using Eq. 2.2.5 and compare this value with the critical value. The last step is to make conclusions. If the t value is greater than the critical value, the correlation is considered to be significant.

2.3 Ensemble simulations

Three sets of ensembles were analyzed to explore the benefits of the ensemble approach in regional climate simulations. Specifically, the first ensemble was the existing NARCCAP RCM multimodel ensemble, consisted of seven models as listed in Table 2.1 (WRFG, RCM3, HRM3, MM5I, CRCM, ECPC and ECP2). The second ensemble was the 10-km resolution WRF downscaling simulations driven by five NARCCAP RCM datasets (WRFG, RCM3, HRM3, MM5I and CRCM), hence it has 5 members. The third ensemble was the so-called stochastic WRF ensemble. In addition to the five members in the second ensemble, nine members were added by employing the stochastic kinetic energy backscatter (SKEB) scheme (Shutts, 2005) in the WRF model to form the 14-member ensemble. The SKEB scheme adds temporally and

spatially correlated perturbations to the rotational wind components and the potential temperature. Berner et al. (2011) showed that the ensemble with SKEB scheme performs better in improving the ensemble weather forecast than the multiple physics scheme ensemble. The effect of the SKEB scheme is most remarkable in the low-level wind fields (Charron et al. 2010; Berner et al., 2011). Since the SKEB scheme is very promising in producing a good ensemble, it is tested here for ensemble regional climate simulations. The time periods of the first two ensemble simulations were both from 1991 to 1998, while the last one was from 1997 to 1998. The ensemble mean and spread of the temperature and precipitation were computed and compared to observations and the CFSR data. The uncertainties in regional climate simulations are discussed.

Chapter 3: Assessment of NARCCAP data and the observations

This chapter shows the analyses of the NARCCAP RCM simulations, NCEP-CFSR reanalysis data and some of the station observations. The NARCCAP data contains 7 RCM model simulations over North America for 26 years from 1979 to 2004.

3.1 Temperature analysis

3.1.1 Time series

In this thesis, we focused on evaluating surface (2-m) air temperature. To compare with the observations from the chosen 8 stations (Fig. 2.1), the gridded model data was interpolated onto the station locations. In this research, the natural neighbour interpolation was chosen to obtain the model data at 8 stations. The basic equation in 2D natural neighbour interpolation is $G(x,y) = \sum_{i=1}^{n} w_i f(x_i, y_i)$, where $G(x,y)$ is the value at the interpolation point (x,y). $f(x_i, y_i)$ is gridded model data at (x_i, y_i), and w_i are the corresponding weights. The weights w_i is computed using the Thiessen polygon network of neighboring points. Finally, the interpolated data and the observations at 8 stations were averaged to represent the area-mean value over Ontario.

The data was divided into four seasons defined in Table 3.1.

Table 3. 1: The distributions of the four seasons.

	Spring	Summer	Fall	Winter
Months	March, April, May	June, July, August	September, October, November	December, January, February

Because the simulations started in January 1st 1979, the winter season in 1979 only includes January and February.

Figure 3-1 shows the time series of the annual average and seasonal average temperature in seven models and observations over Ontario. For the observations, it is obvious to see that the annual temperature fluctuates from the late 1970s to the late 1990s followed by a sudden rise (shown later in the standardization time series in Fig. 3.2). Comparisons of the average temperature in four seasons show that the sudden increase of the annual average temperature in the late 20th century is mainly due to a sudden rise of winter and spring average temperature (Fig. 3.1 b,e and Fig.3.2 b,e). Although all of the four seasons show an increasing trend during the chosen period, the increase of the temperature in summer is not as big as that in winter. In fall, the temperature in 2004 becomes the highest during this period.

The temperatures in seven model simulations follow the observations reasonably well. For the annual average temperature, HRM3 and ECPC have constantly higher temperature than the observations, while RCM3, CRCM and MM5I are lower. WRFG gives the least error. RCM3 has

the coldest bias especially due to its cold bias mainly in spring and summer. HRM3 has the warmest bias, especially because of its greatest warm bias in winter.

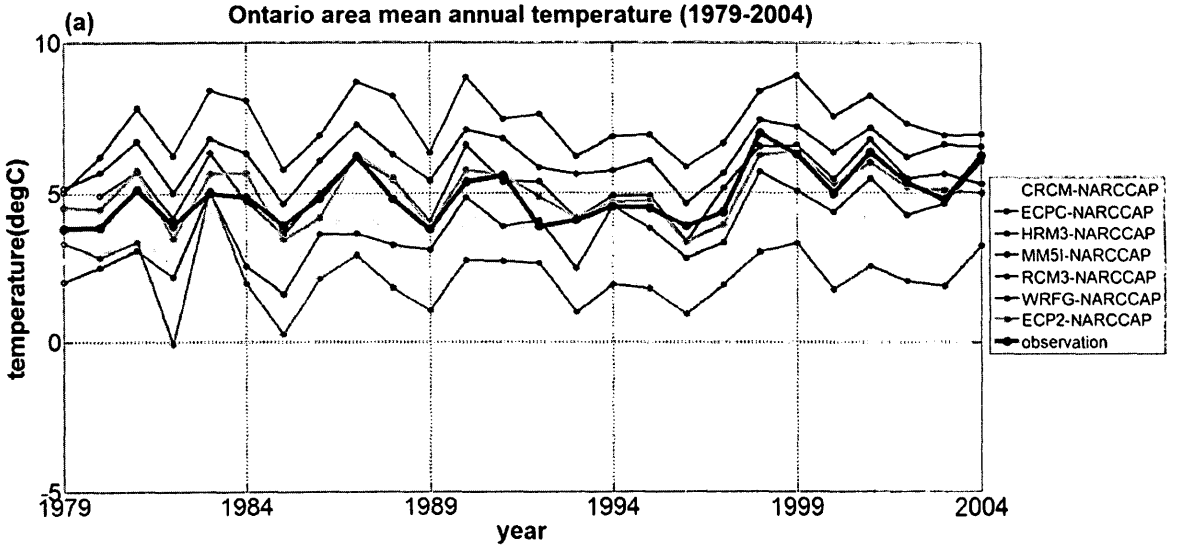

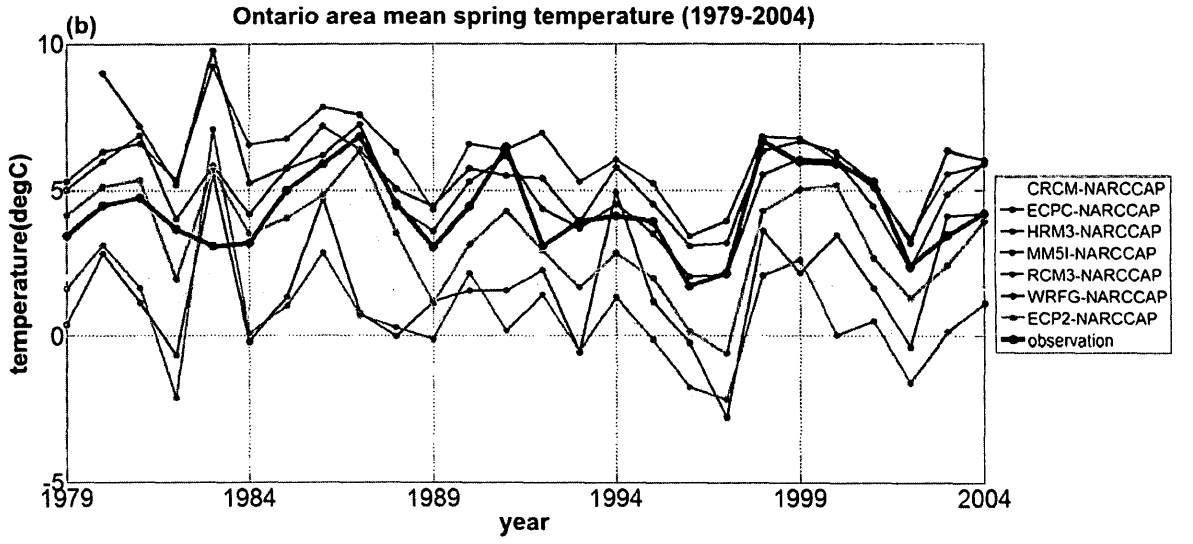

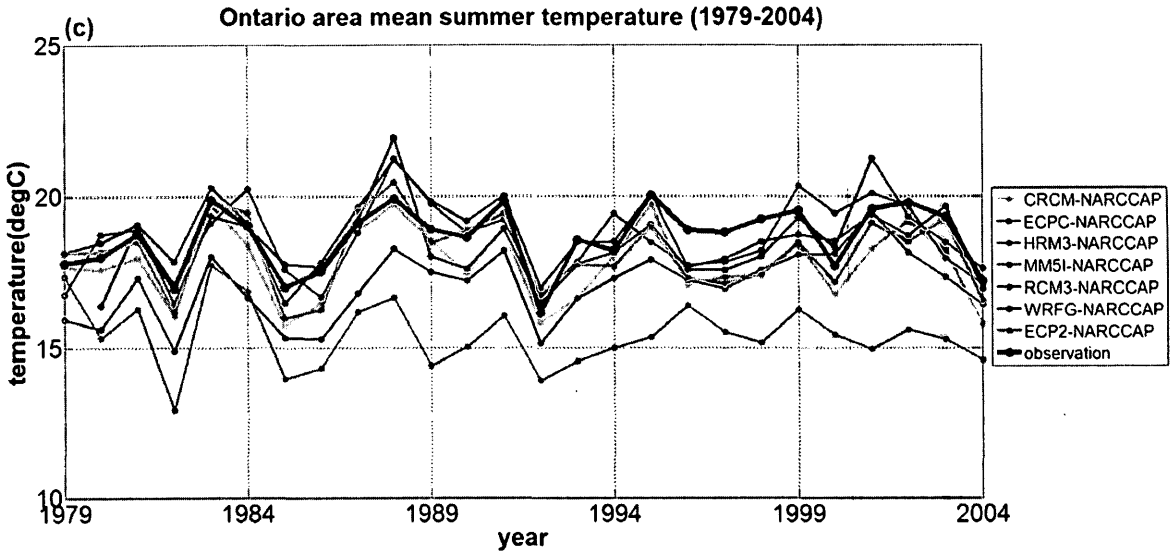
(c)
Ontario area mean summer temperature (1979-2004)
temperature(degC)
year
CRCM-NARCCAP
ECPC-NARCCAP
HRM3-NARCCAP
MM5I-NARCCAP
RCM3-NARCCAP
WRFG-NARCCAP
ECP2-NARCCAP
observation

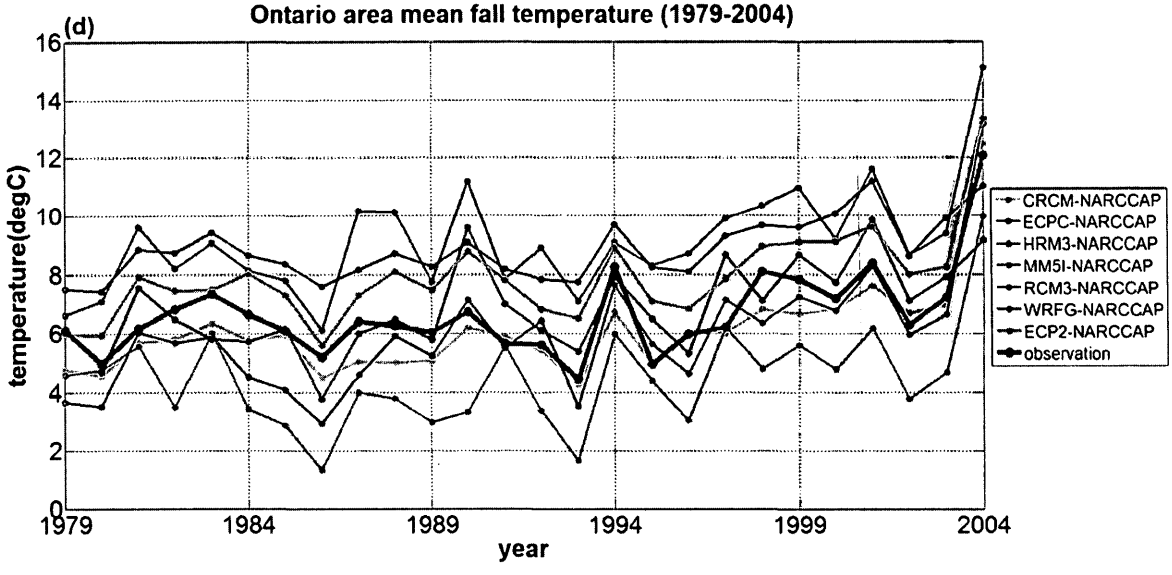
(d)
Ontario area mean fall temperature (1979-2004)
temperature(degC)
year
CRCM-NARCCAP
ECPC-NARCCAP
HRM3-NARCCAP
MM5I-NARCCAP
RCM3-NARCCAP
WRFG-NARCCAP
ECP2-NARCCAP
observation

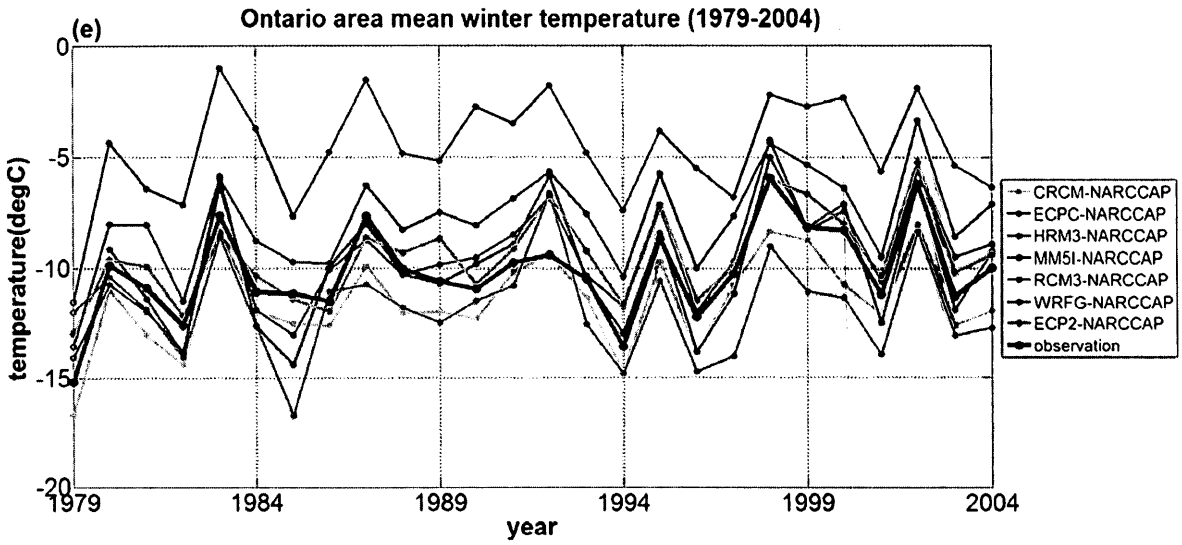

Figure 3. 1: Ontario 8-station mean temperature time series of observations (in red) and seven model data (°C). (a) Annual average temperature, (b) spring average temperature, (c) summer average temperature, (d) fall average temperature, and (e) winter average temperature.

After standardization (Eq. 2.1.1), an increasing trend of annual observed temperature was identified (Fig. 3.2 a). The trend also in the four seasons (Fig.3.2 b-e). The low frequency variations of annual temperature in Ontario can be divided into 4 periods: cold period 1979-1985, warm period 1985-1991, cold period 1991~1997 and warm period 1998~2004. In the late 1980s and the early 1990s there is a warm period, but not as significant as the one occurred from the end of the 20th century. The temperature in Ontario begins to rise remarkably from 1998. This tendency is revealed in spring, fall and winter. In summer, this tendency starts several years earlier. All the four seasons contribute to the significant temperature increase from the late 1990s, and winter contributes the most. In spring, the temperature trend stays almost constant, while the other three seasons all show an increasing trend during the whole studied period.

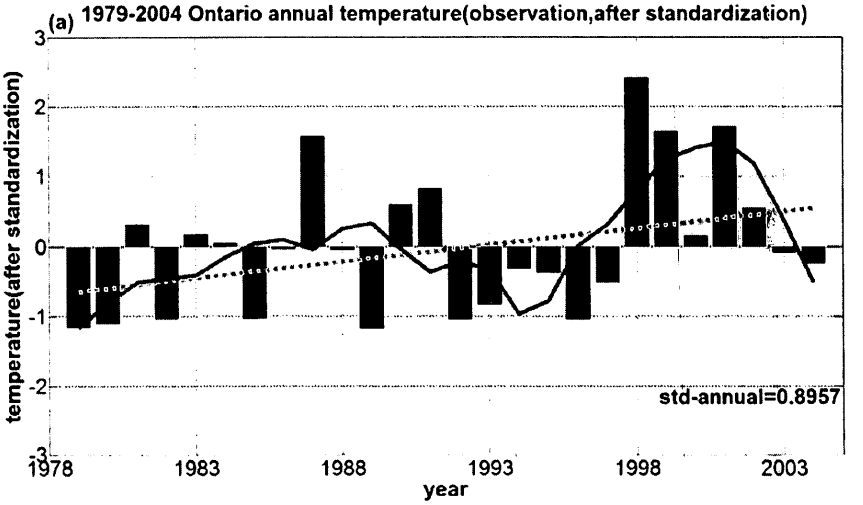
(a) 1979-2004 Ontario annual temperature(observation,after standardization)
temperature(after standardization)
year
std-annual=0.8957

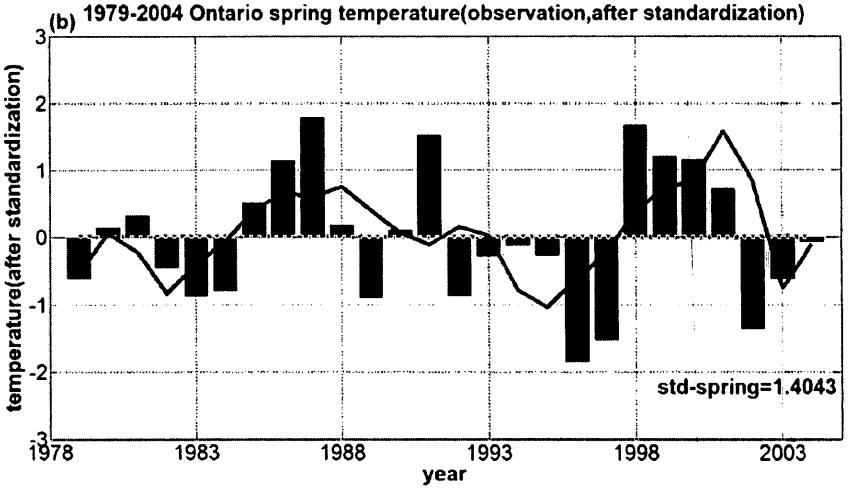
(b) 1979-2004 Ontario spring temperature(observation,after standardization)
temperature(after standardization)
year
std-spring=1.4043

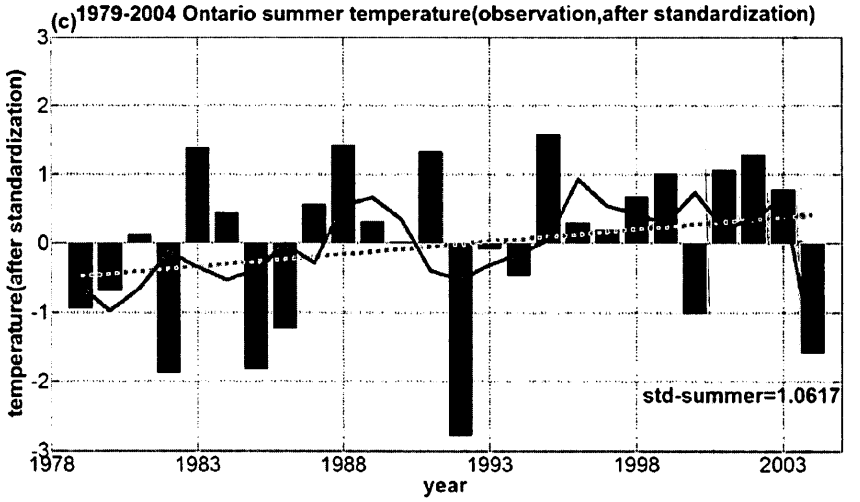
(c)1979-2004 Ontario summer temperature(observation,after standardization)
temperature(after standardization)
year
std-summer=1.0617

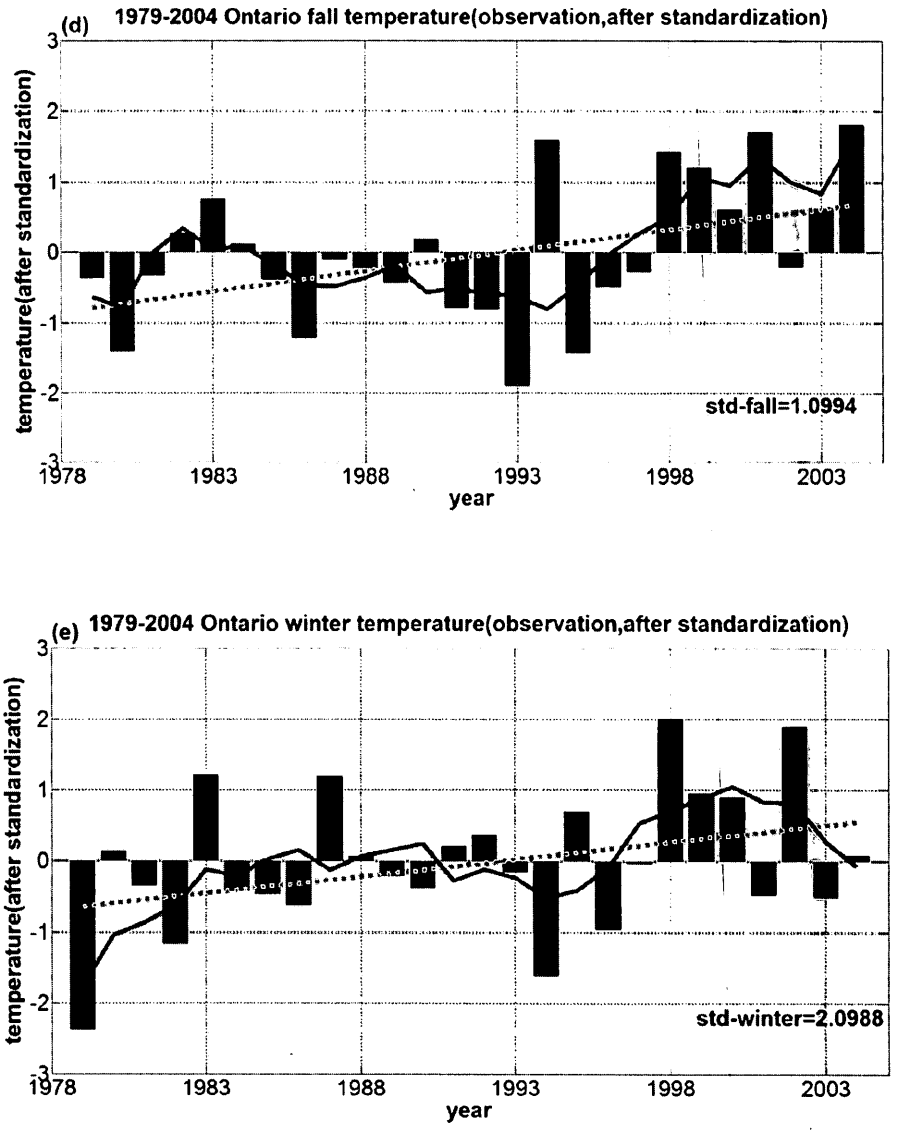

Figure 3. 2: Standardized time series of the 8-station mean temperature observation in Ontario. (a) Annual temperature, (b) spring temperature, (c) summer temperature, (d) fall temperature, (e) winter temperature. The linear trend is in green dash line. The low frequency variation is in red. The standard deviation (°C) is labeled in each panel.

Since WRFG has the least error, we chose WRFG as one example for comparison after standardization. In Fig. 3.3, the annual, summer, fall and winter temperatures have similar peaks and valleys corresponding to the observed temperatures. These three seasons contribute to the

late 1990s temperature upward tendency, and the biggest contribution is from winter. In spring, the WRFG simulation does not perform well since it shows a decreasing trend opposite to the observations. Both the observation and the WRFG annual temperatures show two peaks in the late 1980s and the late 1990s (Fig. 3.2 a and Fig. 3.3 a). The increasing summer, fall and winter temperature in the late 1990s can also be captured in both standardization series (Fig.3.2 c-e and Fig. 3.3 c-e).

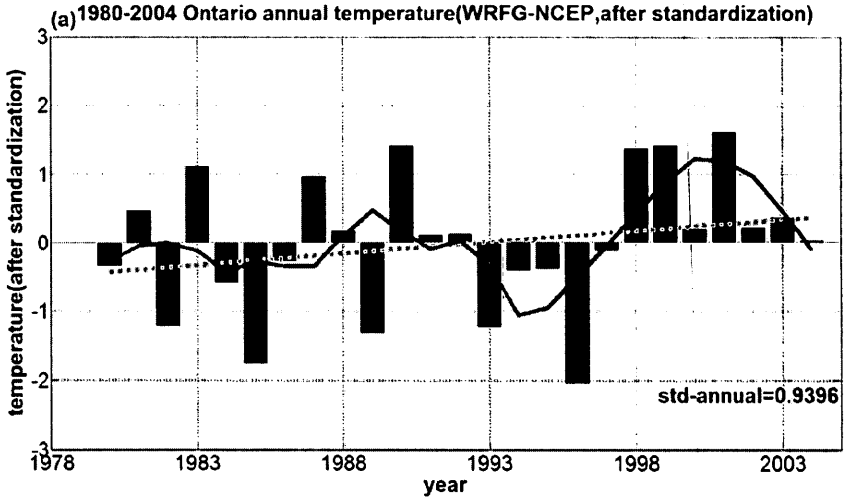

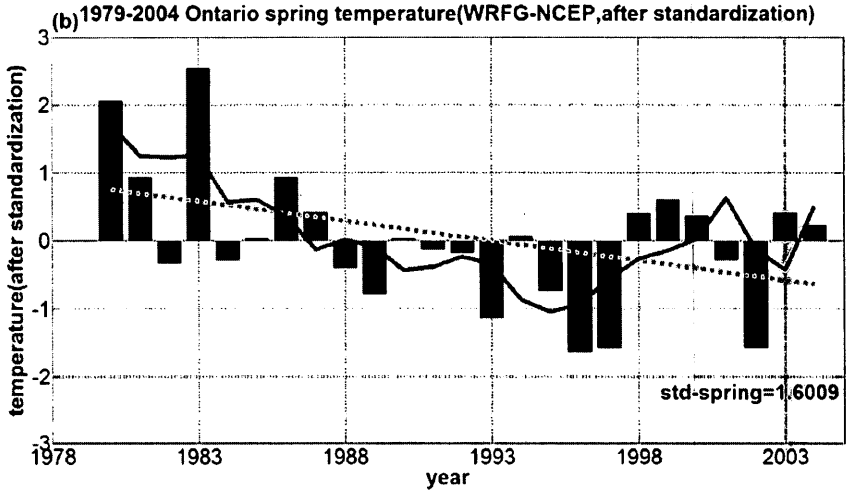
(b)1979-2004 Ontario spring temperature(WRFG-NCEP,after standardization)
temperature(after standardization)
year
std-spring=1.6009

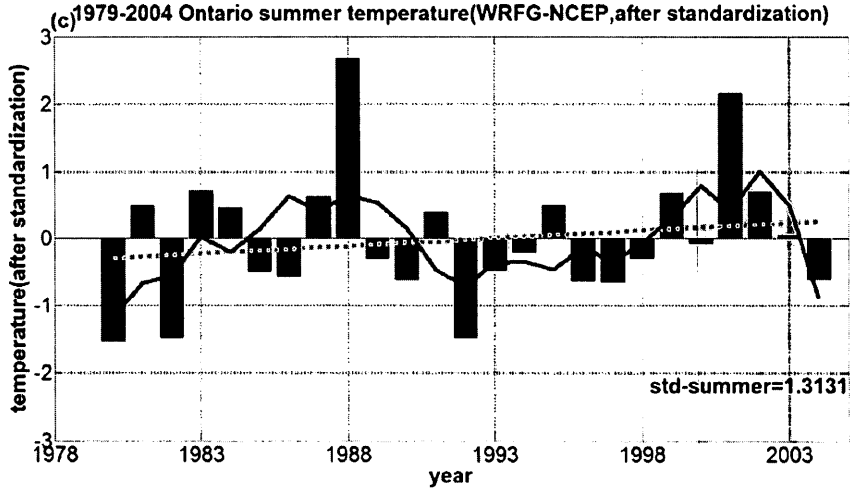
(c)1979-2004 Ontario summer temperature(WRFG-NCEP,after standardization)
temperature(after standardization)
year
std-summer=1.3131

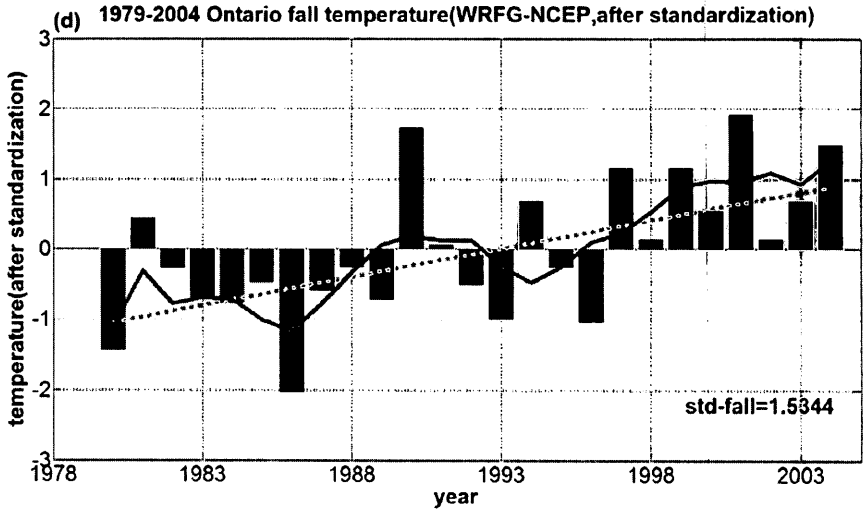
(d) 1979-2004 Ontario fall temperature(WRFG-NCEP,after standardization)
temperature(after standardization)
year
std-fall=1.5344

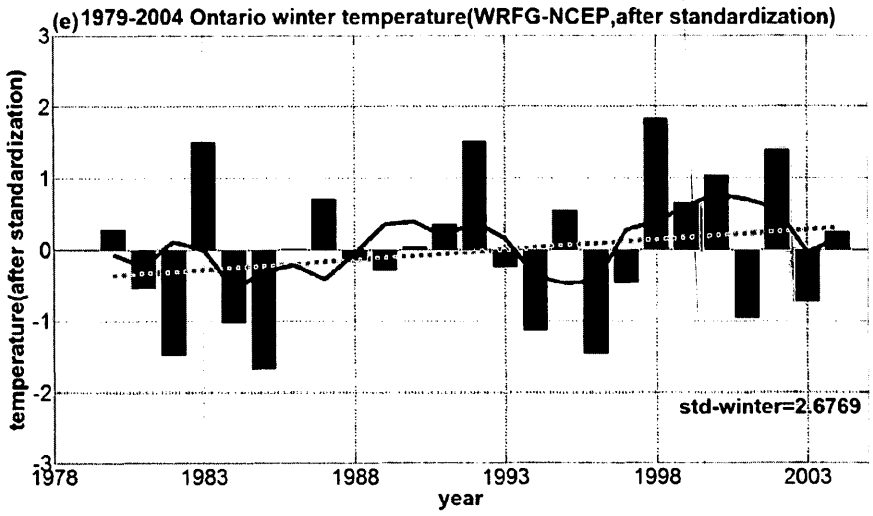

Figure 3. 3: Standardized time series of the 8-station mean WRFG temperature in Ontario. (a) Annual temperature, (b) spring temperature, (c) summer temperature, (d) fall temperature, (e) winter temperature. The linear trend is in green dash line. The low frequency variation is in red. The standard deviation (°C) is labeled in each panel.

For the observations, the standardization curves show some extremely warm and cold years and seasons. In order to study the circulation characteristics and the mechanisms leading to these extreme temperature periods, we defined an anomalous low/high temperature year as 'its standardized temperature value is smaller/greater than -1 or 1.

Table 3. 2: Extremely warm and cold summer and winter as defined as temperature anomalies in excess of ±1.

	Extremely cold (T_{std}<-1)	Extremely warm (T_{std}> 1)
Years (summer)	1982,1985,1986,1992,2004	1983,1988,1991,1995,2002
Years(winter)	1979,1982,1994	1983,1987,1998 ,2002

To some extent, the winter temperature variation follows the annual temperature variation during the entire period. The low frequency variations of winter temperature can also be divided into a

similar 4 periods: cold period 1979-1985, warm period 1985-1991, cold period 1991~1997 and warm period 1998~2004. It can be seen that cold winter events usually occur in cold periods while warm winters usually occur in warm periods.

The summer temperature variation can be divided into 5 periods as well: cold period 1979-1987, warm period 1987-1991, cold period 1991-1994, warm period 1994-2003 and one cold year 2004. The figure and the table reveal that cold summer events usually occur in cold periods while warm summers usually occur in warm periods (except 1983). For these 26 years, summer temperature in Ontario has a slight increasing trend, compared with the winter variation during the same period.

Using the NCEP-DOE reanalysis II data, several factors contributing to the extremely cold and warm winters were discussed in Appendix A. The circulations which favor extremely cold winters include: stronger North American High, stronger North American Trough, stronger jet stream south to the average location and negative temperature advection. The circulations which favor extremely warm winters turn to be opposite: weaker North American High, weaker North American Trough, weaker jet stream north to the average location and positive temperature advection (Fig. A. 1-4).

3.1.2 Spectral analysis

The purpose of conducting spectral analysis for the time series is to find climate variability at all possible frequencies. The periodicity of temperature (and precipitation) is very important to climate studies.

For annual observed temperature over Ontario, the two peaks are clearly shown in Fig. 3.4 a. The most significant period is 3.7 years and the second most significant period is 13 years. The similar 3.7-year period appears in WRFG, CRCM, ECP2, ECPC and HRM3 annual temperature data. Among these 5 models, the power spectra of CRCM and ECP2 are closer to the observations. Compared with other models and observed data, MM5I and RCM3 simulate the 3.7-year period as well, but they miss some other significant periods. The 8.7-year (frequency 3/26 $year^{-1}$) power spectra are similar for most of the NARCCAP models, except MM5I and RCM3. For summer seasons and winter seasons, there are agreements and disagreements among the power spectra of these seven models and the observations. In winter (Fig. 3.6 a), a 3.7-year period is seen in the power spectra of all the models and the observations, which is the most significant variation period (in some of the models it is the second most significant period). However, the observations and ECPC show their most significant period of 2.1-year period. Some of the models and the observations have peaks at the 13-year period and 8.7-year period, but not as significant as 2.1-year and 3.7-year periods. For summer case (Fig.3.5), two main periods are 3.7 years (the most significant period) and 6.5 years (the second most significant period) are shown obviously. In summary, all the seven models and observations show a 3.7-year period of temperature variation. Except MM5I and RCM3, the other five models simulate the period of 13 years in annual and winter temperature variations, and the 6.5-year period in summer variations very well. Interestingly, HRM3 annual temperature variation power spectrum indicates that its most significant period is 13 years and the second most significant period is 3.7 years, which are in the opposite order as those in the observation.

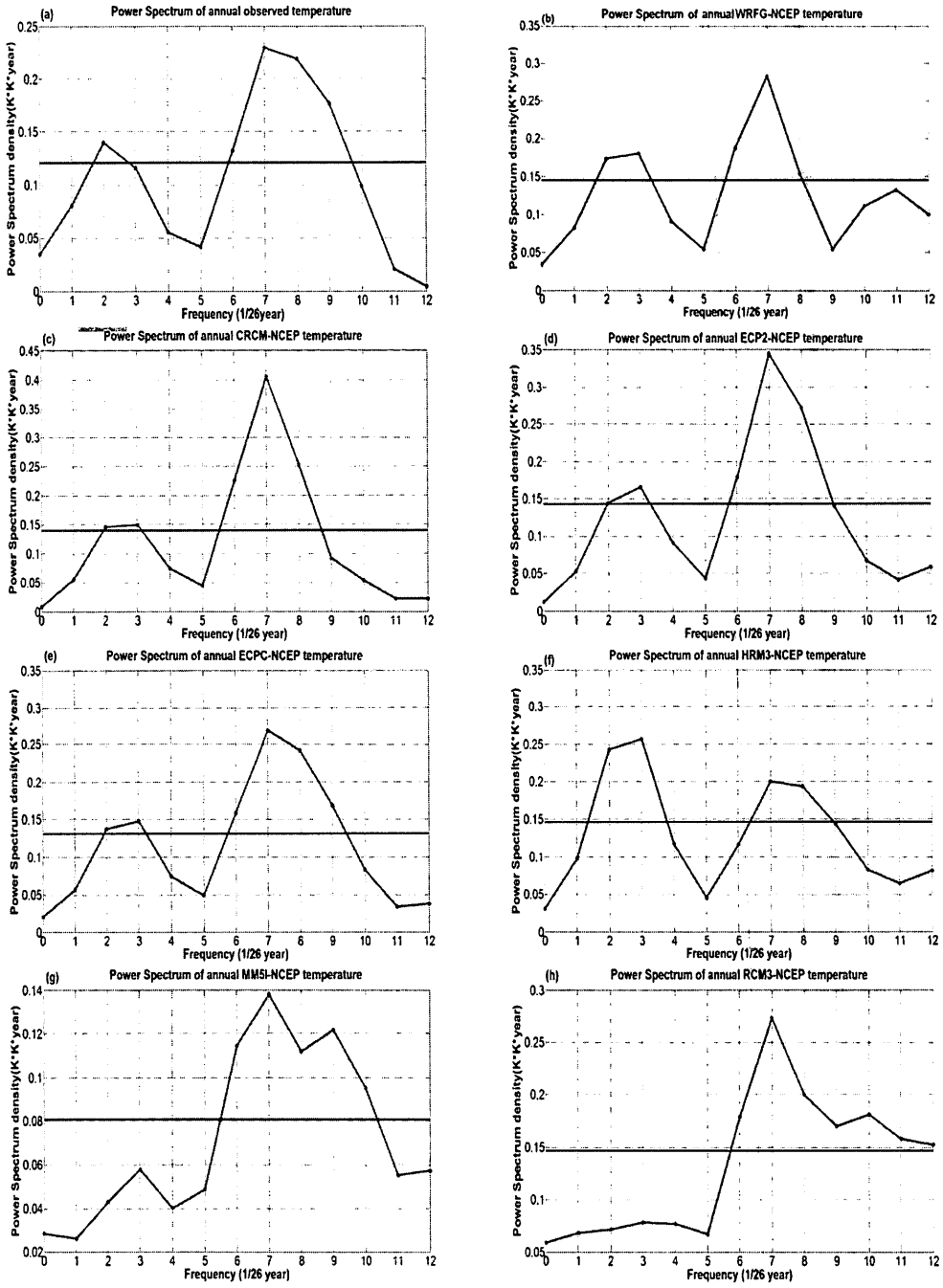

Figure 3. 4: Power spectra of annual average temperatures in Ontario in observations and seven NARCCAP simulations. (a) Observation, (b) WRFG, (c) CRCM, (d) ECP2, (e) ECPC, (f) HRM3, (g) MM5I, (h) RCM3. The red lines are power spectrum criterion (The x-axis is frequency (1/26 year^{-1}) and the y-axis is the power spectrum (K^2 year)).

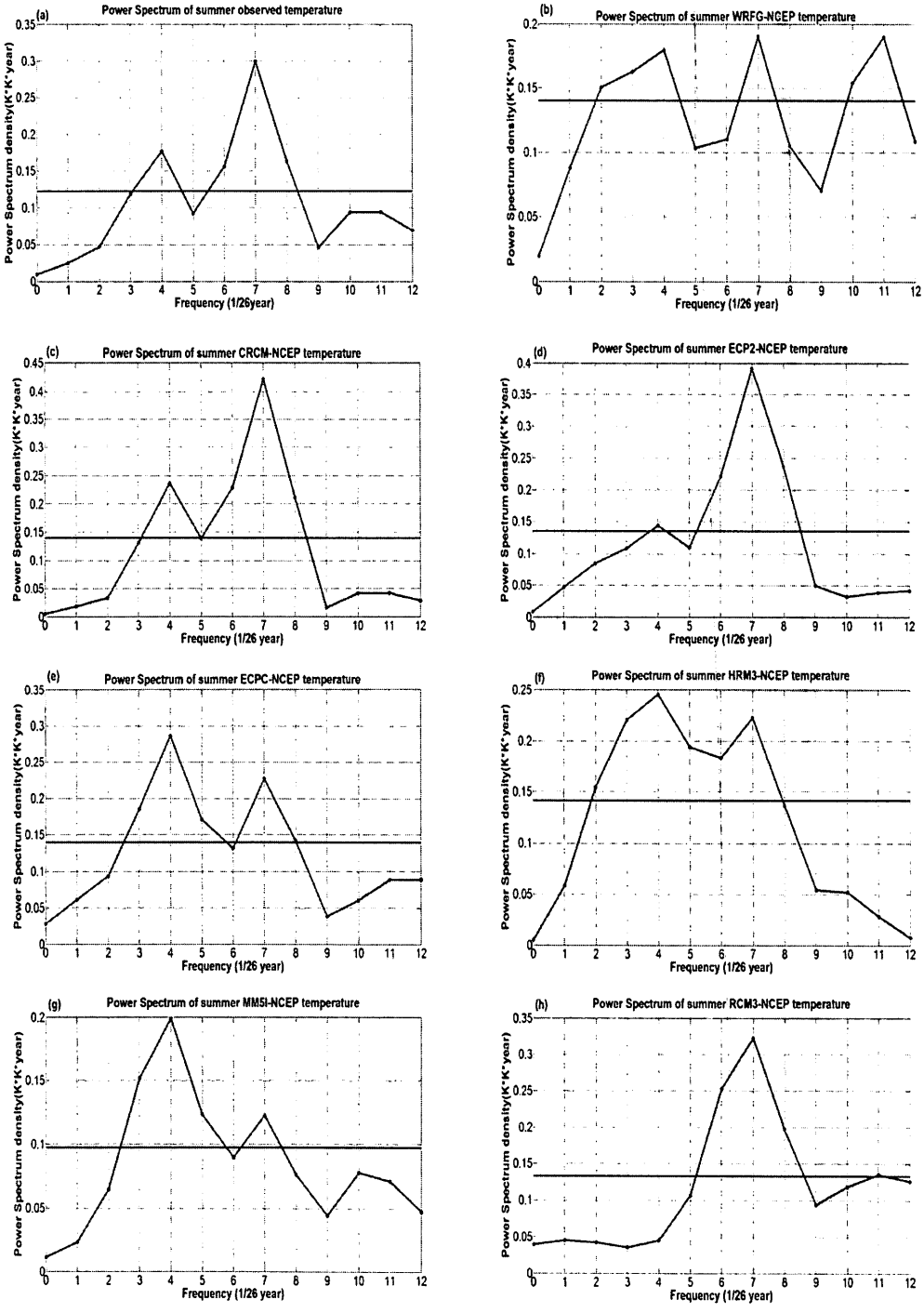

Figure 3. 5: Power spectra of summer average temperatures in Ontario in observations and seven NARCCAP simulations. (a) Observation, (b) WRFG, (c) CRCM, (d) ECP2, (e) ECPC, (f) HRM3, (g) MM5I, (h) RCM3. The red lines are power spectrum criterion (The x-axis is frequency (1/26 year^{-1}) and the y-axis is the power spectrum (K^2 year)).

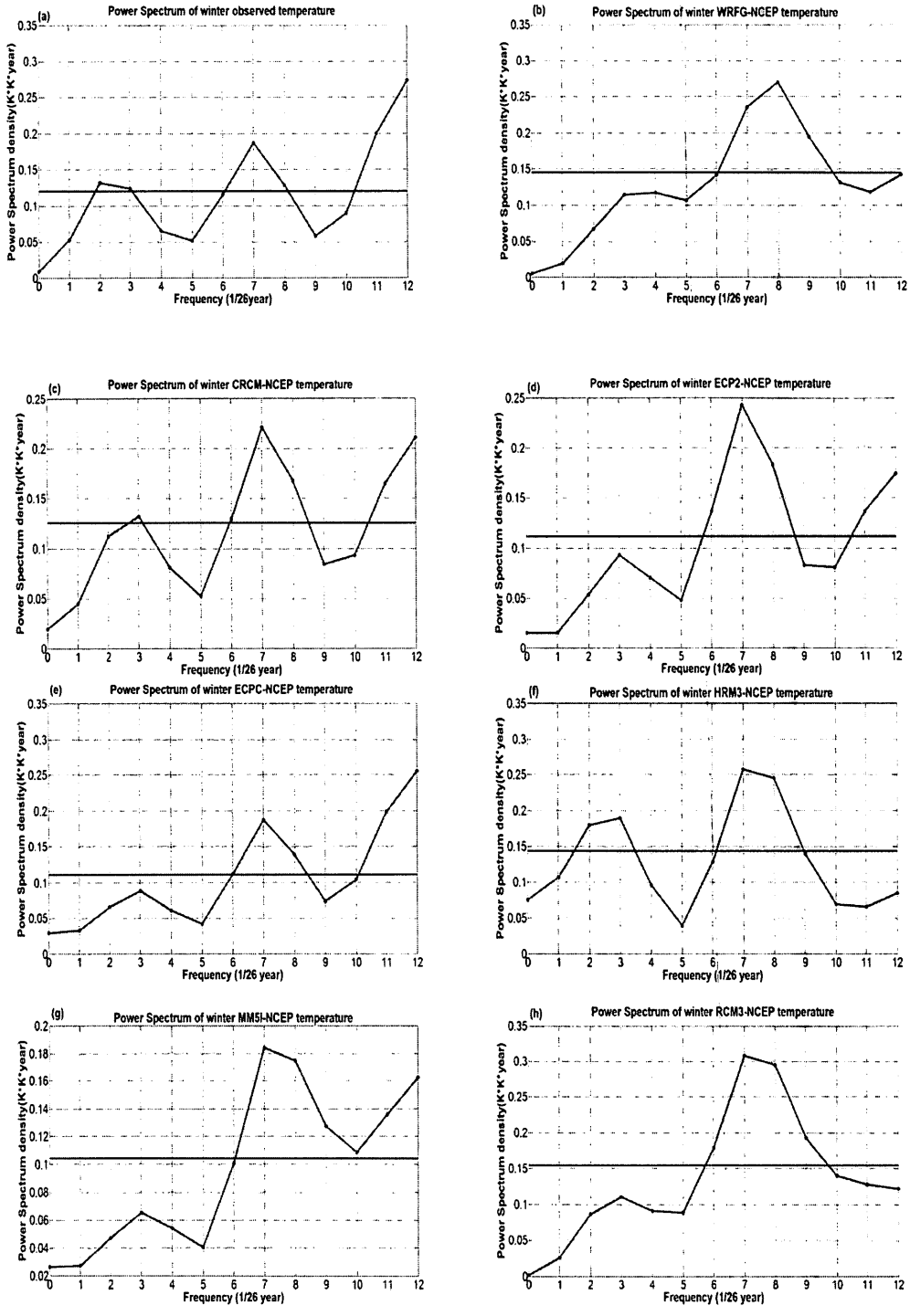

Figure 3. 6: Power spectra of winter average temperatures in Ontario in observations and seven NARCCAP simulations. (a) Observation, (b) WRFG, (c) CRCM, (d) ECP2, (e) ECPC, (f) HRM3, (g) MM5I, (h) RCM3. The red lines are power spectrum criterion (The x-axis is frequency (1/26 year^{-1}) and the y-axis is the power spectrum (K^2 year)).

3.1.3 EOF analysis

Empirical Orthogonal Functions (EOF) technique has become one of the most widely used methods to study both the spatial distribution and temporal variation of climatological variables (Hannachi et al., 2009; Zeng et al., 2006). In this research, the EOF analysis was applied to NCEP-DOE reanalysis II data and each NARCCAP model data over Ontario to identify the capability of the models in capturing the climate variability. Because the results from all the models and the reanalysis data give similar EOF patterns, only the EOF analysis results for the WRFG data and the NCEP-DOE reanalysis II data are shown here.

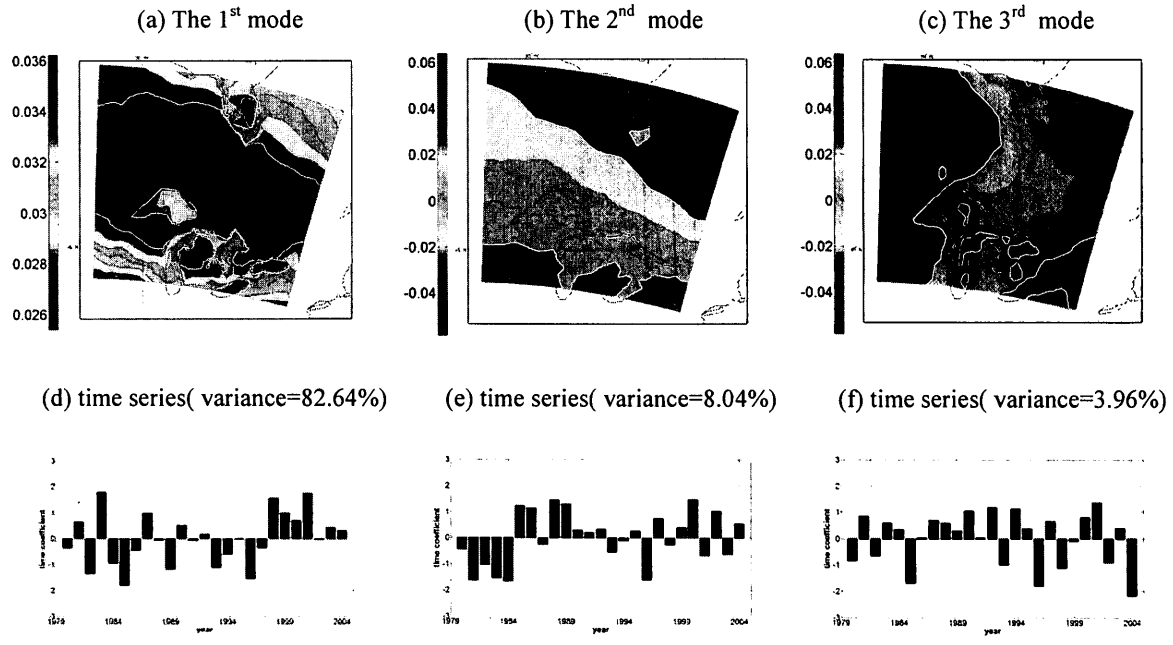

Figure 3. 7: The spatial distributions (a-c) and temporal variations (d-f) of the first 3 leading EOF modes for WRFG annual temperature (a,d: 1st mode, b,e: 2nd mode, c,f: 3rd mode).

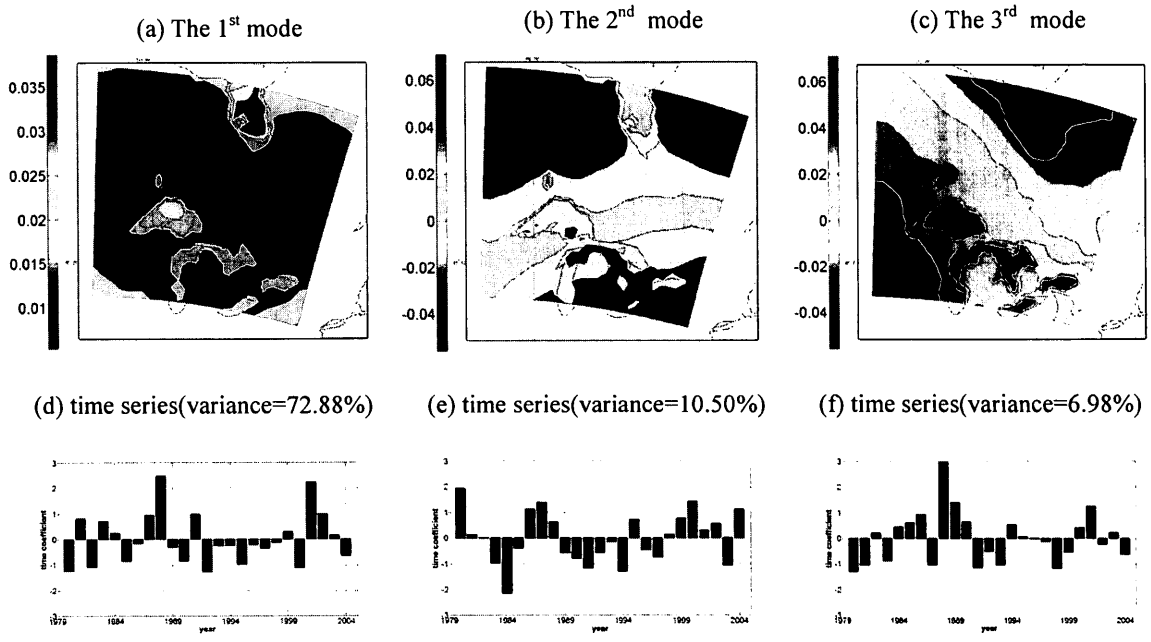

Figure 3. 8: The spatial distributions (a-c) and temporal variations (d-f) of the first 3 leading EOF modes for WRFG summer temperature (a,d: 1st mode, b,e: 2nd mode, c,f: 3rd mode).

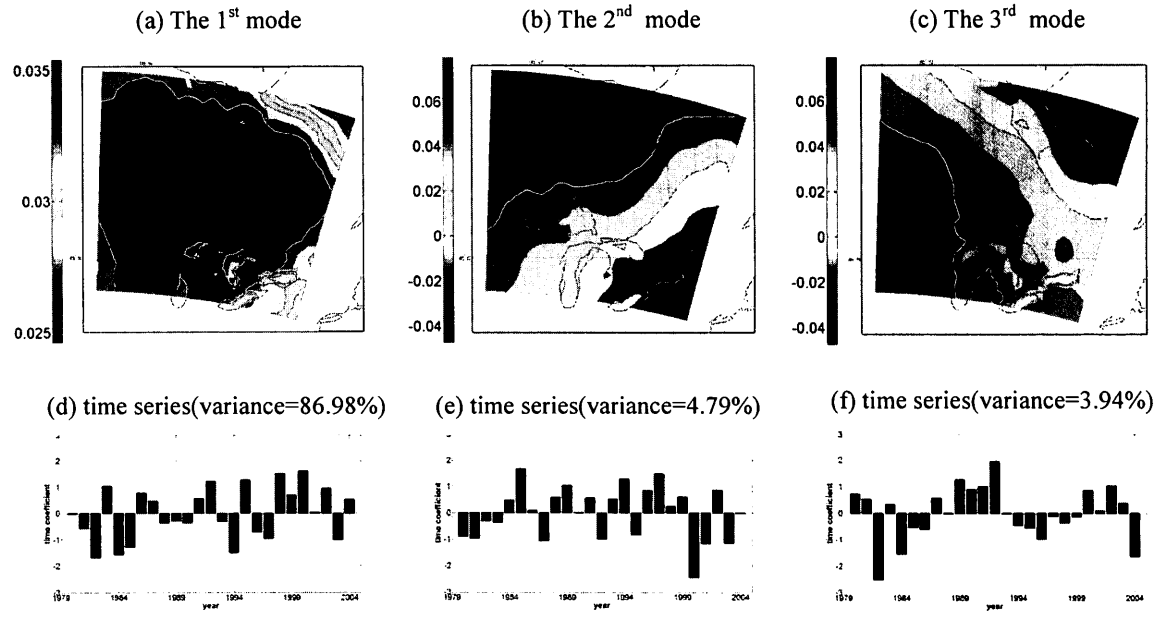

Figure 3. 9: The spatial distributions (a-c) and temporal variations (d-f) of the first 3 leading EOF modes for WRFG winter temperature (a,d: 1st mode, b,e: 2nd mode, c,f: 3rd mode).

Firstly the annual temperature variation is discussed. The first mode variance contribution accounts for 82.64%, which is definitely dominant among all the modes. From Fig. 3.7 (a), it can be clearly seen that the correlation coefficients in Ontario are all positive, which means that the annual temperature throughout Ontario changes in the same phase. The annual temperature variations in both west and east Ontario show great accordance. The area of large variability is in the middle of Ontario north to the Great Lakes. Interestingly, the values over water surface such as the Hudson Bay and the Great Lakes are obviously lower than surrounding areas over land. It is probably because of the different heat capacities between land and water. Figure 3.7 d is the time coefficient series of the first mode. Positive values represent that annual temperature of the whole region rises while negative values stand for a decreasing trend of temperature in the corresponding years. When comparing this time coefficient series with the observed data time series (Fig. 3.10 d), it shows a similar feature that from 1998 the annual temperature rises remarkably after decades of fluctuations.

The second mode variance contribution accounts for only 8.04%, much smaller than the first mode. It shows a great difference in temperature variation between north (negative value) and south (positive value) Ontario. A positive time coefficient means that annual temperature in north Ontario rises while temperature in south Ontario drops, and vise versa. The third mode has 3.96% of the variance contribution, and the patterns are opposite in west (positive value) and east (negative value) Ontario.

In total, the leading three modes, with more than 90% accumulated variance contribution, are sufficient to describe the spatial and temporal distribution of the annual temperature variation.

In summer (Fig. 3.8), the variance contribution of the first mode only accounts for 72.88%, which is relatively smaller than that of annual and winter (86.98%). The correlation coefficients in Ontario are positive in both summer and winter, and the high center is in the middle part of Ontario. In summer, Lake Superior and the south part of the Hudson Bay share low coefficients, but still positive. The coefficients do not have great differences in the first mode of winter. At this time of year, the low coefficients of temperature only appear at the top right corner and the bottom right corner of the domain. Overall, from the first modes of summer and winter, the temperature variations show good accordance. Moreover, the time series of the first mode in winter explains 86.98% of the covariance that in the late 1990s, the temperature is rising.

It is noticeable that the patterns of the 2nd and the 3rd modes in summer and winter are similar. The coefficients of both summer and winter 2nd modes have a northwest-southeast increasing trend. So the differences of temperature variations are shown that the northwest and southeast parts do not share the same phase. The third mode accounts much less than the leading 2 modes. The summer and winter 3rd modes both show a pattern that the northeast (negative) and the southwest (positive) are in different phases. Not surprisingly, the differences between summer and winter EOF patterns are over the lakes. This is because that in winter, the lakes are covered with freezing ice and the temperature over the lakes is considered to be similar to the adjacent land area. In summer, when the ice over the lakes melts, due to the different heat capacity of land and water, the coefficients over the lakes are different from the coefficients over the land.

EOF analyses of all other six models result in similar conclusions. The first mode takes up the largest percentage of variance contribution at around 80%-90%, and has similar spatial distribution to that of WRFG model. For the temporal patterns, there are some differences in fluctuations before 1998 among the models. All time coefficient series of the seven models show a remarkable temperature rise in 1998.

The EOF analyses of the NCEP-DOE reanalysis II data shows similar spatial and temporal patterns displayed below in Fig. 3.10 to Fig. 3.12. The first modes of annual, summer and winter temperature variations are all positive and take up around 70% of their total variance. Although there are some differences in the 2nd and the 3rd modes between model and the NCEP-DOE data, the variance of these two modes accounts for much smaller percentage than the first mode. Thus, the first mode is the predominant one which can depict the temperature variations, to some extent. It can be seen from the first modes of annual and winter NCEP-DOE temperature (Fig.3.10 d and Fig. 3.12 d) that the significant temperature increase occurs in the late 1990s.

The EOF analyses of the model data and the NCEP-DOE data suggested that all models are capable of simulating the main annual, summer and winter temperature variation in Ontario.

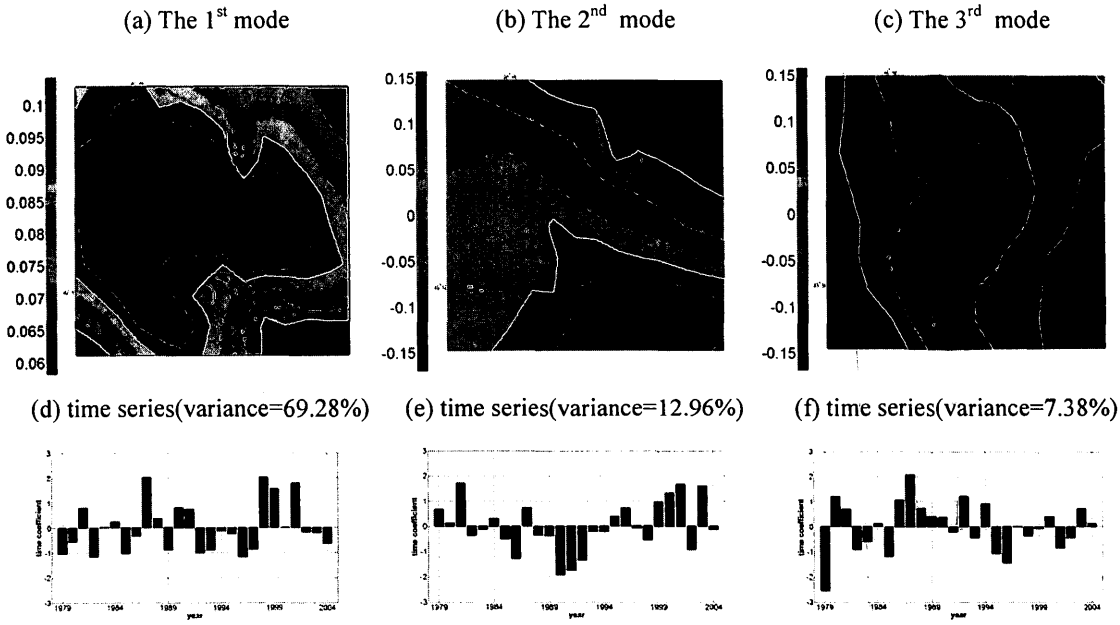

Figure 3. 10: The spatial distributions (a-c) and temporal variations (d-f) of the first 3 leading EOF modes for the observed annual temperature (a,d: 1st mode, b,e: 2nd mode, c,f: 3rd mode).

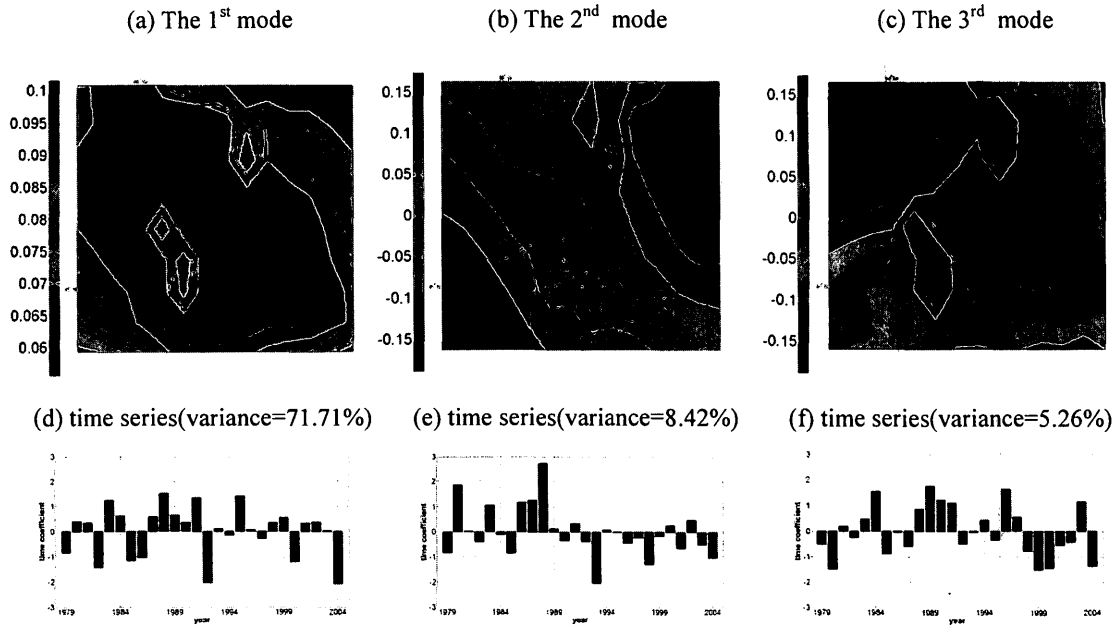

Figure 3. 11: The spatial distributions (a-c) and temporal variations (d-f) of the first 3 leading EOF modes for the observed summer temperature (a,d: 1st mode, b,e: 2nd mode, c,f: 3rd mode).

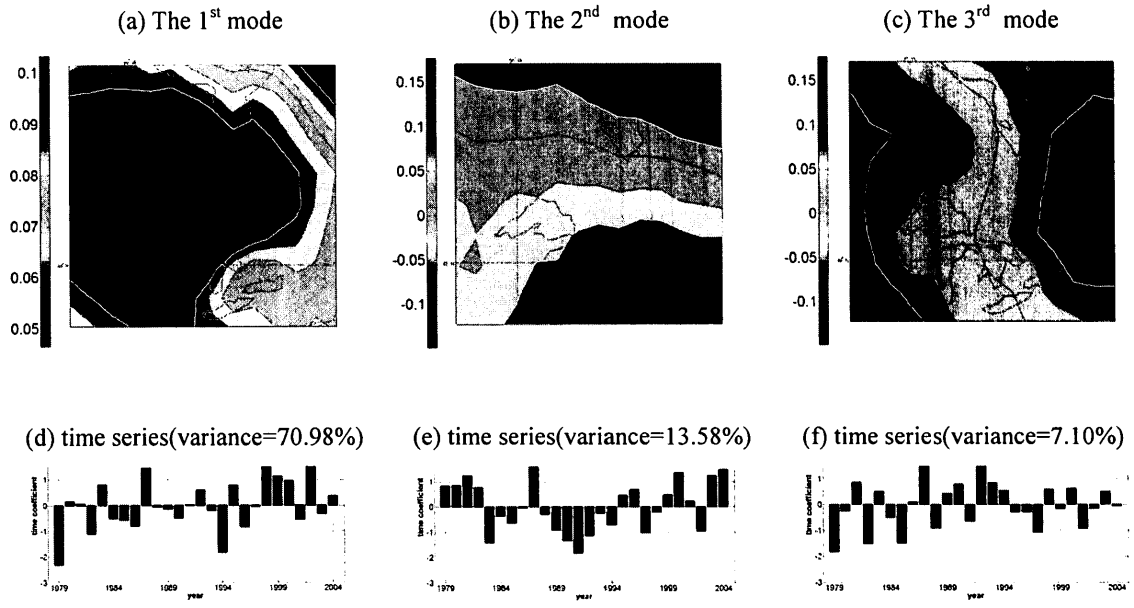

Figure 3. 12: The spatial distributions (a-c) and temporal variations (d-f) of the first 3 leading EOF modes for the observed winter temperature (a,d: 1st mode, b,e: 2nd mode, c,f: 3rd mode).

3.2 Maximum and minimum temperature analysis

To obtain the averaged maximum temperature (TMAX) and minimum temperature (TMIN) defined in this section, the annual or seasonal averaged daily maximum and minimum temperatures were interpolated onto 8 stations and then averaged. The maximum and minimum temperatures discussed in later sections were also obtained by this method. Figure 3.13 and 3.14 show Ontario 8-station mean maximum and minimum temperature time series. Since the maximum and minimum temperatures are not provided in ECPC, ECP2 and MM5I, only four out of seven models are plotted, and some of them do not cover the entire period.

For the annual mean of the daily maximum and minimum temperature during the entire period, a remarkable rising trend is shown in 1998 in both time series. CRCM has a warm bias in fall and winter for both maximum and minimum temperature, which leads to its warm bias in annual maximum and minimum temperature. RCM3 has a cold bias in spring, summer and fall maximum temperature time series, and this contributes to its cold bias of annual maximum temperature. HRM3 has the lowest annual minimum temperature. This is mainly due to its cold bias in winter and spring minimum temperature. All the three models (WRFG, RCM3 and HRM3) have colder minimum temperature than the observations in summer.

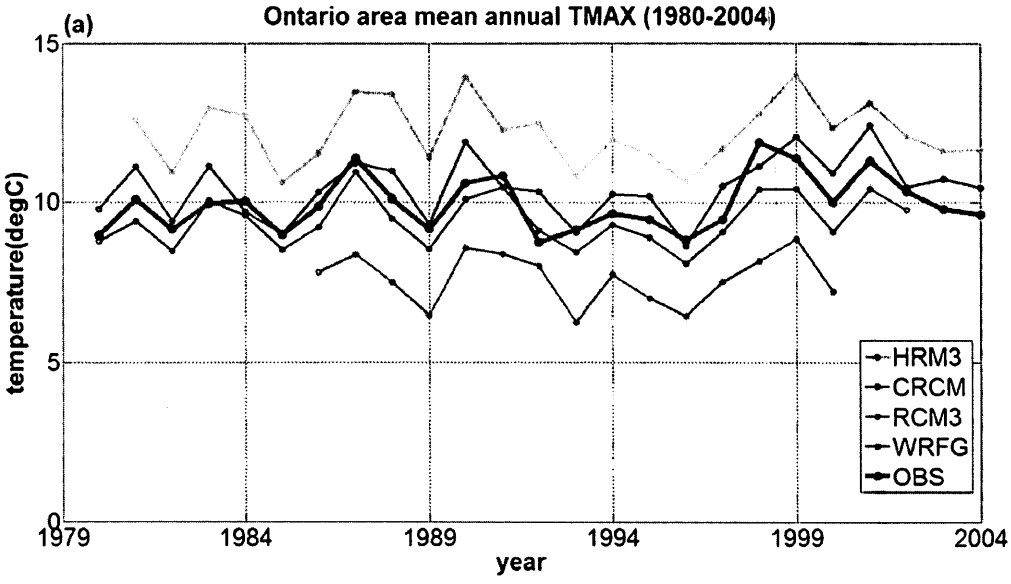

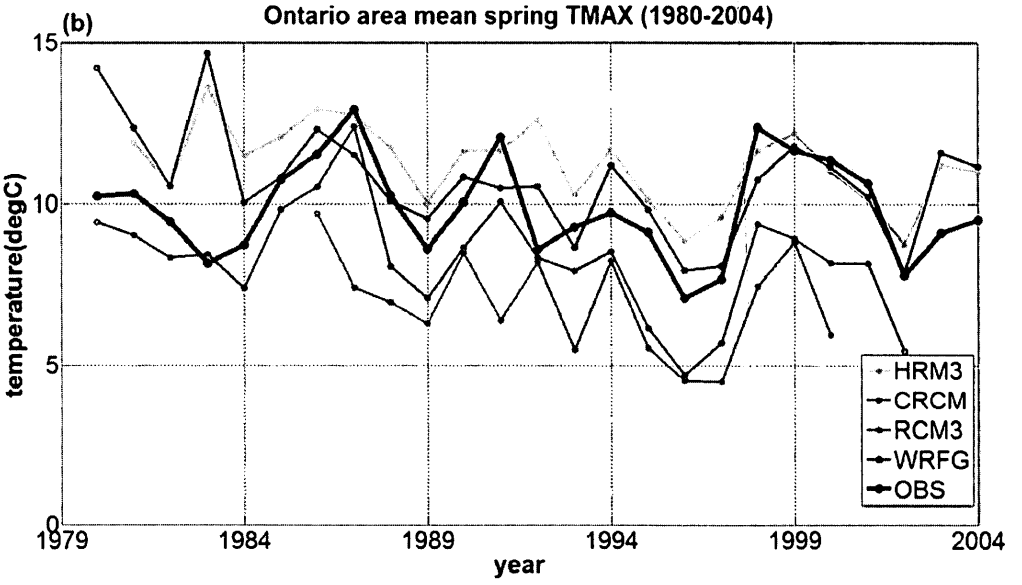
(b)
Ontario area mean spring TMAX (1980-2004)
temperature(degC)
year
HRM3
CRCM
RCM3
WRFG
OBS

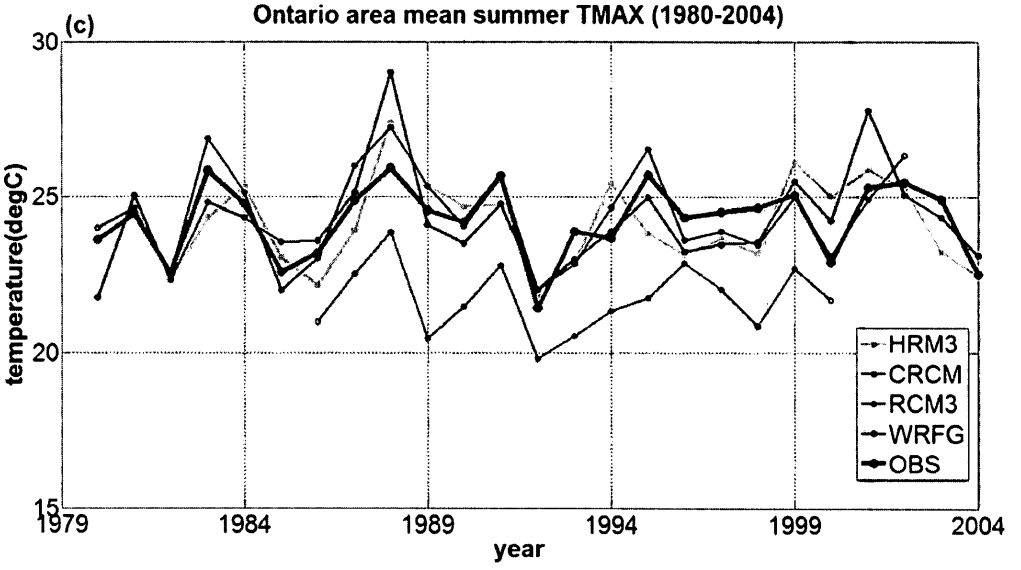
(c)
Ontario area mean summer TMAX (1980-2004)
temperature(degC)
year
HRM3
CRCM
RCM3
WRFG
OBS

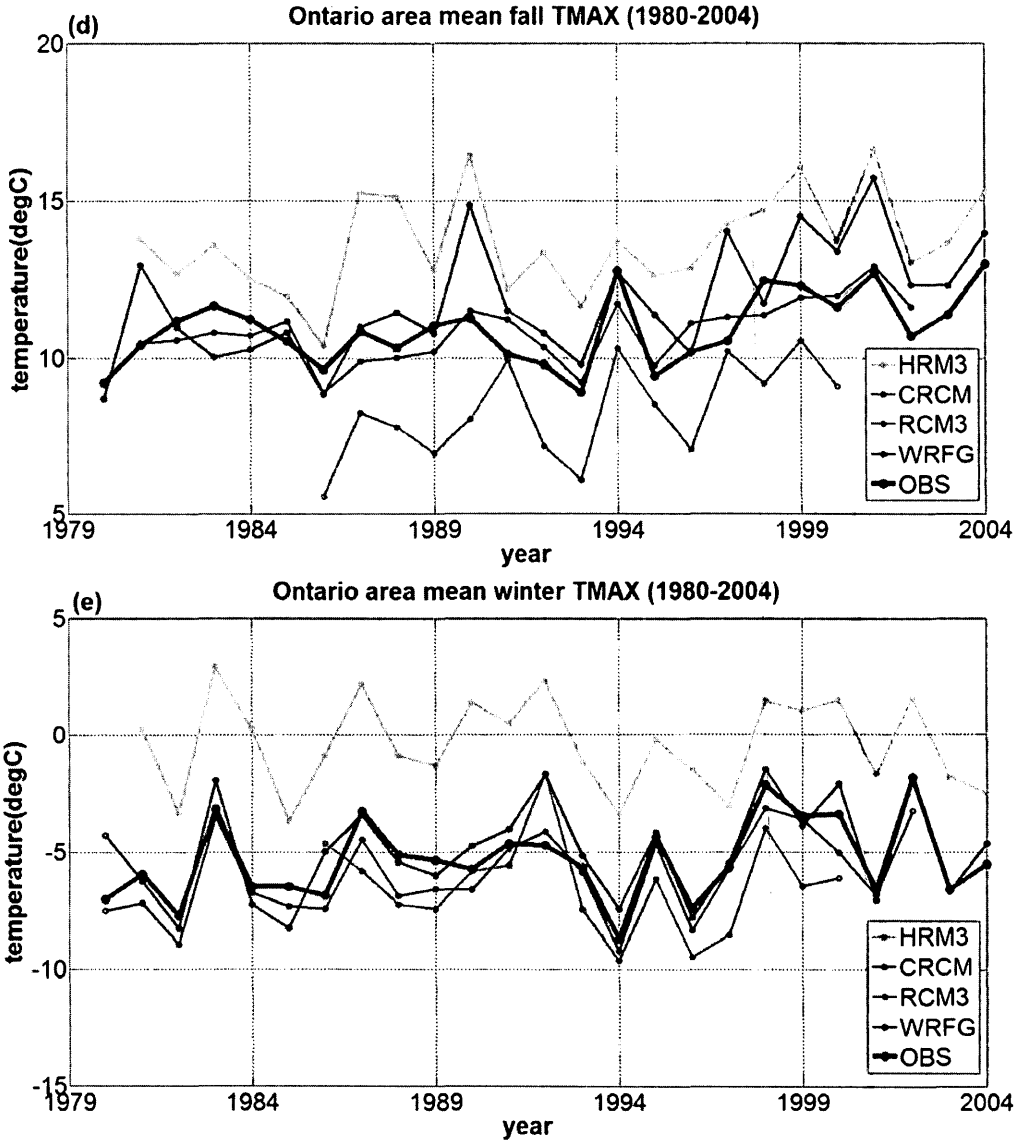

Figure 3. 13: Ontario 8-station mean maximum temperature time series of observations and four model data (unit: degC). The red line represents observation data. (a) Ontario annual area mean maximum temperature, (b) Ontario spring area mean maximum temperature, (c) Ontario summer area mean maximum temperature, (d) Ontario fall area mean maximum temperature, (e) Ontario winter area mean maximum temperature.

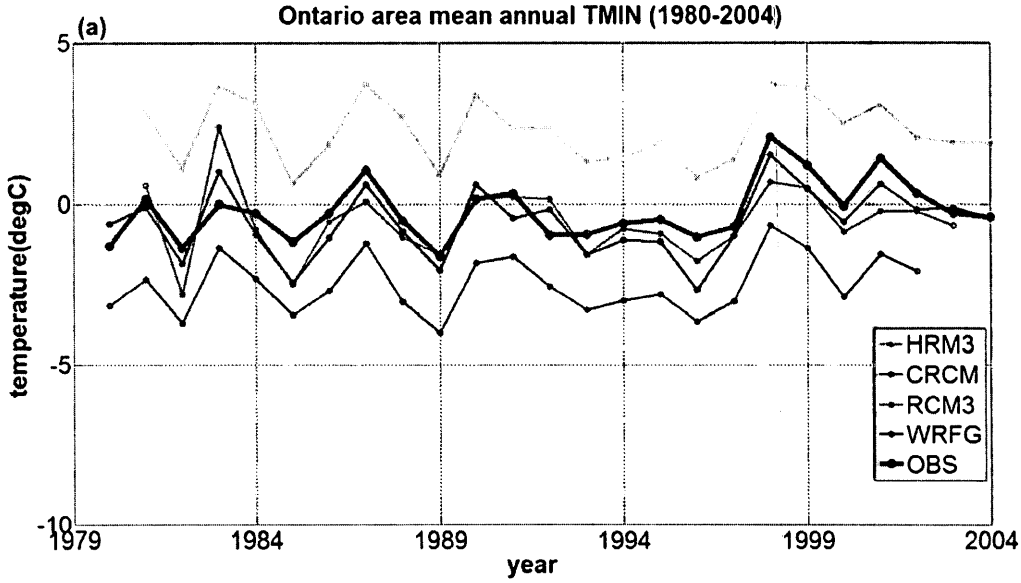
(a)
Ontario area mean annual TMIN (1980-2004)
temperature(degC)
year
HRM3
CRCM
RCM3
WRFG
OBS

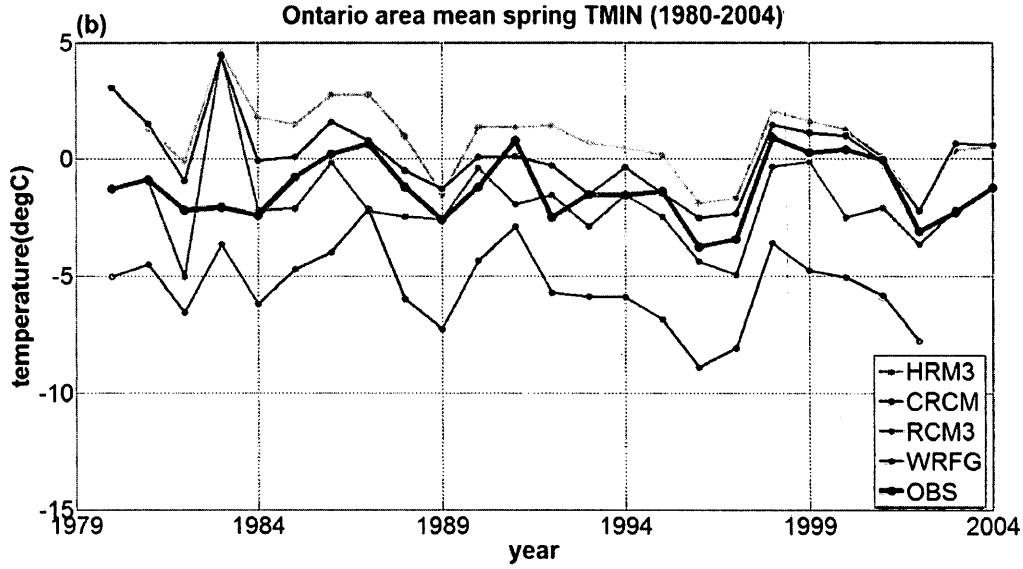
(b)
Ontario area mean spring TMIN (1980-2004)
temperature(degC)
year
HRM3
CRCM
RCM3
WRFG
OBS

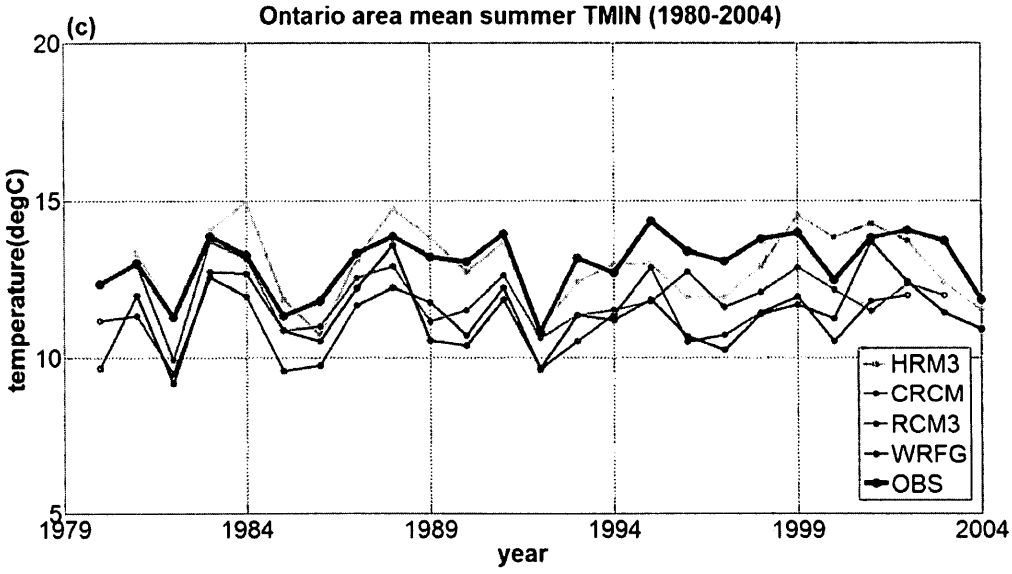
(c)
Ontario area mean summer TMIN (1980-2004)
temperature(degC)
year
HRM3
CRCM
RCM3
WRFG
OBS

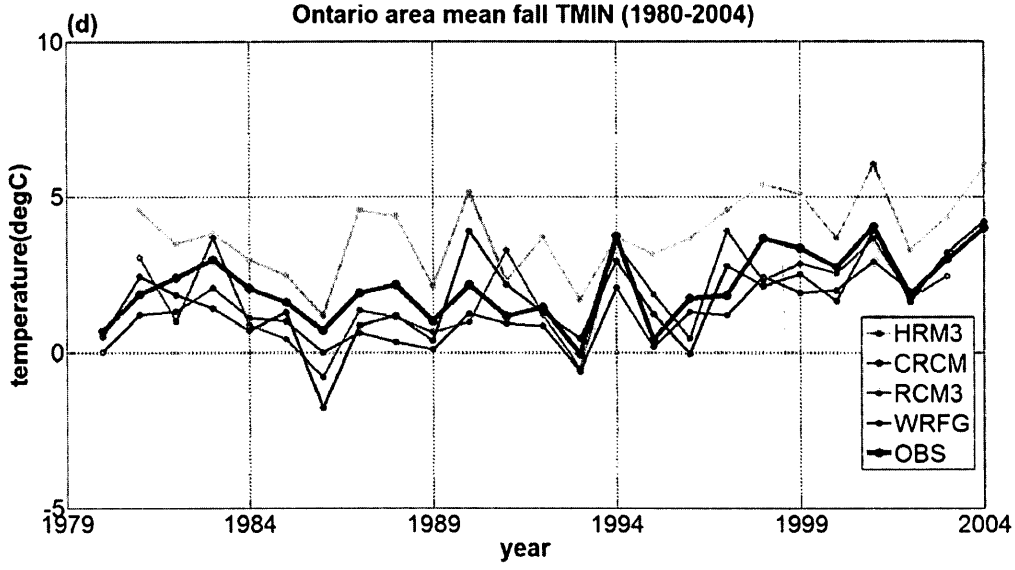
(d)
Ontario area mean fall TMIN (1980-2004)
temperature(degC)
year
HRM3
CRCM
RCM3
WRFG
OBS

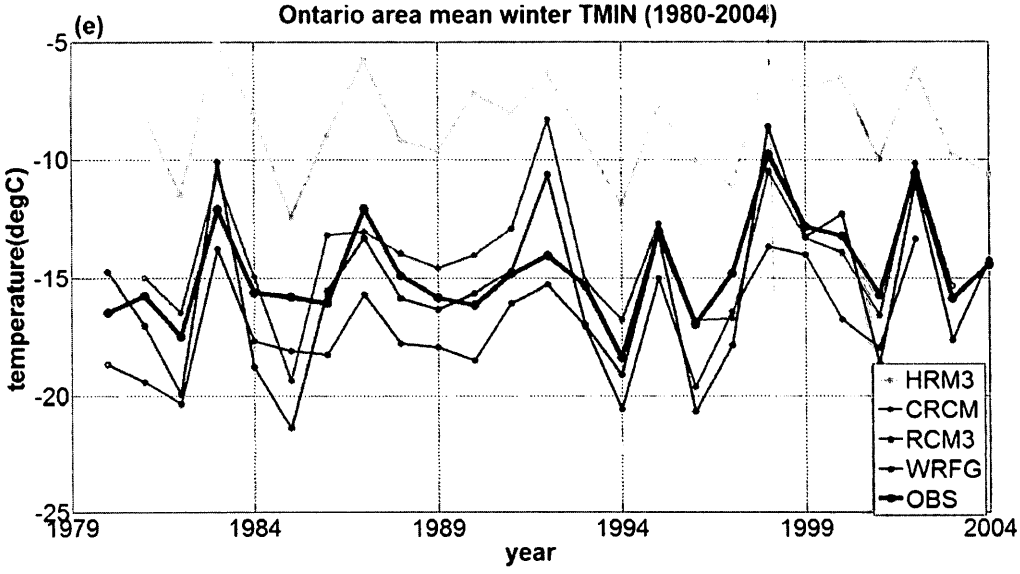

Figure 3. 14: Ontario 8-station mean minimum temperature time series of observations and four model data (unit: degC). The red line represents observation data. (a) Ontario annual area mean minimum temperature, (b) Ontario spring area mean minimum temperature, (c) Ontario summer area mean minimum temperature, (d) Ontario fall area mean minimum temperature, (e) Ontario winter area mean minimum temperature.

3.3 Precipitation analysis

3.3.1 Time series

The time series of 8-station mean precipitation is shown below in Fig. 3.15, for (a) annual, (b) spring, (c) summer, (d) fall and (e) winter. Some models including ECPC, ECP2, RCM3 reveal an obviously higher precipitation amount during this period. The high biases in ECPC and ECP2 appear in both winter and summer seasons, while the winter precipitation of RCM3 remains close to the observations. The annual precipitation amounts of the rest models stay close to the

observations. Summer precipitation processes, in particular convective precipitation, cannot be well resolved by the models. However, winter precipitation is mainly caused by synoptic systems and less by convection. In later sections, winter precipitation (dry and wet years) will be discussed. Compared with the temperature series, the precipitation discrepancies between the observations and the model results are much greater than those of the temperature.

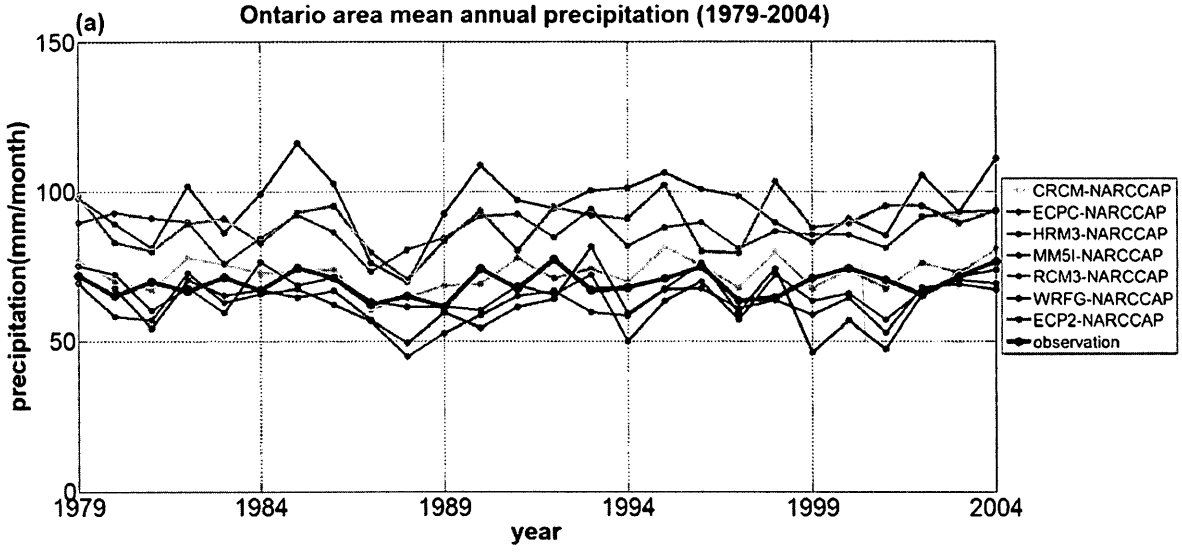

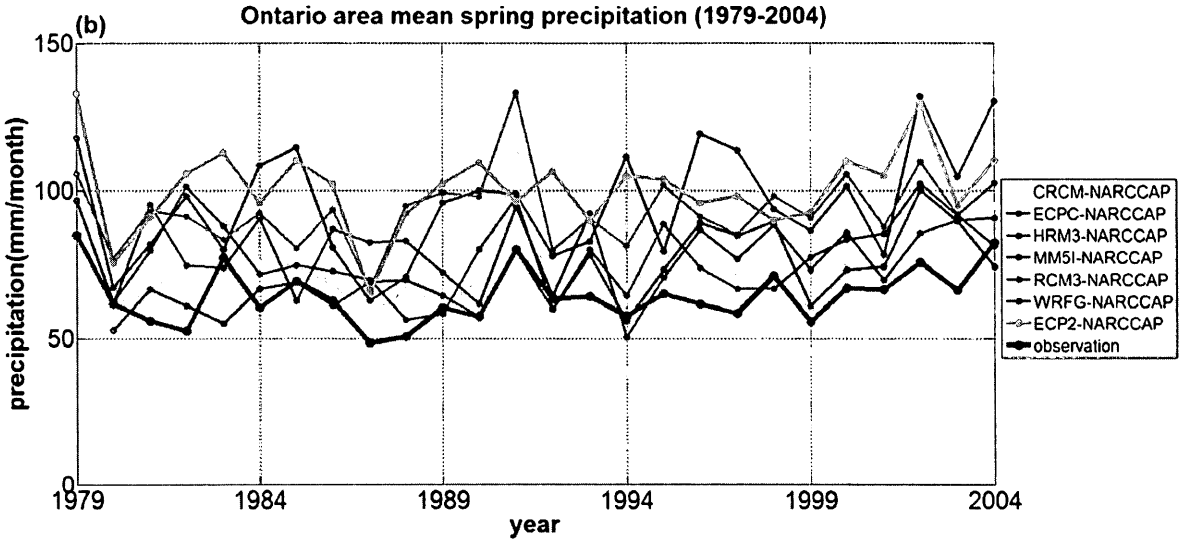
(b)
Ontario area mean spring precipitation (1979-2004)
precipitation(mm/month)
year
CRCM-NARCCAP
ECPC-NARCCAP
HRM3-NARCCAP
MM5I-NARCCAP
RCM3-NARCCAP
WRFG-NARCCAP
ECP2-NARCCAP
observation

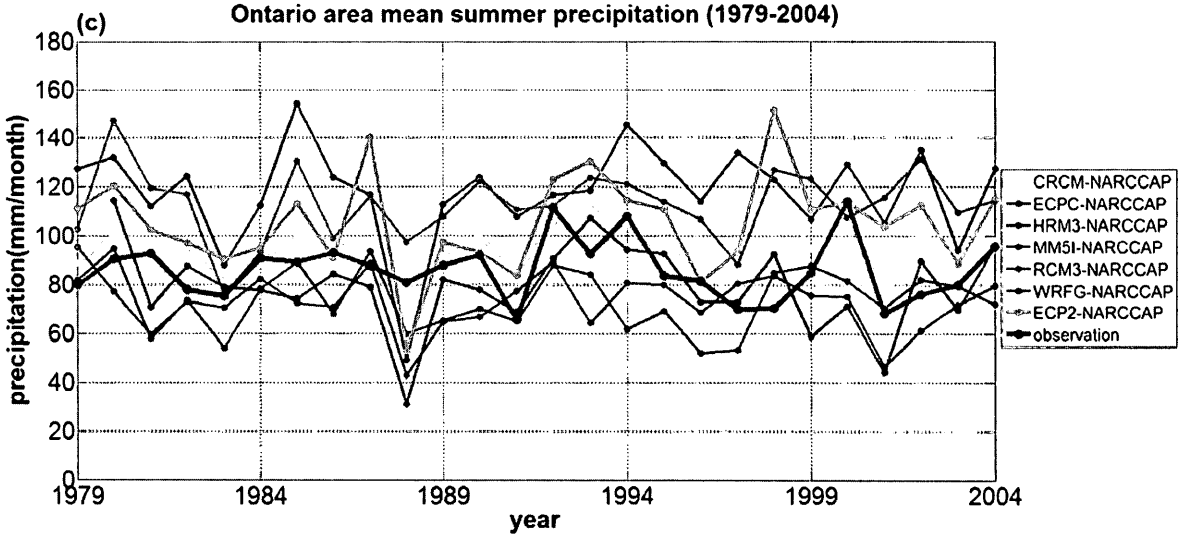
(c)
Ontario area mean summer precipitation (1979-2004)
precipitation(mm/month)
year
CRCM-NARCCAP
ECPC-NARCCAP
HRM3-NARCCAP
MM5I-NARCCAP
RCM3-NARCCAP
WRFG-NARCCAP
ECP2-NARCCAP
observation

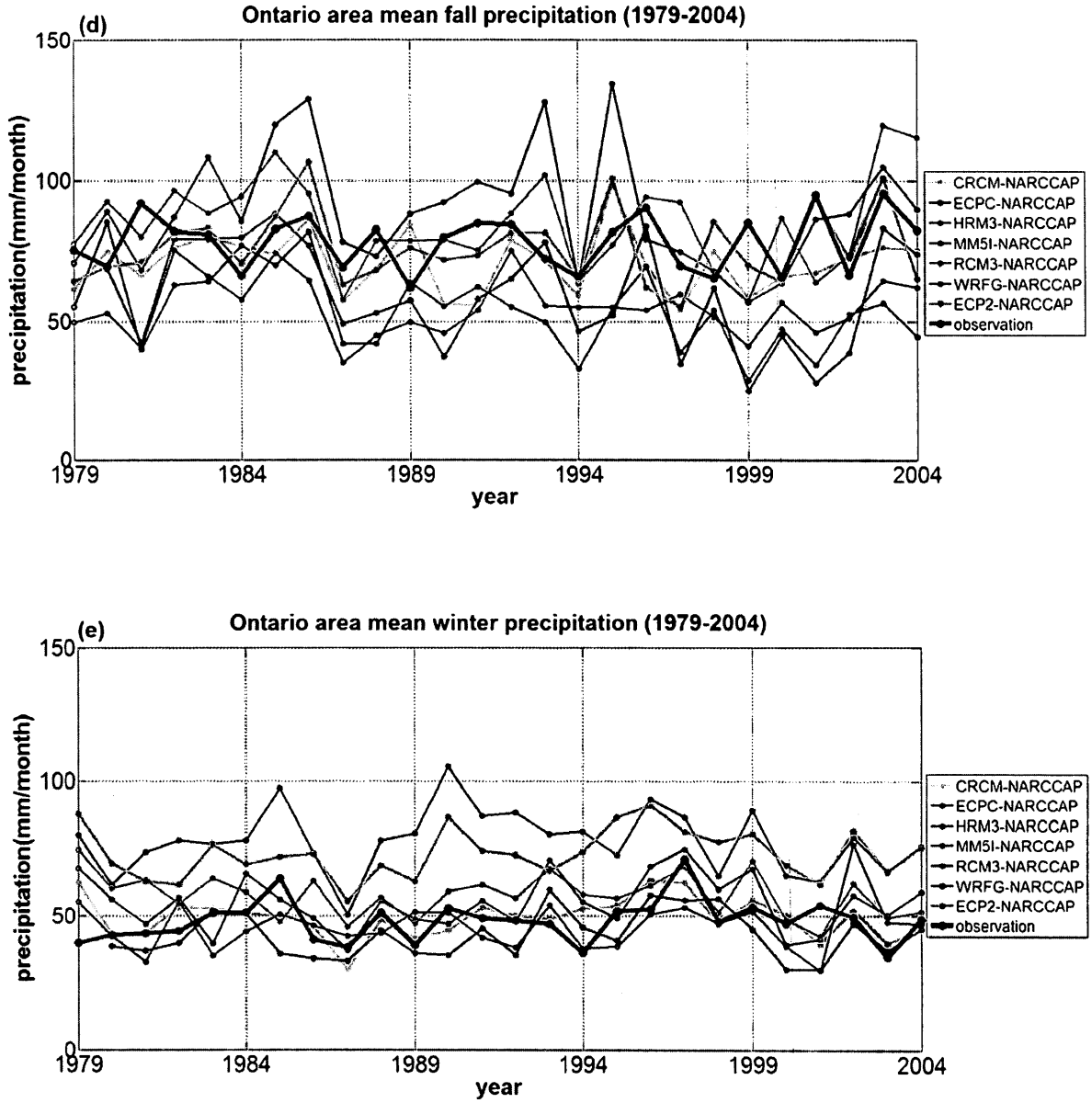

Figure 3. 15: Observed and model simulated time series of 8-station mean precipitation in Ontario (mm month^{-1}). For (a) annual precipitation, (b) spring precipitation, (c) summer precipitation, (d) fall precipitation, (e) winter precipitation. The red line represents observation data.

The 9-point temporal smoothing average was used to identify precipitation anomalies (Fig. 3.16). The annual precipitation remains at a stable level during the chosen period. The dry period is

from middle 1980s to early 1990s, while some moist years are in late 1970s and middle 1990s. But with a sudden rise from 2000, the precipitation increases to its peak in 2004, which is mostly related to the increase in spring and summer (Fig. 3.16 b and c).

For the smoothed precipitation trend, there are similarities in the peaks and valleys of the model data and the observations. The precipitation variations are more stable than those of temperature. WRFG and ECPC reveal different peaks from the observations at 1995 and different valleys at around 2001 and 2002, according to the annual precipitation (Fig. 3.16 a). In spring, WRFG and ECPC have a high precipitation period in the mid 1990s, while the observations and other models do not show this wet period. For the summer case, the valleys of the model data match the observations in late 1980s but with different precipitation amounts. The fall observed precipitation always has smaller quantity than the model precipitation, except ECPC and RCM3. For the winter case, all the models show an obvious peak in middle 1990s and match the observations. In the last year (2004), the only two models which show the similar decreasing precipitation tendency to the observations are ECPC and ECP2.

The standardization analysis of the observed precipitation is show in Fig. 3.17. This figure shows the linear trend of the observed precipitation using the least-square method. It can be seen clearly that the area mean precipitation indeed varies at a very stable level, since that the linear trend of the annual precipitation is almost a horizontal line. There is a slight decreasing tendency in summer precipitation amount and a moderate increasing trend in precipitation amounts in the other three seasons. In the mid 1990s, the annual precipitation depicts a wet period and this is mainly due to the high precipitation in summer. Dry years occur in the late 1980s and the late 1990s. Spring contributes the most to the 1980s dry years. Although in the late 1990s, the

precipitation in winter is relatively high, the other three seasons contribute more negatively leading to a dry period of the annual precipitation.

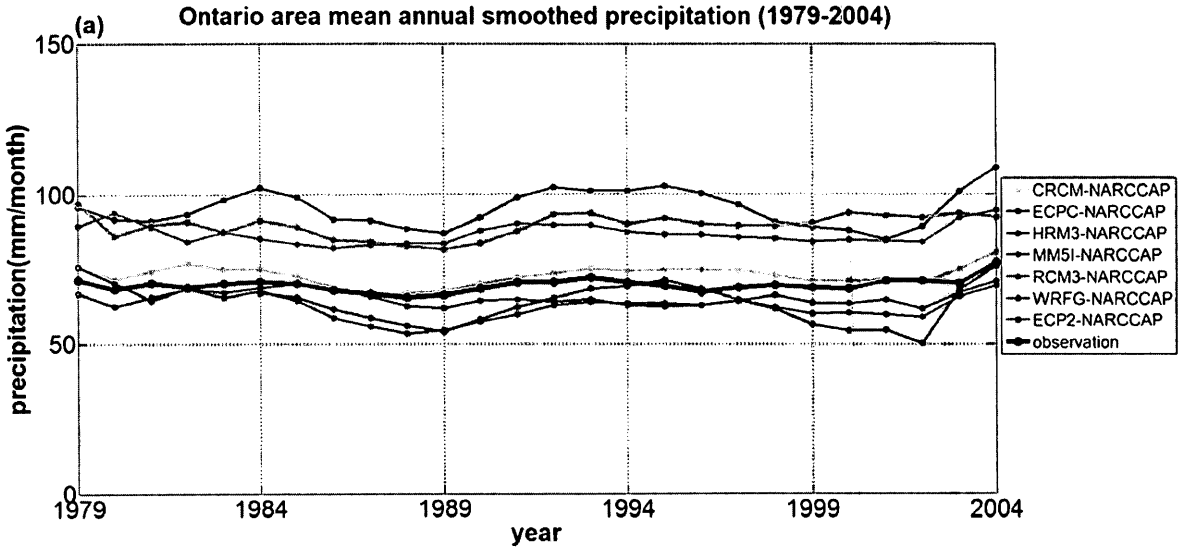

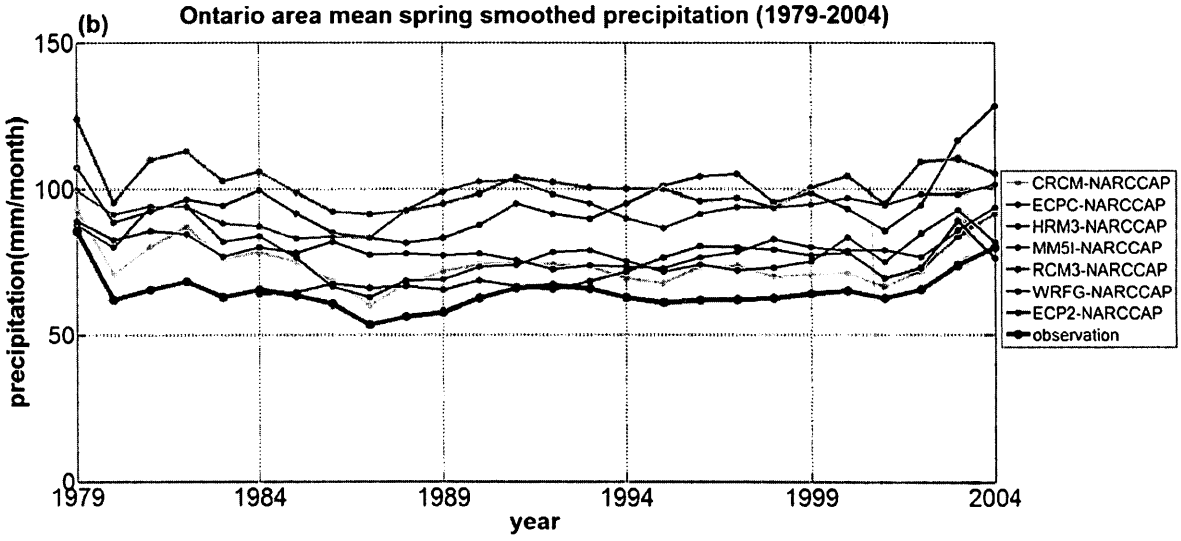

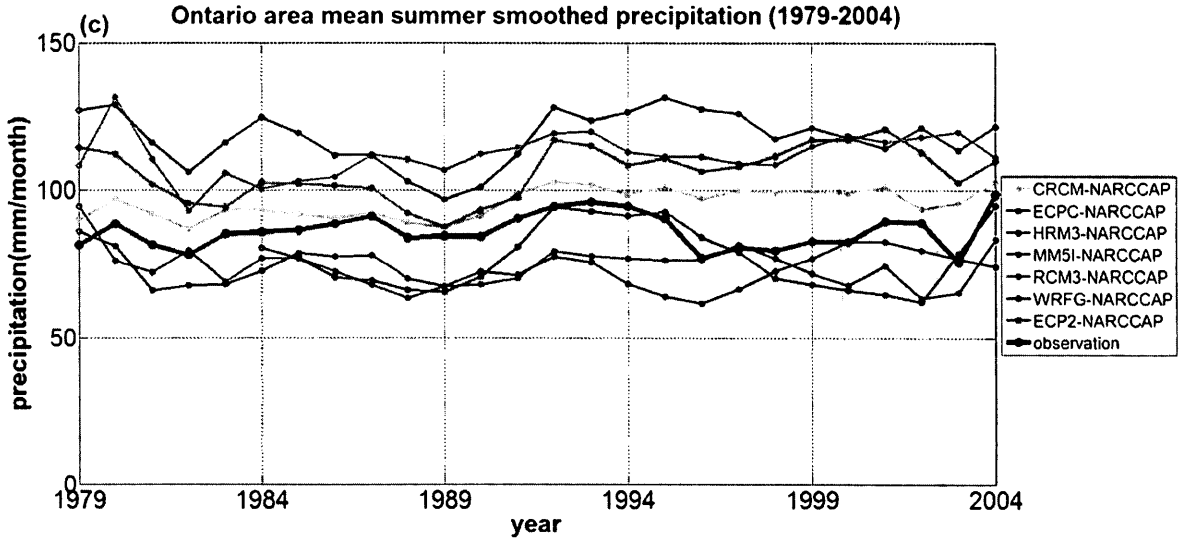
(c)
Ontario area mean summer smoothed precipitation (1979-2004)
precipitation(mm/month)
150
100
50
0
1979
1984
1989
1994
1999
2004
year
CRCM-NARCCAP
ECPC-NARCCAP
HRM3-NARCCAP
MM5I-NARCCAP
RCM3-NARCCAP
WRFG-NARCCAP
ECP2-NARCCAP
observation

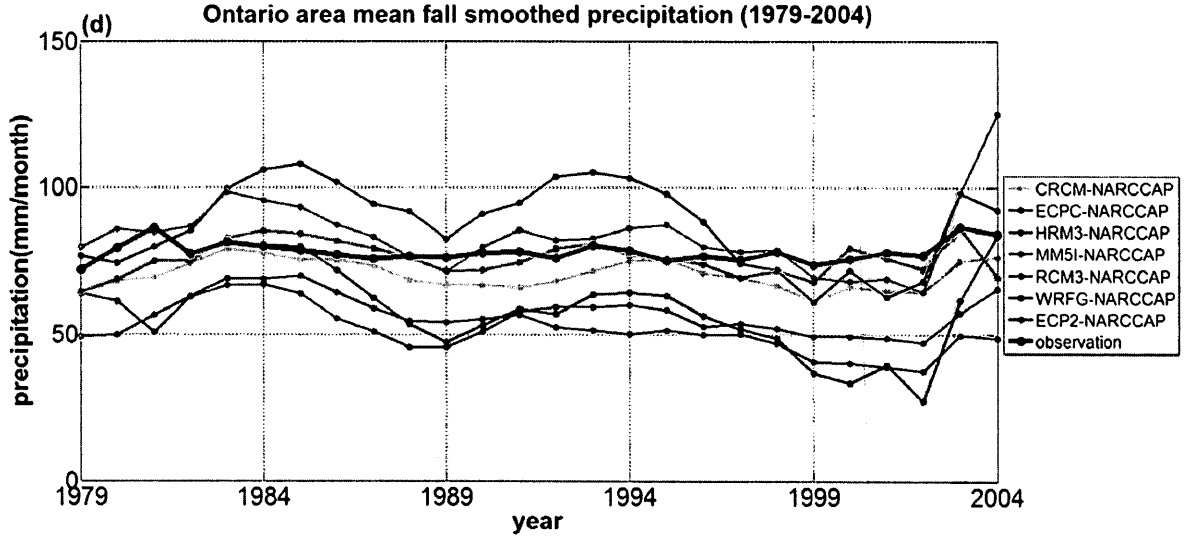
(d)
Ontario area mean fall smoothed precipitation (1979-2004)
precipitation(mm/month)
150
100
50
0
1979
1984
1989
1994
1999
2004
year
CRCM-NARCCAP
ECPC-NARCCAP
HRM3-NARCCAP
MM5I-NARCCAP
RCM3-NARCCAP
WRFG-NARCCAP
ECP2-NARCCAP
observation

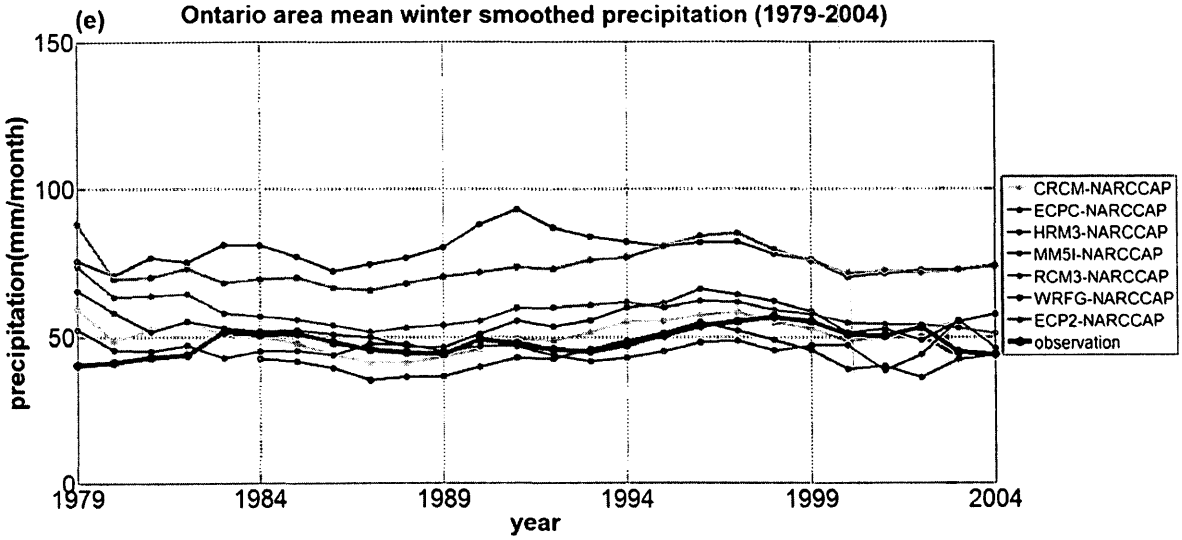

Figure 3. 16: Observed and model simulated time series of 8-station mean precipitation in Ontario (after 9-point smooth average) (mm month^{-1}). For (a) annual precipitation, (b) spring precipitation, (c) summer precipitation, (d) fall precipitation, (e) winter precipitation. The red line represents observation data.

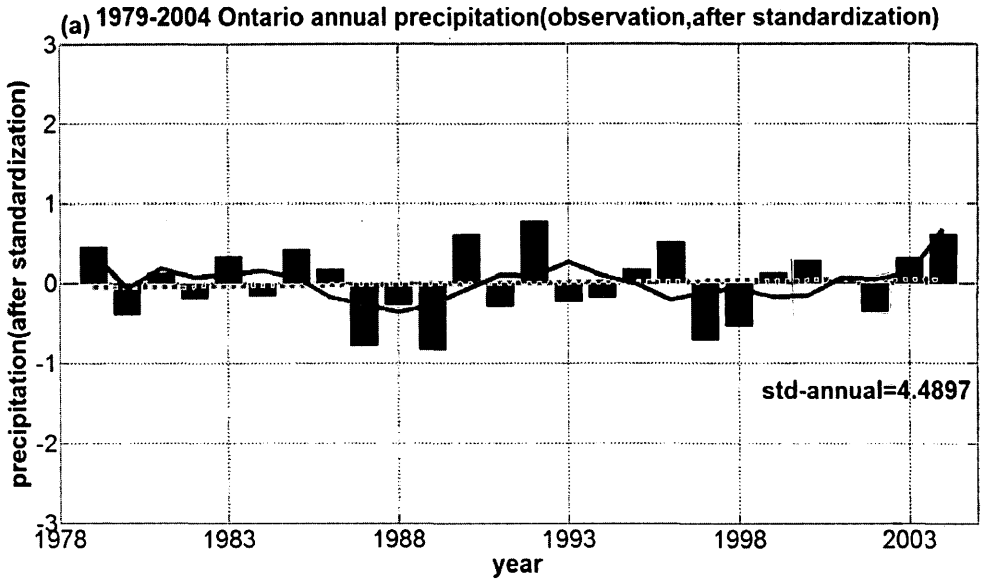

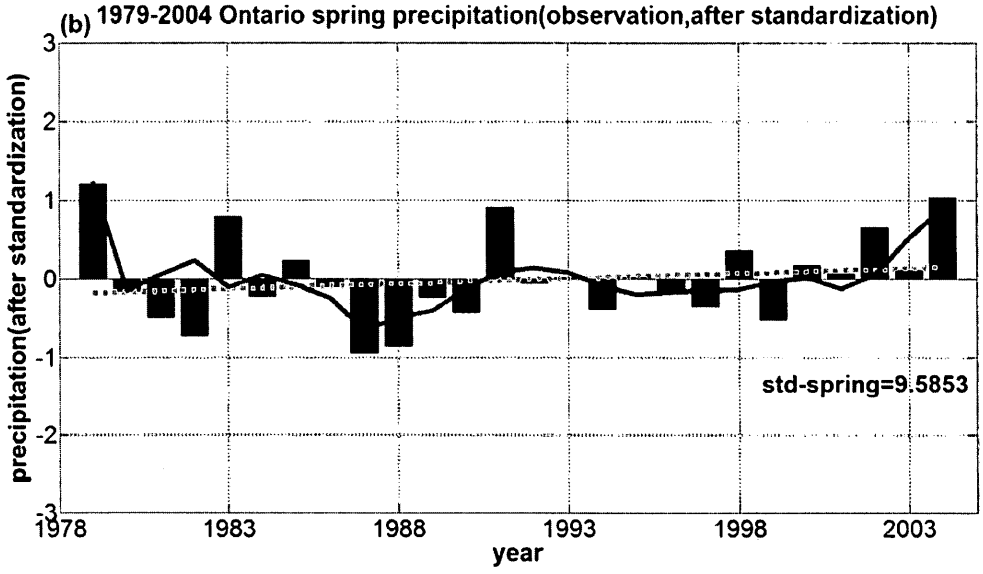
(b) 1979-2004 Ontario spring precipitation(observation,after standardization)
precipitation(after standardization)
year
std-spring=9.5853
3
2
1
0
-1
-2
-3
1978
1983
1988
1993
1998
2003

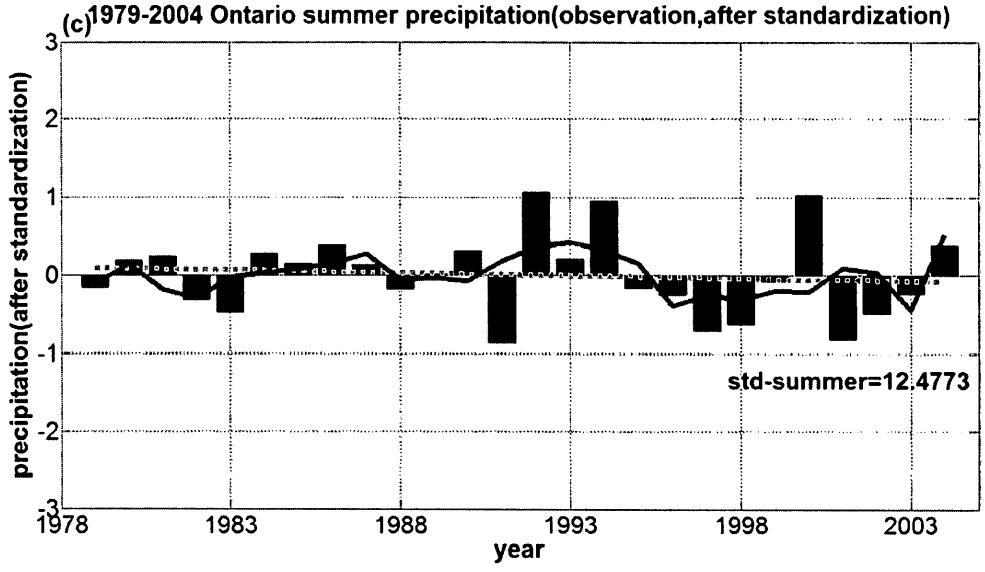
(c)1979-2004 Ontario summer precipitation(observation,after standardization)
precipitation(after standardization)
year
std-summer=12.4773
3
2
1
0
-1
-2
-3
1978
1983
1988
1993
1998
2003

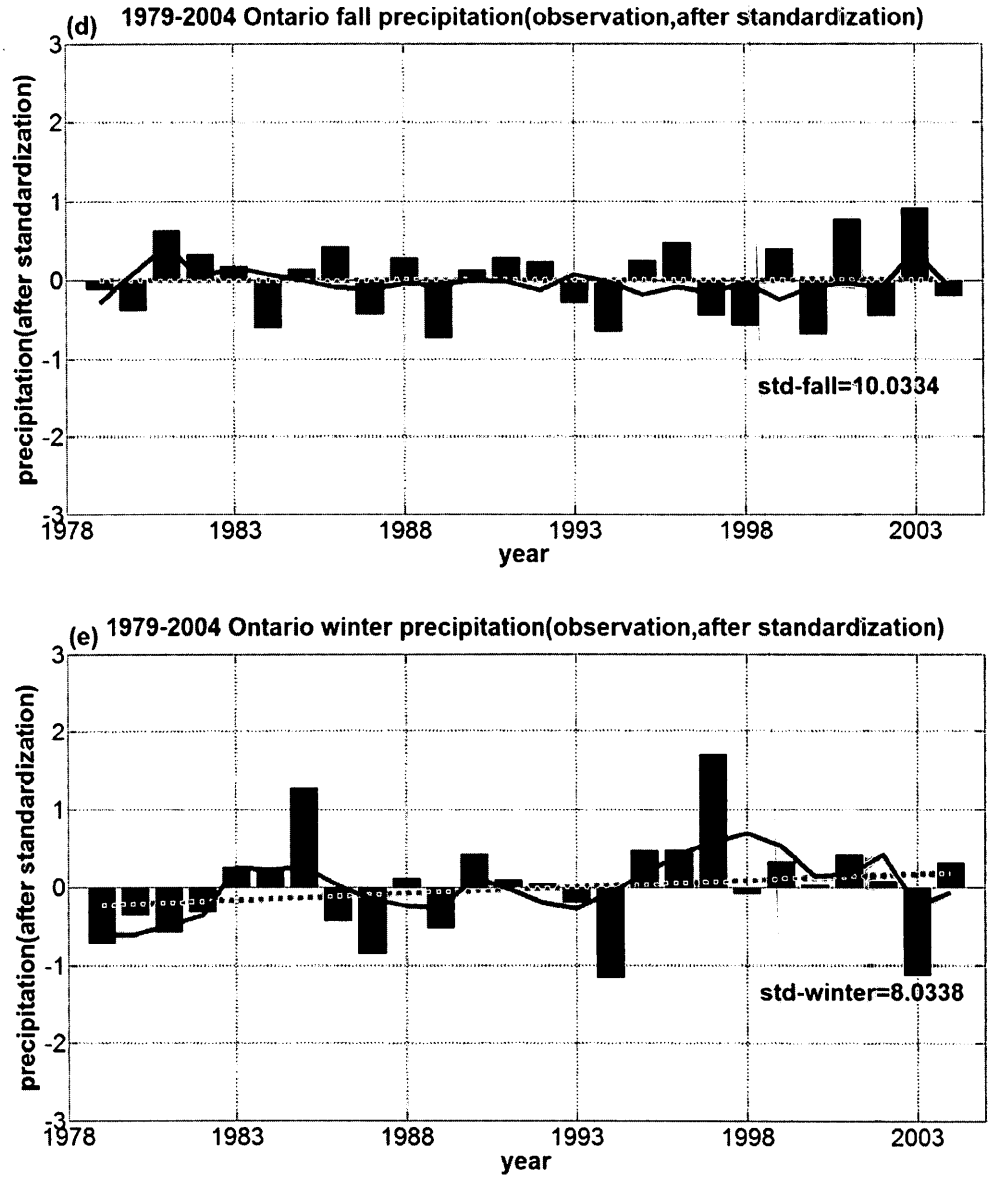

Figure 3. 17: Standardized time series of the 8-station mean precipitation observation in Ontario (unitless). For (a) annual precipitation, (b) spring precipitation, (c) summer precipitation, (d) fall precipitation, (e) winter precipitation. (Linear trend is in green dash line. Low frequency variation is in red).

Table 3. 3: Extremely dry and wet summer and winter as defined as precipitation anomalies in excess of ±1.

	Extremely dry(P_{std}<-1)	Extremely wet (P_{std}> 1)
Years(summer)		1992,2000
Years(winter)	1994,2003	1985,1997

Similarly, we can define extremely dry and wet year/season if its anomaly exceeds one standard deviation. Compared with extremely cold and warm events, the number of extremely dry and wet events is smaller. Altogether there are only 6 years reaching the standard (Table 3.3), which reveals that the precipitation variation during this period is more stable than that of temperature.

Although the precipitation variability is not as significant as temperature variability, there are still some extremely dry and wet winters which are shown in Fig. 3.17 (e). Since the summer precipitation processes are mainly due to unresolved convections, the analysis to discuss the reason why there are dry or wet seasons are applied to winters. In winter, there is a positive precipitation anomaly in middle 1980s and late 1990s, while a negative anomaly during late 1970s, early 1980s, late 1980s and early 1990s.

The NCEP-DOE reanalysis II data were used to study the factors contributing to the extremely dry and wet winters in Appendix B. The favorable conditions to form a wet winter include anomalous southerly wind, sufficient moisture and a large scale upward motion lifting moisture to high levels.

3.3.2 Spectral analysis

The periodicities of annual, summer and winter precipitation during 1980 to 2004 were analyzed similarly as those for the temperature. For annual mean precipitation (Fig. 3.18), the most significant period is 2.1-year and the second most significant one is 4.3 years. Unlike the temperature periodicity, different models show quite different precipitation periodicities, which also suggested the predictability of precipitation is low. WRFG, CRCM and RCM3 reflect a dominant 13-year period in their annual precipitation. ECPC, HRM3 and MM5I all show a 6.5-year period. Compared to the observations, the same 2.1-year period is shown only in WRFG, CRCM and MM5I. The 4.3-year period only presents in RCM3.

In summer (Fig. 3.19), the observed data has its most significant period of 6.5 years, with the second most significant period of 3.7 years. CRCM, ECPC2, HRM3 and MM5I all have this period as their most significant period in their summer precipitation variations. Some different periods appear in WRFG (13 years), ECPC (5.2 years) and RCM3 (4.3 years).

In winter (Fig. 3.20), discrepancies still exist among the observations and the model data. The observations show a 2.1-year period as its most significant period, which is the same as the annual precipitation variation. But in fact, none of the seven models precipitation variations show such period. The discrepancies among the periodicities of winter precipitation of seven model data are much greater than those of summer and annual precipitation. The only two similar periods is a 13-year period in WRFG and CRCM, and 6.5-year period in ECPC and ECP2. HRM3 and MM5I both show a 2.8-year period, but with different weights.

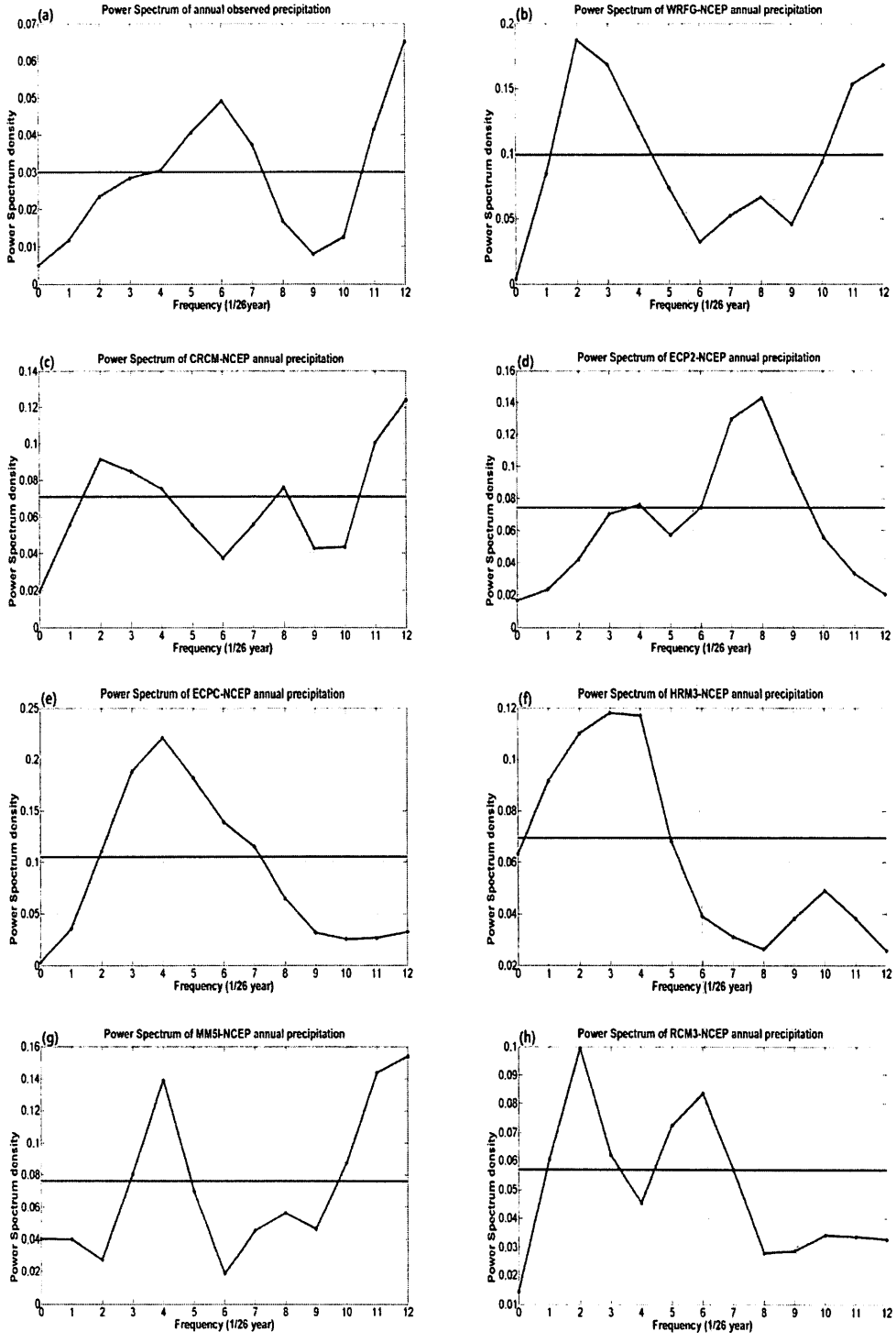

Figure 3. 18: Power spectra of annual precipitation in Ontario in observations and seven NARCCAP simulations. (a) Observation, (b) WRFG, (c) CRCM, (d) ECP2, (e) ECPC, (f) HRM3, (g) MM5I, (h) RCM3 (The x-axis is frequency (1/26 year^{-1}) and the y-axis is the power spectrum ((mm month^{-1})^2 year)).

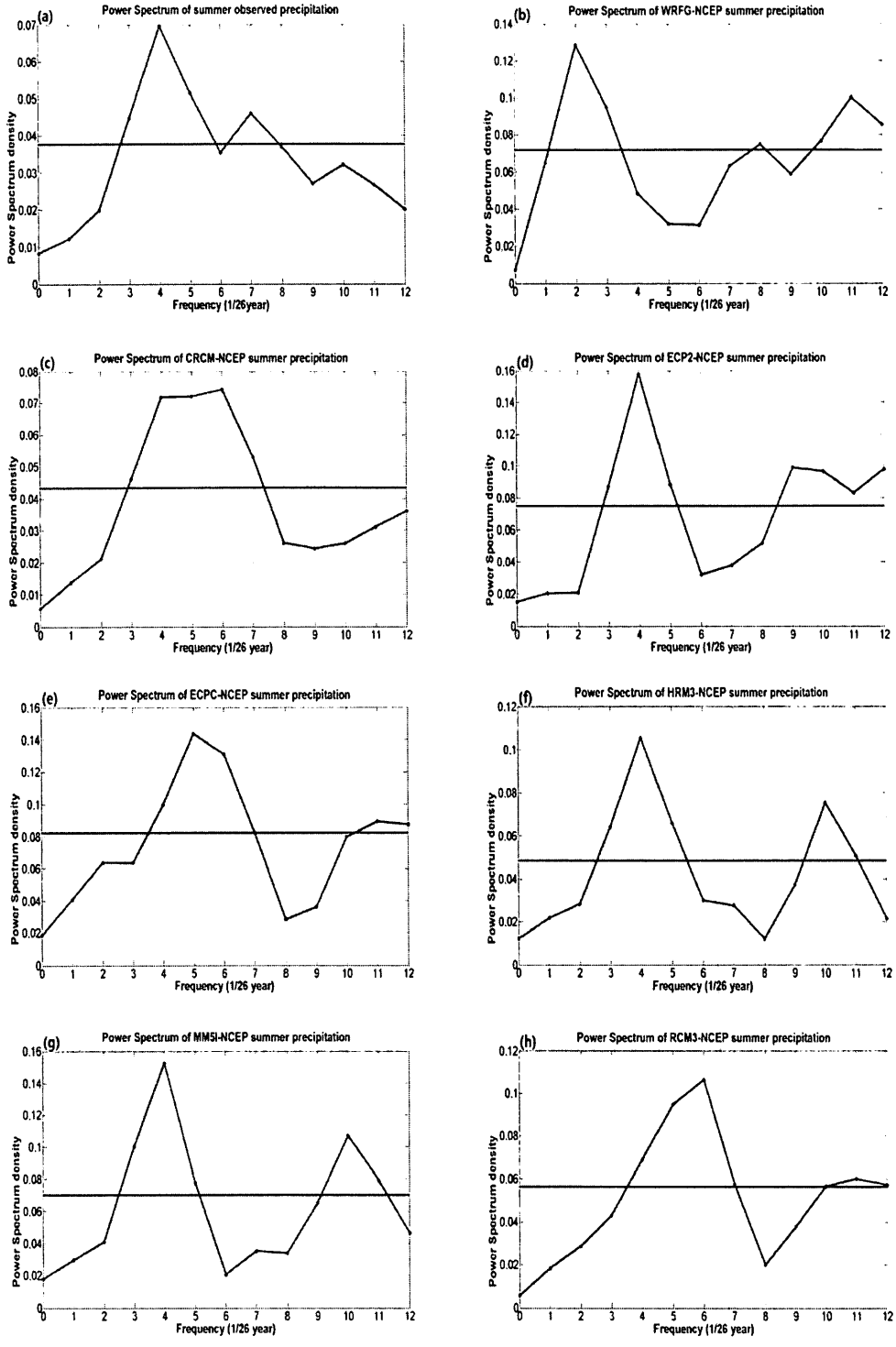

Figure 3. 19: Power spectra of summer precipitation in Ontario in observations and seven NARCCAP simulations. (a) observation, (b) WRFG, (c) CRCM, (d) ECP2, (e) ECPC, (f) HRM3, (g) MM5I, (h) RCM3 (The x-axis is frequency (1/26 year^{-1}) and the y-axis is the power spectrum ((mm month^{-1})^2 year).

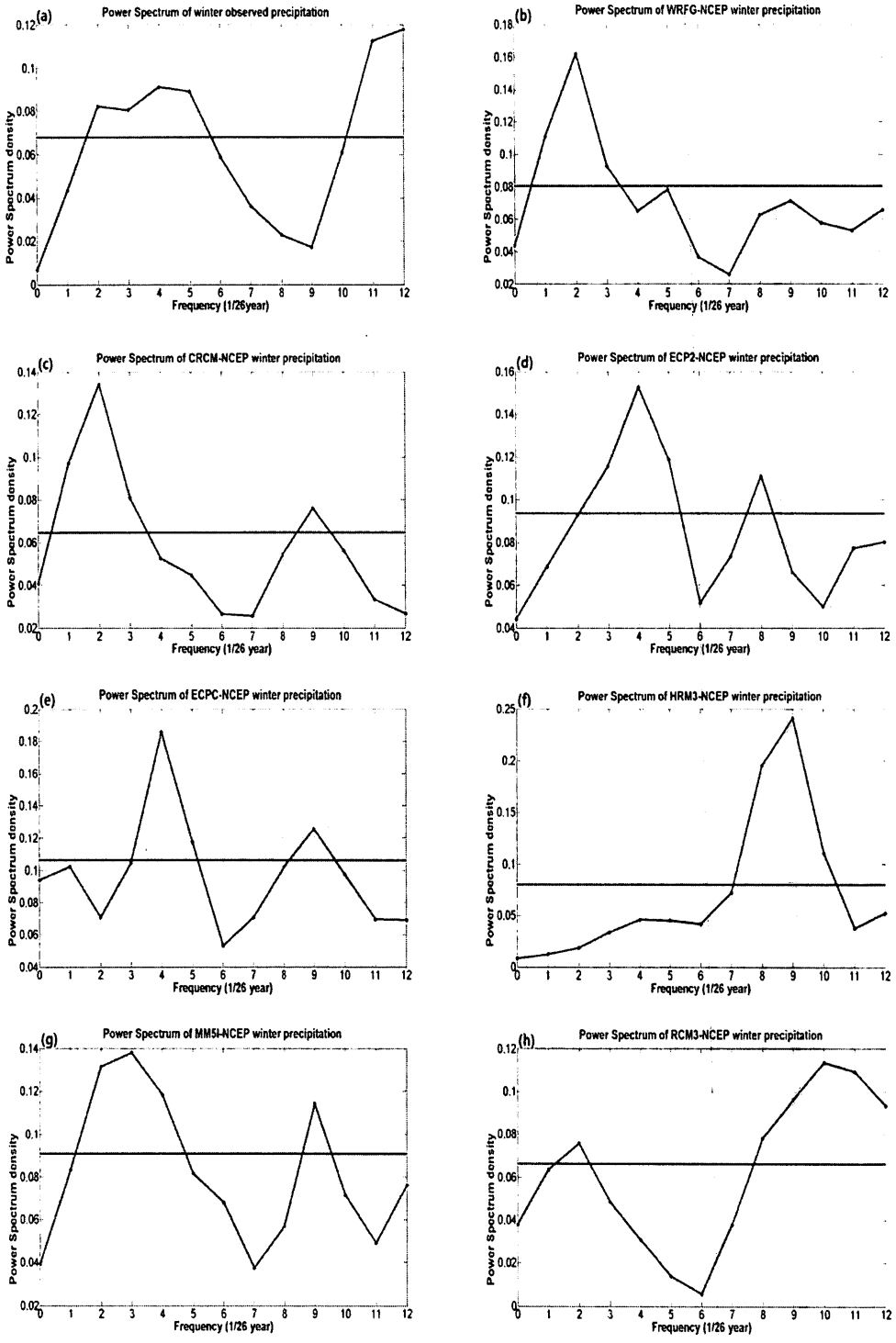

Figure 3. 20: Power spectra of winter precipitation in Ontario in observations and seven NARCCAP simulations. (a) observation, (b) WRFG, (c) CRCM, (d) ECP2, (e) ECPC, (f) HRM3, (g) MM5I, (h) RCM3 (The x-axis is frequency (1/26 year^{-1}) and the y-axis is the power spectrum ((mm month^{-1})^2 year).

3.4 Trend validation

Since the 25-year period (1980-2004) is relatively short to have reliable climatological trend analysis, it is necessary to validate the trends of both temperature and precipitation during 1980 and 2004. As described in OURANOS' report (Bourdages and Huard, 2010), last 5 years of the entire period is removed to get a subsample to validate the trends.

Fig. 3.21 portrays the time series of mean annual temperature, summer temperature and winter temperature, taken from the 8-station mean time series. Figure 3.22 shows the time series of the mean annual precipitation, summer precipitation and winter precipitation.

All the time series are indicated in 2 different colors: the red lines represent the 1980-2004 time period, whereas the black dash-dot lines cover the 1980-1999 period. Table 3.4 summarizes the comparison of the mean and trends of temperature and precipitation, calculatedfirst with the 1980-2004 dataset and the subsample without the last 5 years (1980 to 1999). In this particular case, removing the last 5 years of dataset results in all most identical increasing or decreasing trend of both temperature and precipitation.

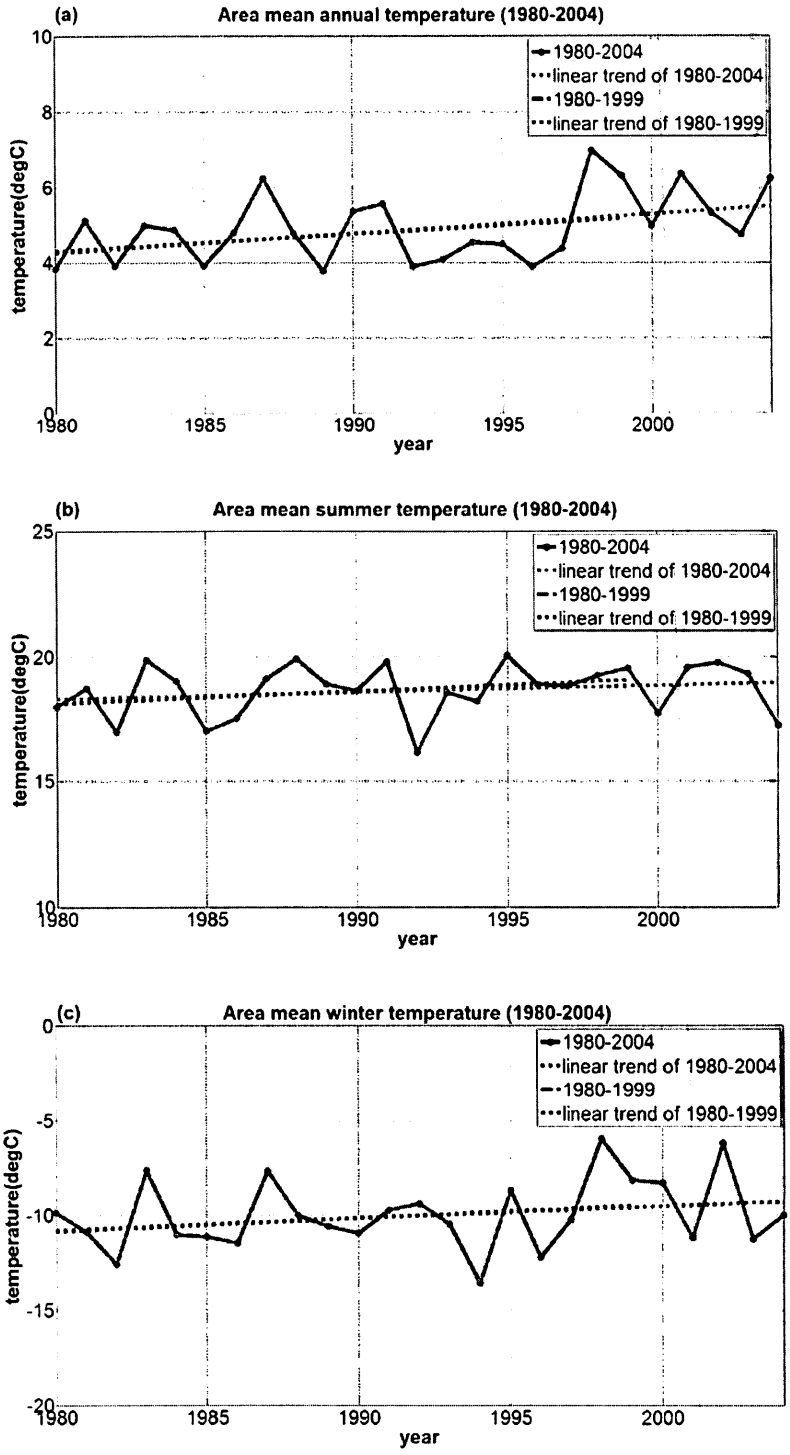

Figure 3. 21: The time series of the 8-station mean temperature. (a) Annual temperature, (b) summer temperature and (c) winter temperature. Two periods are shown in the figures: 1980-2004 in red and 1980-1999 in black dash-dot line.

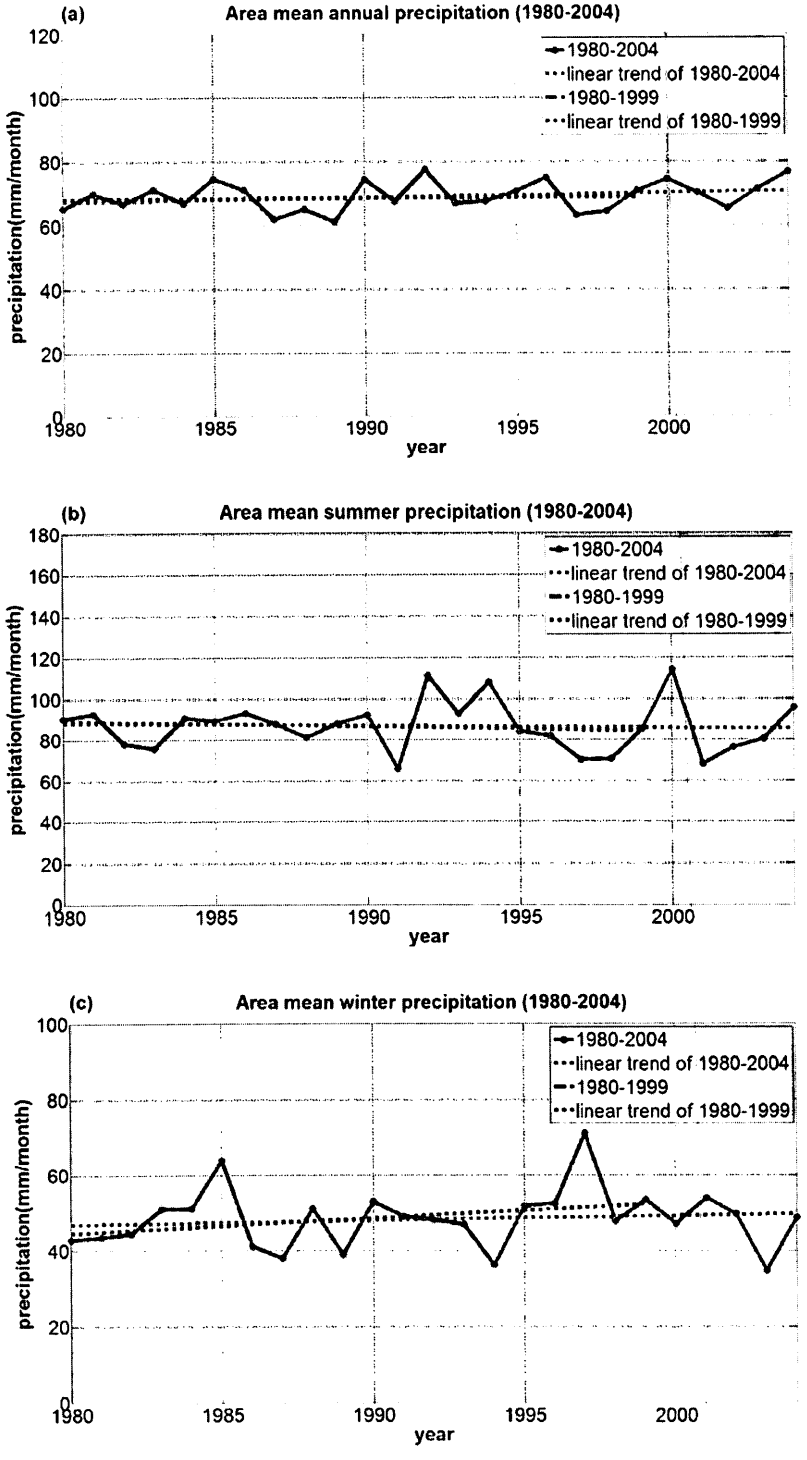

Figure 3. 22: The time series of the 8-station mean precipitation. (a) Annual precipitation, (b) summer precipitation and (c) winter precipitation. Two periods are shown in the figures: 1980-2004 in red and 1980-1999 in black dash-dot line.

Table 3. 4: Comparison of mean and trends of annual, summer and winter mean temperature (and precipitation), for the domain area mean, using a dataset covering the 1980-2004 and 1980-1999 periods (shown in Figure and Figure). Differences are presented with respect to the 25-year period (1980-2004).

	Annual:1980-1999	Annual:1980-2004	%difference
Mean T	4.79°C	4.94°C	3.04%
Trend T	4.37°C $(100year)^{-1}$	5.06°C$(100year)^{-1}$	13.64%
Mean P	68.65mm $month^{-1}$	69.26 mm $month^{-1}$	0.88%
Trend P	3.36mm $month^{-1}$ $(100year)^{-1}$	13. mm $month^{-1}$ $(100year)^{-1}$	74.87%

	Winter:1980-1999	Winter:1980-2004	%difference
Mean T	-10.11°C	-9.97°C	1.40%
Trend T	6.91°C$(100year)^{-1}$	6.01°C$(100year)^{-1}$	-14.98%
Mean P	48.86 mm $month^{-1}$	48.46 mm $month^{-1}$	-0.83%
Trend P	39.56 mm $month^{-1}$ $(100year)^{-1}$	11.63 mm $month^{-1}$ $(100year)^{-1}$	-240.15%

	Summer:1980-1999	Summer:1980-2004	%difference
Mean T	18.65°C	18.67°C	0.11%
Trend T	4.81°C$(100year)^{-1}$	2.64°C$(100year)^{-1}$	-82.20%
Mean P	86.32 mm $month^{-1}$	86.41 mm $month^{-1}$	0.10%
Trend P	-26.25 mm $month^{-1}$ $(100year)^{-1}$	-13.62 mm $month^{-1}$ $(100year)^{-1}$	-92.73%

3.5 Verification of CFSR data

Since the observations (only eight stations) did not cover the entire region of the WRF domain, CFSR data was selected to be compared with the WRF simulations which would be shown in the next chapter. CFSR is chosen because of its fine resolution (38km×38km) compared with NCEP-DOE (2.5°×2.5°). Before conducting the comparison between the WRF simulations and CFSR data, it is necessary to verify CFSR data. In this section, a brief comparison between CFSR data and the 8-station observations are shown.

The gridded CFSR data were first interpolated onto the eight stations. Then the mean temperature and precipitation over these eight stations were calculated and compared to the mean observed values. For the temperature, the winter mean series of the CFSR data is 3.17 degrees higher than the mean observation, while the summer mean series of the CFSR data is similar in magnitudes but with different slope of the linear trend. Overall, the annual temperature in CFSR is 1.52 degrees higher than the observations, mainly due to the warm bias in winter. Both of these series reveal an increasing trend from 1980 to 2004.

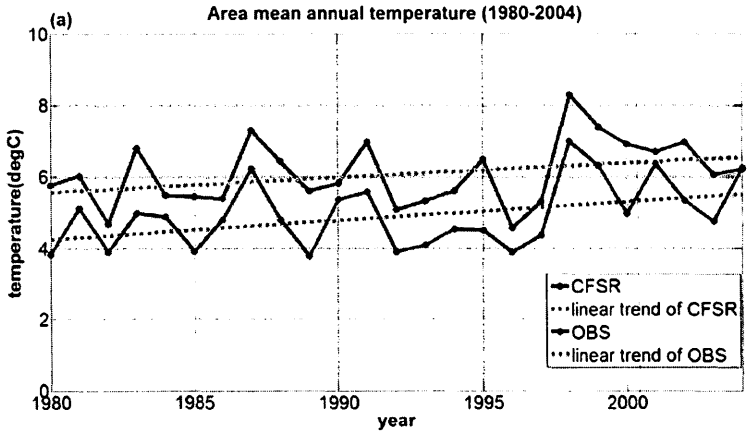

Correlation: 0.85

Y(CFSR)=0.0408X-75.1859

Y(OBS)=0.0527X-100.0986

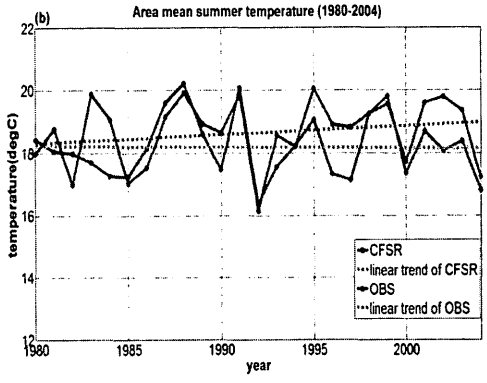

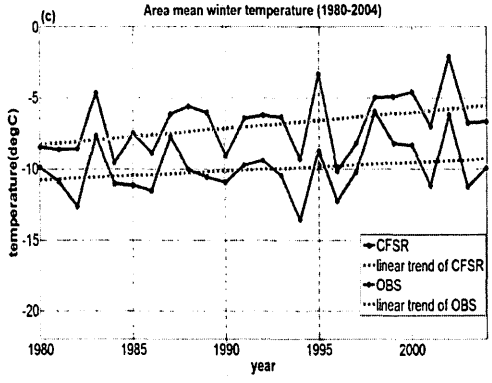

Correlation: 0.77

Y(CFSR)=-0.0033X+24.7368

Y(OBS)=0.0276X-36.2854

Correlation: 0.91

Y(CFSR)=0.1112X-228.2801

Y(OBS)=0.0626X-134.7139

Figure 3. 23: Verification of CFSR temperature data, compared to the observations, of 8-station mean. (a) Annual temperature, (b) summer temperature, and (c) winter temperature. Unit: °C.

Table 3. 5: The 8-station mean temperature between 1980 and 2004. Unit: °C.

	CFSR	Station data
Annual mean temperature	6.24	4.72
Summer mean temperature	18.2	18.67
Winter mean temperature	-6.79	-9.96

For precipitation, there is neither significant increasing nor decreasing trend during this period of 1980 and 2004. There is a +20.68 mm month^{-1} discrepancy between the CFSR and the observed winter precipitation, which contributes mostly to the differences in the annual precipitation (13.05 mm month^{-1} higher in CFSR). The amounts of summer precipitation in both the CFSR data and the observations are similar during the chosen period.

Moreover, there is a similarity in the correlations between the CFSR data and the observations of temperature and precipitation. The correlations of the temperature and precipitation in summer (0.77 and 0.67, respectively) are smaller than those in winter (0.91 and 0.92 respectively). For annual temperature and precipitation time series, the correlations are 0.85 and 0.82 respectively, whose values are between their summer and winter correlation values. All the correlations are at 90% confidence level.

Table 3. 6: The 8-station mean precipitation between 1980 and 2004. Unit: mm month^{-1}.

	CFSR	Station data
Annual mean precipitation	83.27	70.22
Summer mean precipitation	84.38	86.66
Winter mean precipitation	69.14	48.46

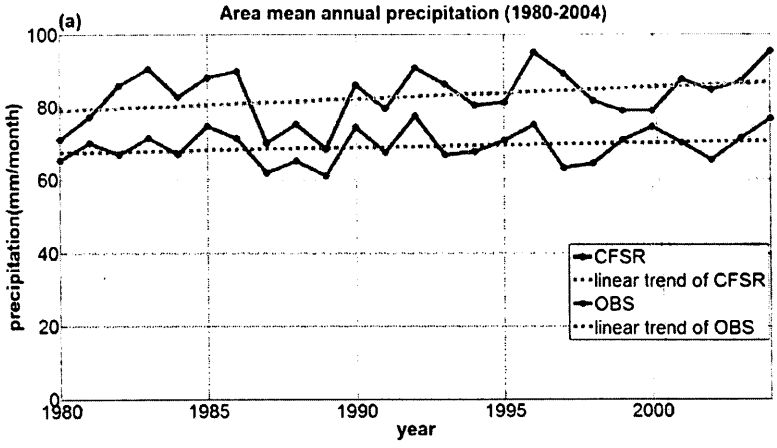

Correlation:0.82

Y(CFSR)=0.3305X-575

Y(OBS)=0.1392X-208.08

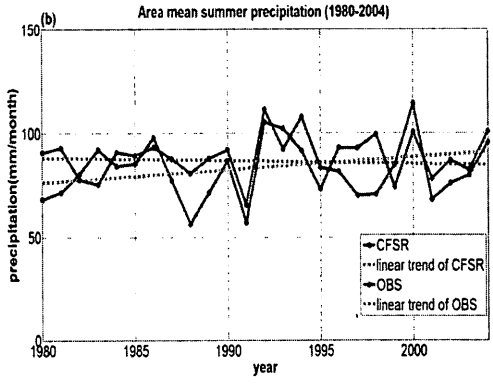

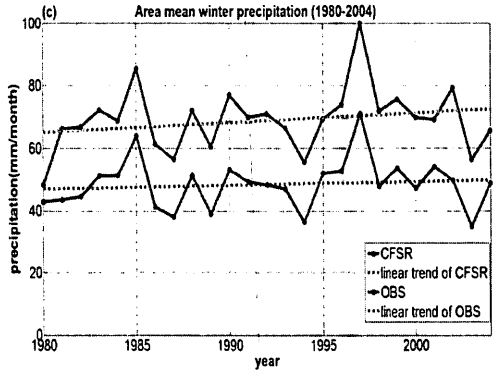

Correlation:0.67

Y(CFSR)=0.6149-1140

Y(OBS)=-0.1419+369.0

Correlation:0.92

Y(CFSR)=0.311X-550.3787

Y(OBS)=0.1211X-192.863

Figure 3. 24: Verification of CFSR precipitation data, compared to the observations, of 8-station mean. (a) Annual precipitation, (b) summer precipitation, and (c) winter precipitation. Unit: mm month^{-1}.

Chapter 4 Evaluation of the WRF Simulations

In this chapter, high-resolution simulations from January 1991 to December 1998 using the WRF model was conducted to see how well the downscaling simulation could improve the representation of the regional climate over Ontario. As in previous chapter, this chapter is divided into 2 main parts, the analyses of the temperature and the precipitation. When comparing the domain-averaged values, the domain average was obtained by averaging the values over the entire WRF model domain excluding the outer 15 points along each side of the lateral boundaries. The NARCCAP and CFSR data were first interpolated onto the same WRF model grid before the domain average were computed.

Instead of discussing individual downscaling simulations, we focused more on the discussions of two sets of ensembles. One is the 7-member NARCCAP ensemble, which consists 7 NARCCAP model data (CRCM, ECPC, ECP2, HRM3, RCM3, MM5I and WRFG). The other ensemble constitutes 5 members, which were the WRF downscaling simulations driven by 5 NARCCAP model data (CRCM, HRM3, RCM3, MM5I and WRFG). Incomplete datasets have prevented us to conduct simulations with the WRF model driven by ECPC and ECP2.

4.1 Temperature in the WRF simulations

The temperature variation in the WRF mode domain is analyzed in this section.

4.1.1 Time series

While containing a high degree of variability, the simulated annually averaged temperature show a warming trend with some slight fluctuates across the simulated 8 years between 1991 and 1998. Figure 4.1 shows the time series of the annual (Fig. 4.1 a) and the seasonal (Fig. 4.1 b-e) domain mean temperature from 1991 to 1998. In each panel, thick cyan, green and red lines represent the 7-member NARCCAP ensemble mean temperature, the CFSR temperature and the 5-member WRF simulation ensemble mean temperature, respectively. Each WRF simulation result and its corresponding driving NARCCAP data are plotted in the same color but the former is in solid line and the latter in dashed line. All annual temperatures reveal a significant increasing trend in the last two years. All the five WRF simulations with different initial and boundary conditions show relatively colder temperatures compared with their corresponding NARCCAP simulations. In general, the warmer the driving NARCCAP model is, the warmer the WRF downscaling simulation is. HRM3 produced the warmest area mean temperature, similar to its warmest 8-station mean temperature shown in previous chapter.

In winter, the NARCCAP ensemble mean has a warm bias while the WRF ensemble mean has a cold bias, compared to the CFSR data. Spring also portrays a similar bias, except the year 1992 and 1994. In summer, most of the WRF simulations reveal a temperature minimum in 1992, except the one driven by HRM3, which shows the temperature valley in 1993. The differences between model data (both NARCCAP ensemble mean and WRF ensemble mean) and the CFSR data are the smallest in summer among the four seasons. In fall, both NARCCAP ensemble and

the WRF simulation ensemble show a cold bias between 1991 and 1998. This is the only season in which both ensembles show a cold bias.

Among all the 4 seasons, spring and winter have the two most significant upward trends in the last two years of the period, i.e., 1997 and 1998, compared with the moderate increase in summer and fall. It is because that in high latitude areas, cold periods often last till March or April. And in this thesis, spring includes these two cold months by definition. So the trend of spring temperature follows the tendency of the winter temperature in the same year.

The mean of the annual and the four-season temperature from 1991 to 1998 are calculated in Table 4.1 to Table 4.5. According to the tables, the differences between the WRF ensemble mean and the CFSR data are greater than the differences between the NARCCAP ensemble mean and the CFSR data in fall and winter, the former becomes smaller in the other two seasons. However, it has been shown in the previous chapter, that the 8-station interpolated CFSR data is approximately 1~2 °C warmer than the station data in this period (c.f. Fig. 3.23). Due to this fact, it is believed that the differences between the WRF ensemble mean and the observations are smaller than the differences between the NARCCAP ensemble mean and the observations in general. We will verify it again shortly (c.f. Table 4.7).

Table 4.6 depicts the correlations and the root mean square errors (RMSE) between CFSR and each ensemble mean. The correlations are all significant at the 90% confidence level. According to the table, the correlation between CFSR and the WRF ensemble mean is greater than that between CFSR and the NARCCAP ensemble mean in spring, fall and in the annually averaged sense. Only in summer it has the opposite situation. Most of the RMSE between CFSR and the

WRF ensemble mean are smaller than those between CFSR and the NARCCAP ensemble mean. The only exception is the winter temperature. Overall, the WRF ensemble mean shows slight increase in correlations and reduction in RMSEs. Although the differences do not pass the 90% confidence test, it suggests the dynamic downscaling and ensemble simulations are at least promising in improving the temperature prediction in regional climate study.

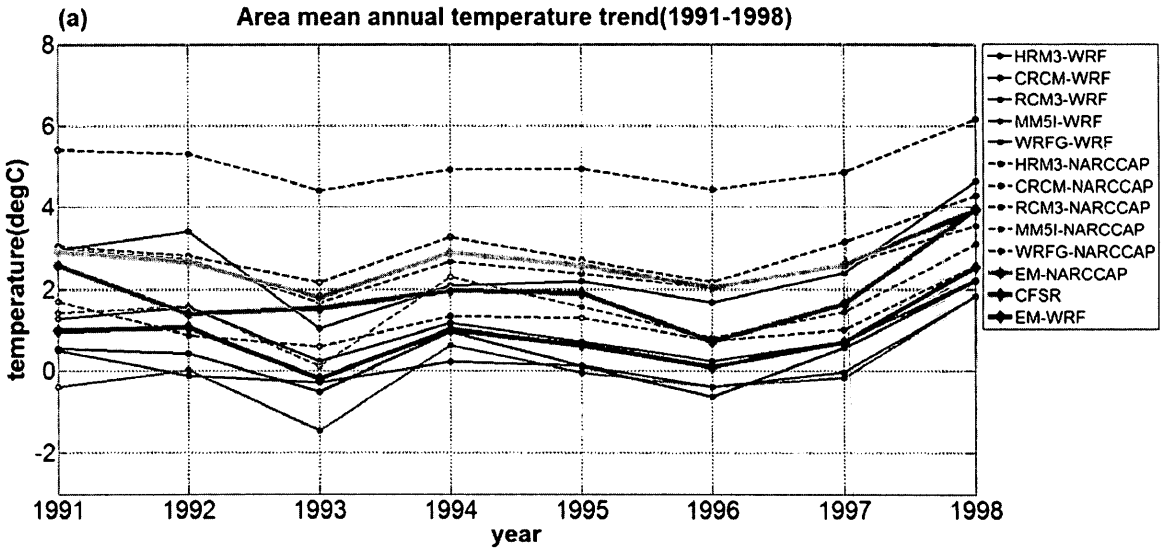

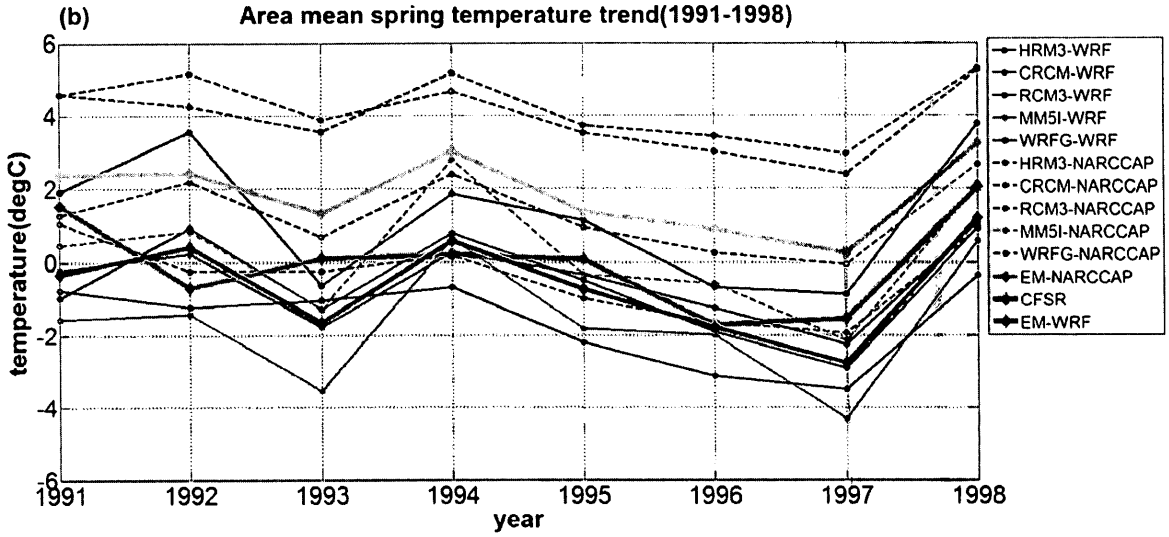
(b)
Area mean spring temperature trend(1991-1998)
temperature(degC)
year
HRM3-WRF
CRCM-WRF
RCM3-WRF
MM5I-WRF
WRFG-WRF
HRM3-NARCCAP
CRCM-NARCCAP
RCM3-NARCCAP
MM5I-NARCCAP
WRFG-NARCCAP
EM-NARCCAP
CFSR
EM-WRF

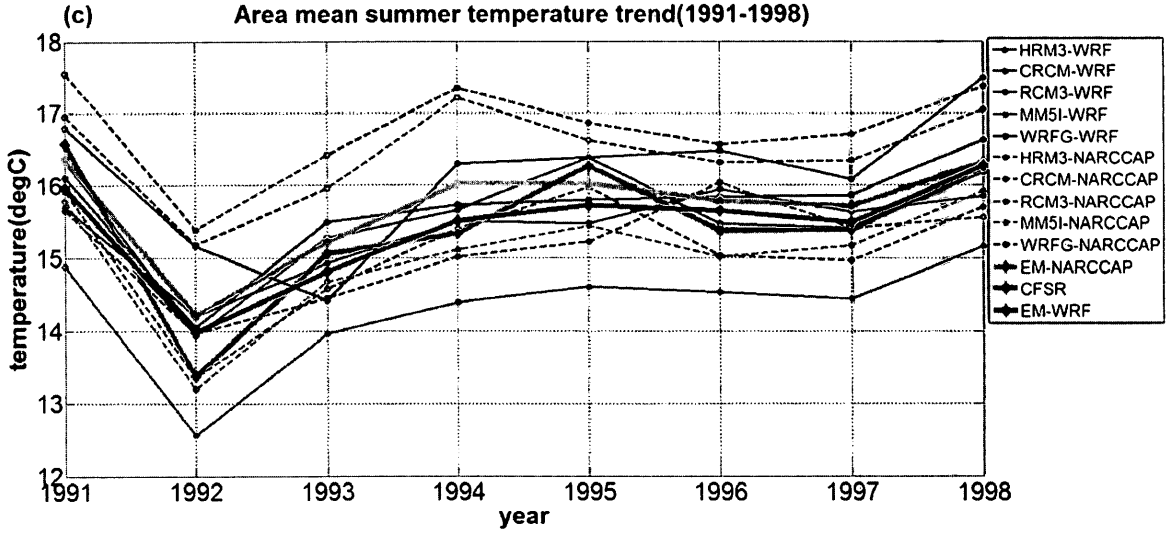
(c)
Area mean summer temperature trend(1991-1998)
temperature(degC)
year
HRM3-WRF
CRCM-WRF
RCM3-WRF
MM5I-WRF
WRFG-WRF
HRM3-NARCCAP
CRCM-NARCCAP
RCM3-NARCCAP
MM5I-NARCCAP
WRFG-NARCCAP
EM-NARCCAP
CFSR
EM-WRF

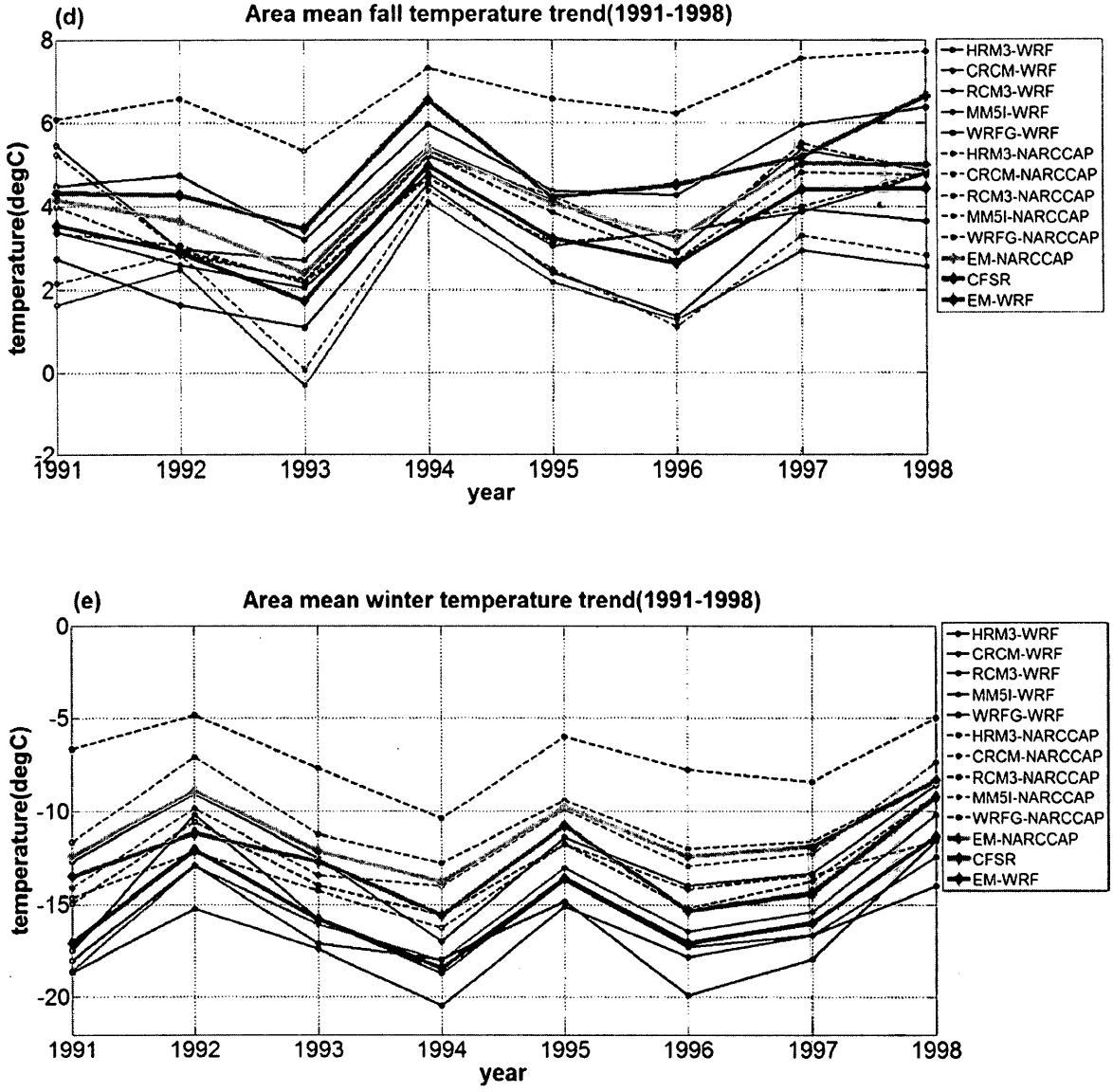

Figure 4. 1: Area mean temperature (T2 in each model data). (a) Annual temperature, (b) spring temperature, (c) summer temperature, (d) fall temperature, (e) winter temperature. Unit: °C.

Each thin solid or dashed curve represents a model data. For example, HRM3-NARCCAP is the HRM3 data in NARCCAP, and HRM3-WRF indicates a WRF simulation driven by HRM3-NARCCAP data. EM-NARCCAP and EM-WRF represent for the 7-member NARCCAP

ensemble mean and the 5-member WRF ensemble mean. This is also applied in later-section figures.

Table 4. 1: Annual mean temperature of different models between 1991 and 1998

	Mean (°C)	
	NARCCAP	WRF
HRM3	5.05	2.55
CRCM	1.27	0.23
RCM3	2.57	1.02
MM5I	1.54	0.01
WRFG	2.94	0.46
ENSEMBLE MEAN	2.67	0.86
CFSR	1.96	

Table 4. 2: Spring area mean temperature of different models between 1991 and 1998

	Mean (°C)	
	NARCCAP	WRF
HRM3	4.05	1.26
CRCM	-0.36	-1.61
RCM3	1.30	-0.60
MM5I	0.24	-1.67
WRFG	2.11	-0.53
ENSEMBLE MEAN	1.87	-0.63
CFSR	0.01	

Table 4. 3: Summer area mean temperature of different models between 1991 and 1998

	Mean (°C)	
	NARCCAP	WRF
HRM3	16.45	16.14
CRCM	15.12	15.59
RCM3	15.17	15.41
MM5I	15.04	14.32
WRFG	16.78	15.69
ENSEMBLE MEAN	15.71	15.43
CFSR	15.45	

Table 4. 4: Fall area mean temperature of different models between 1991 and 1998

	Mean (°C)	
	NARCCAP	WRF
HRM3	6.66	4.91
CRCM	3.56	3.48
RCM3	4.13	4.22
MM5I	2.40	2.11
WRFG	3.80	2.67
ENSEMBLE MEAN	4.77	3.47
CFSR	4.89	

Table 4. 5: Winter area mean temperature of different models between 1991 and 1998

	Mean (°C)	
	NARCCAP	WRF
HRM3	-7.08	-12.29
CRCM	-13.52	-16.89
RCM3	-10.50	-15.26
MM5I	-11.72	-15.07
WRFG	-13.10	-16.26
ENSEMBLE MEAN	-11.18	-15.16
CFSR	-12.80	

Table 4. 6: Correlation (COR) coefficient and RMSE (units: °C) between CFSR and each ensemble mean temperature.

		Spring	Summer	Fall	Winter	Annual
Correlation	NARCCAP ENSEMBLE MEAN	0.76	0.95	0.85	0.93	0.86
	WRF ENSEMBLE MEAN	0.80	0.93	0.89	0.93	0.89
RMSE	NARCCAP ENSEMBLE MEAN	2.03	0.45	1.50	1.91	1.41
	WRF ENSEMBLE MEAN	1.15	0.39	0.97	2.26	1.16

Figure 4.2 and table 4.7 show comparisons between the 8-station mean observations and the ensemble mean. The same comparisons will be used to analyze precipitation in the next section. The annual WRF ensemble mean is colder than CFSR by about 1.3°C, but it is closer to the observations. In fact, either for the annual, summer or winter temperature, the WRF ensemble

mean is always the closest to the observations. The two ensemble means, as well as the observations and the CFSR, all depict a remarkable rising tendency from winter 1997. The annual temperature also increases from 1997 to 1998. The WRF ensemble mean also shows the best correlation with the observations, compared to the NARCCAP ensemble mean and the CFSR data. The mean annual temperature bias is reduced from more than 1°C in the NARCCAP ensemble mean to less than 0.1°C in the WRF ensemble mean. The bias is also reduced in summer or winter in the WRF downscaling ensemble simulations. Thus, it can be concluded that the WRF ensemble mean performs better than the NARCCAP ensemble mean in simulating temperatures for this 8-year period. So increasing the horizontal resolution improve the model results.

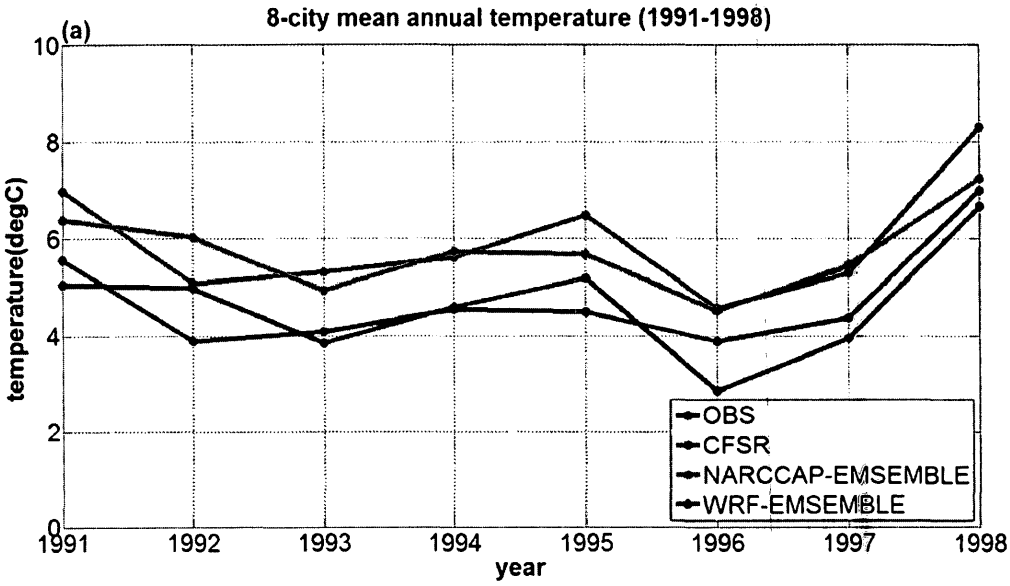
8-city mean annual temperature (1991-1998)
(a)
temperature(degC)
year
OBS
CFSR
NARCCAP-EMSEMBLE
WRF-EMSEMBLE

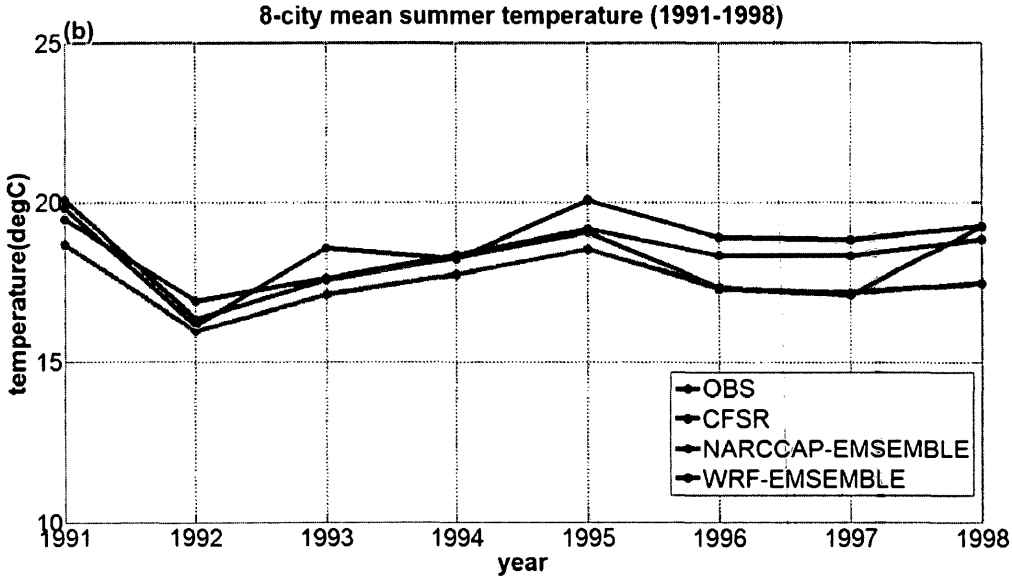
8-city mean summer temperature (1991-1998)
(b)
temperature(degC)
year
OBS
CFSR
NARCCAP-EMSEMBLE
WRF-EMSEMBLE

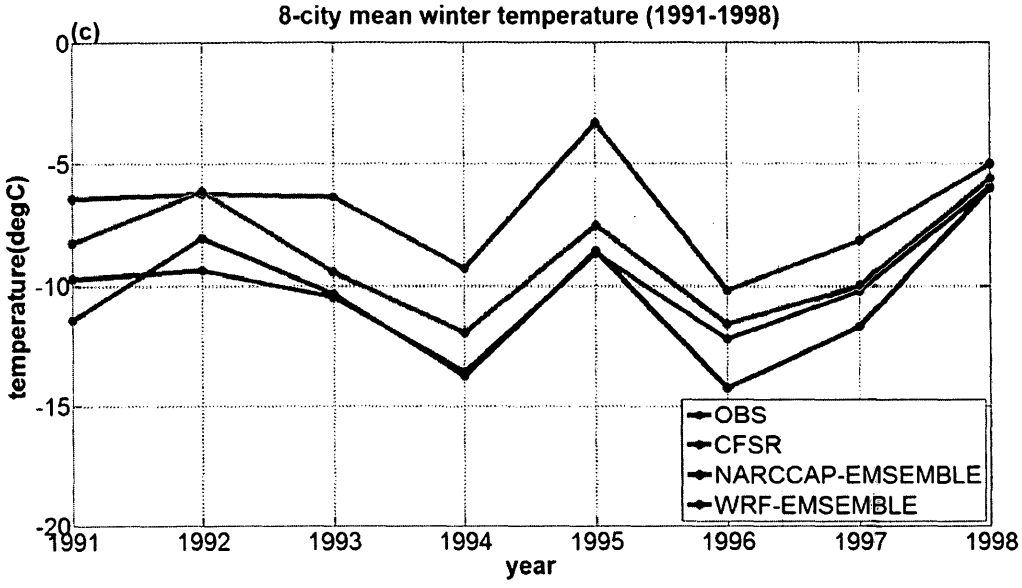

Figure 4. 2: 8-station mean temperature time series between 1991 and 1998. (a) Annual temperature, (b) summer temperature, (c) winter temperature. Unit: °C.

Table 4. 7: The annual, summer, winter temperature of CFSR data, NARCCAP ensemble mean and WRF ensemble mean and their correlation and RMSE with the observations.

		OBS	CFSR	NARCCAP-ENSEMBLE MEAN	WRF-ENSEMBLE MEAN
Annual mean	Temperature	4.73°C	5.95°C	5.75°C	4.65°C
	RMSE with OBS		1.27°C	1.14°C	0.64°C
	Correlation with OBS		0.95	0.90	0.86
Summer mean	Temperature	18.71°C	18.11°C	17.49°C	18.38°C
	RMSE with OBS		0.97°C	1.34°C	0.63°C
	Correlation with OBS		0.87	0.89	0.91
Winter mean	Temperature	-10.03°C	-6.87°C	-8.82°C	-10.51°C
	RMSE with OBS		3.43°C	1.51°C	1.17°C
	Correlation with OBS		0.85	0.91	0.93

4.1.2 Temperature horizontal distributions

The horizontal distributions of the annually averaged temperature of the WRF simulations driven by different models and the ensemble means are depicted in Fig. 4.3. The north to south temperature gradient is obviously observed in all of the model results and the CFSR data. It can be seen clearly from the figure that among the five models, the isotherms are more or less along the zonal direction, except in HRM3-WRF, where the isotherms have a sharper slope to the south of the Hudson Bay. MM5I is the coldest member, since the area with temperature above 0 °C is the smallest among the five ensemble members. There are apparently cold biases in the southwest part of the domain, compared with the CFSR data. Ontario is located in the middle of the domain. All the 5 WRF simulations simulate around 5 °C in southern Ontario and 0°C in northern Ontario and the temperature over the Hudson Bay gradually changes to below 0°C. Some details are captured in the west part of the domain, which is located southwest to the Hudson Bay. And the cold tongue associated with the Appalachian Mountains in the southeast part of the domain is captured by all of the WRF simulations and the CFSR data.

Comparing Fig. 4.3 a, f and h, the WRF ensemble mean temperature is colder than CFSR in the southern part of the domain, where NARCCAP ensemble mean seems resemble the CFSR data. The WRF ensemble mean produces more details related to the local topographic effects. For example, the cold tongue over the Appalachian Mountains is colder in the WRF ensemble mean than in the NARCCAP ensemble mean. Near or over the Appalachian Mountains, it shows several cold centers in the WRF ensemble mean, but not in the NARCCAP ensemble mean. The isotherms are not smooth in the WRF ensemble mean. There are many small cold spots over the entire domain, which are corresponding to small shallow lakes. These small lakes cannot be

resolved in NARCCAP RCM simulations, yet they partly contribute to the colder temperature in the WRFN ensemble mean temperature field in that area. It can be seen that the colder temperature in the WRF ensemble mean is also around the Great Lakes, Lake Winnipeg and the Hudson Bay. It is noticeable that the high-resolution WRF ensemble mean can capture low temperature over the small lakes in the west and east parts of the domain, while the coarse-resolution NARCCAP ensemble mean and CFSR do not show such details. The WRF ensemble mean can also describe the low temperature over the top right corner more specifically. Since it has been mentioned that the annual CFSR temperature maybe a few degrees higher than the station data. If 2 degrees are subtracted from the CFSR data, the WRF ensemble mean performs quite well in the temperature simulation.

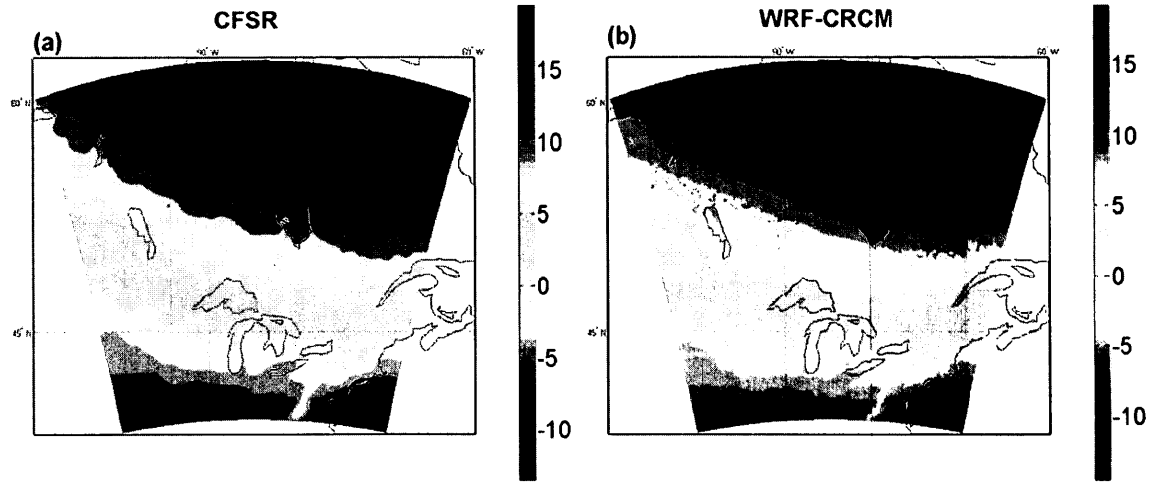

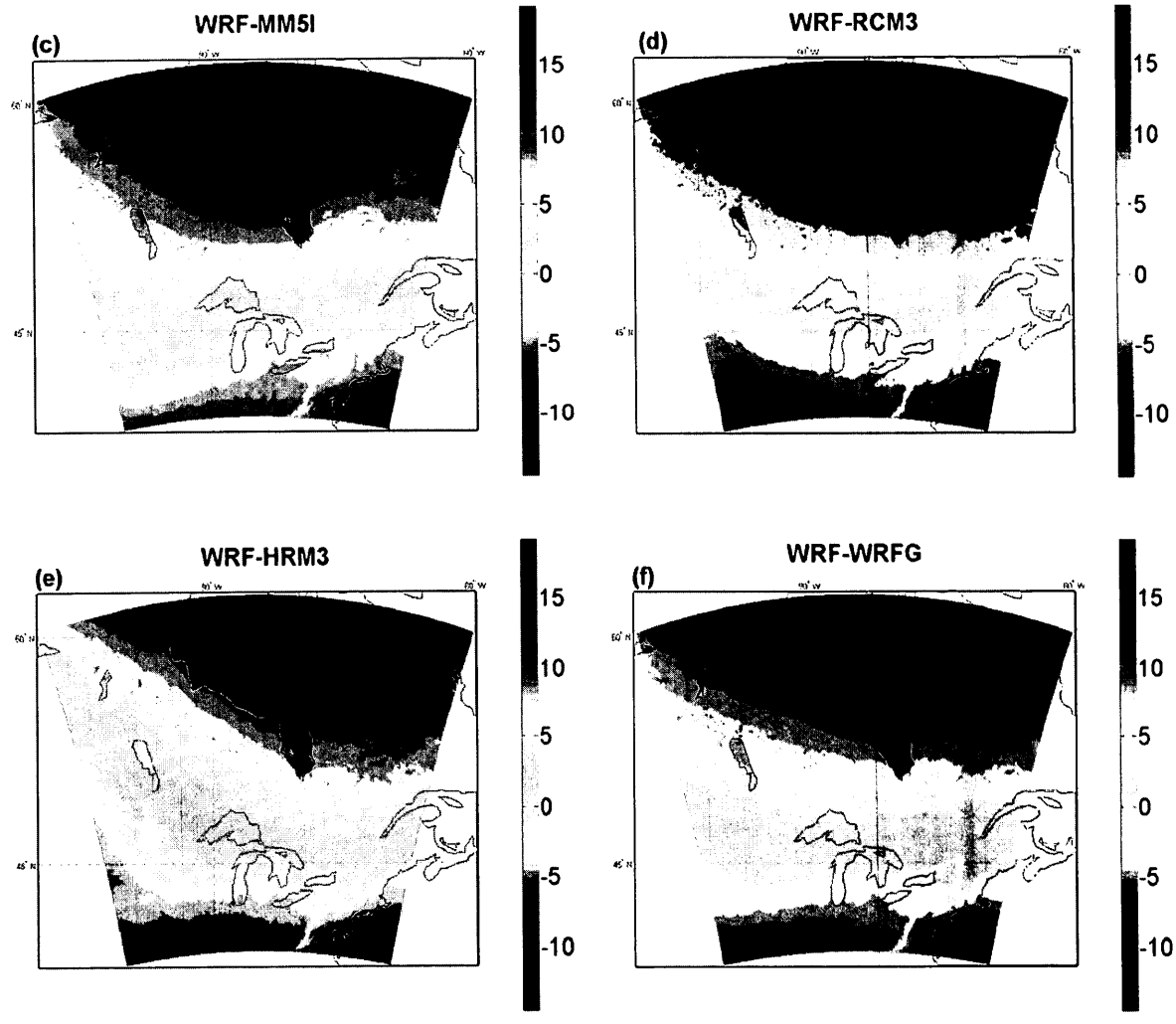
(c)
WRF-MM5I
(d)
WRF-RCM3
(e)
WRF-HRM3
(f)
WRF-WRFG
15
10
-5
-0
-5
-10

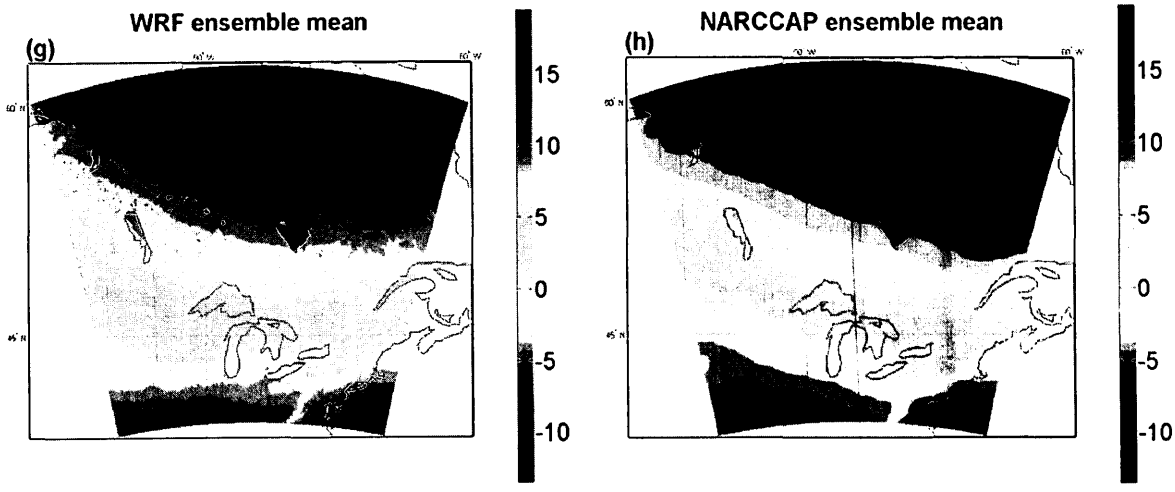

Figure 4. 3: Time mean (1991-1998) temperature patterns (T2 in each model data and the CFSR data) in (a) CFSR, (b) CRCM-WRF, (c) MM5I-WRF, (d) RCM3-WRF, (e) HRM3-WRF, (f) WRFG-WRF, (g) WRF ensemble mean, (h) NARCCAP ensemble mean (Unit: °C).

4.2 Maximum and minimum temperature analysis

The maximum and minimum temperatures in the WRF simulations are discussed in this section. Figures 4.4 and 4.5 present the 8-station mean maximum and minimum temperature from 1991 to 1998 in winter and summer, respectively. Each point in the figures presents the seasonal (winter or summer) mean and 8-station mean maximum or minimum temperature. Since the maximum and minimum temperatures are not included in the NARCCAP MM5I data, simulations from this model are not discussed here.

In winter, WRF predicts lower maximum and minimum temperatures than their corresponding NARCCAP models. The significant upward tendency of the winter 8-station mean maximum and minimum temperatures in 1997 and 1998 is shown in all model time series. Exclude the

initialization stage in the first winter (January and February, 1991), the maximum and minimum temperatures reach a top in 1992 and 1995, and a bottom in 1994, which correspond well to the observations.

In summer, the maximum and minimum temperatures vary more smoothly than that in winter. All 4 WRF simulations show a warmer maximum temperature and a colder minimum temperature, compared to their driving NARCCAP data. It suggests that the temperature diurnal variability over Ontario becomes larger in the WRF downscaling simulations.

Table 4.8 presents the 8-station summer and winter maximum and minimum temperatures of NARCCAP ensemble mean and WRF ensemble mean and their correlations and RMSEs with the observations. The WRF ensemble mean only shows higher correlation and smaller RMSE with the observations than the NARCCAP ensemble mean in winter maximum temperature. In summer, the NARCCAP ensemble mean maximum and minimum temperature are closer to the observations, and so does the NARCCAP ensemble mean minimum temperature in winter. The correlations between the two ensemble means and the observations are similar. All the correlations are significant at 90% confidence level.

In summary, the WRF model simulated a relatively cold maximum and minimum temperature in winter, compared with the NARCCAP data. The maximum temperature is higher while the minimum temperature becomes lower than the observations in summer. It suggests that more extreme temperature events may occur in summer. Compared with the observed maximum and

minimum temperature, the WRF ensemble mean does not perform better than the NARCCAP ensemble mean.

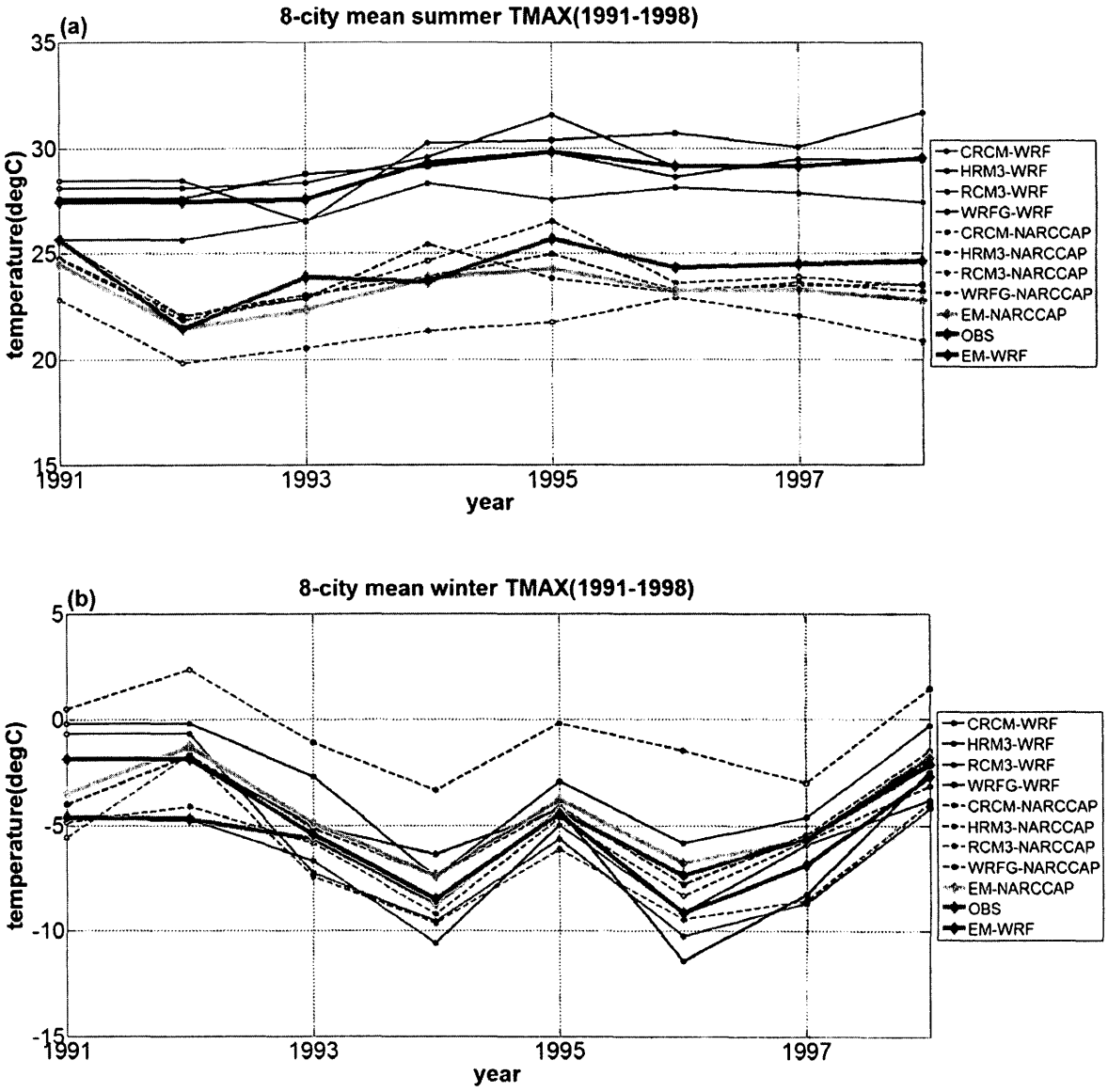

Figure 4. 4: 1991-1998 8-station mean maximum temperature in (a) summer, and (b) winter. (Unit: °C).

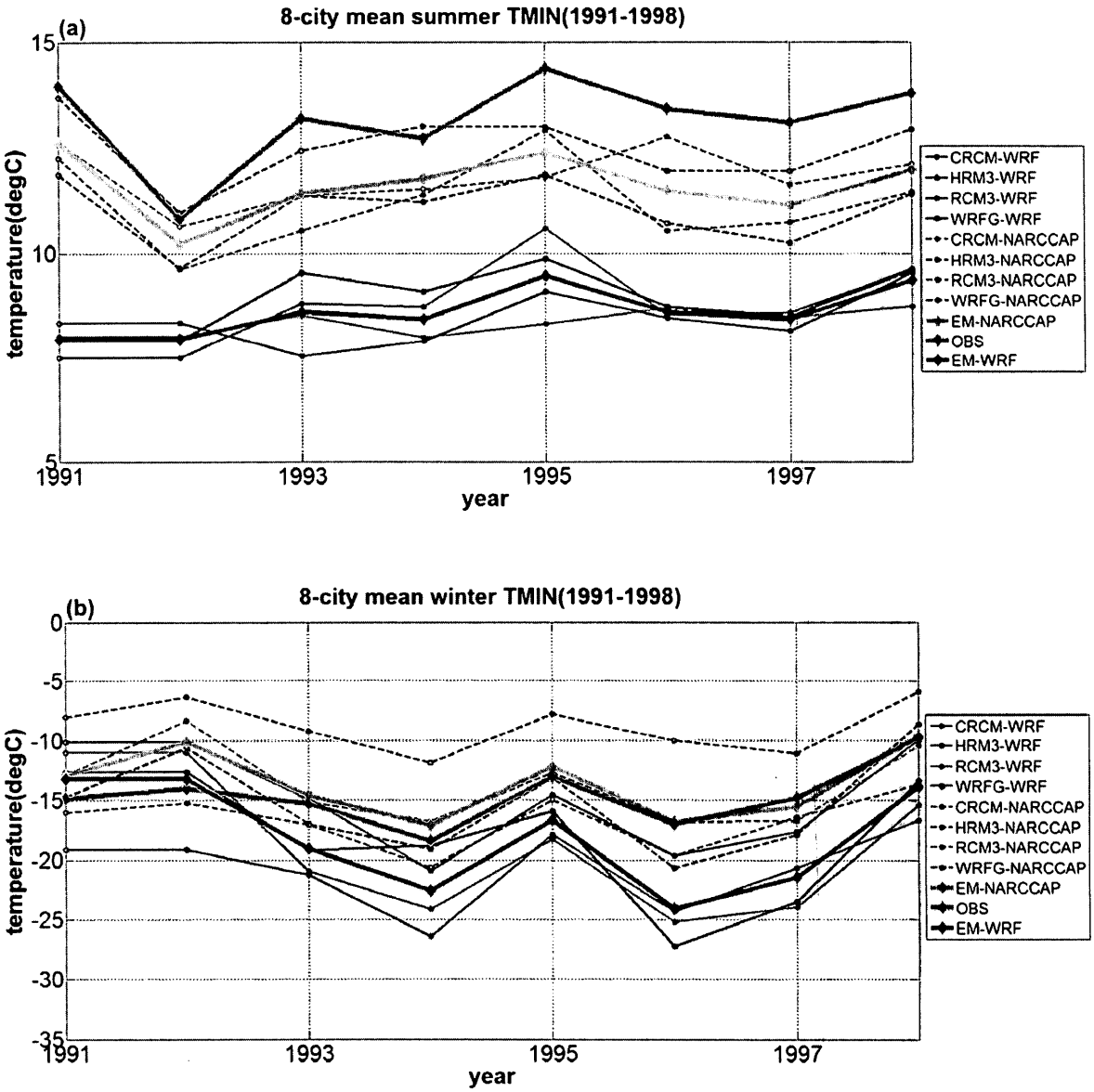

Figure 4. 5: 1991-1998 8-station mean minimum temperature in (a) summer, and (b) winter (Unit: °C).

Table 4. 8: The 8-station summer and winter maximum and minimum temperature of NARCCAP ensemble mean and WRF ensemble mean and their correlation and RMSE with the observations.

			OBS	NARCCAP-ENSEMBLE MEAN	WRF-ENSEMBLE MEAN
Summer mean	TMAX	Mean	24.23	23.26	27.67
		RMSE with OBS		1.41	4.61
		Correlation with OBS		0.65	0.57
	TMIN	Mean	13.16	11.60	8.60
		RMSE with OBS		1.89	4.62
		Correlation with OBS		0.62	0.61
Winter mean	TMAX	Mean	-5.39	-4.48	-5.10
		RMSE with OBS		1.52	1.51
		Correlation with OBS		0.76	0.82
	TMIN	Mean	-14.63	-13.57	-18.00
		RMSE with OBS		2.07	4.46
		Correlation with OBS		0.72	0.71

4.3 Precipitation in the WRF simulations

The precipitation variation in the chosen area is analyzed in this section.

4.3.1 Time series

The area mean annual precipitation rate and seasonal precipitation are discussed below. In Fig.4.6, the same color scheme as in Fig. 4.1 is used. The thick green, cyan, and red lines

represent the CFSR data, the 7-member NARCCAP ensemble mean and the 5-member WRF ensemble mean, respectively.

As shown in Fig.4.6, the annual precipitation amounts of NARCCAP models, WRF downscaling simulations and the ensemble means vary between 50 mm month^{-1} and 100 mm month^{-1}. The highest one is the WRF simulation driven by NARCCAP MM5I model data, which is approximately 20 mm month^{-1} more than the CFSR data. The annual precipitation amounts of both the WRF ensemble mean and NARCCAP ensemble mean are lower than CFSR data. The former is about 10 mm month^{-1} higher than the latter, thus the WRF ensemble mean is closer to the CFSR data.

From the four-season domain area mean monthly precipitation figures, this chosen region has the largest amount of precipitation in summer and the smallest amount in winter. The WRF simulation driven by NARCCAP MM5I model data produces an obviously large precipitation amount throughout the year.

Table 4.9 to 4.13 compare the time mean of the precipitation rate. The annual and seasonal mean precipitation rates for all the models, two ensemble means and the CFSR data are listed in Table 4.9 to 4.13. Most of the models produce precipitations in the amount between 50 mm month^{-1} to 80 mm month^{-1}, except MM5I (more than 90mm month^{-1}).

The annual averaged monthly precipitation amount depicted by CFSR is 80.19 mm month^{-1}. The WRF ensemble mean produces higher precipitation (71.77 mm month^{-1}) than the NARCCAPensemble mean (63.85 mm month^{-1}). Even though both ensemble means show a dry

bias, the WRF ensemble mean is closer to the CFSR data. This behavior appears in all four seasons.

Table 4.14 provides the correlation and the RMSE between CFSR and the ensemble mean precipitation. Similar to Table 4.6, all the correlations are significant at the 90% confidence level. The annual and all seasonal precipitation (except winter) have higher correlations between CFSR and the WRF ensemble mean than the NARCCAP ensemble mean. Moreover, all the RMSEs between CFSR and the WRF ensemble mean are obviously smaller than that between CFSR and the NARCCAP ensemble mean, which means that the WRF ensemble mean is closer to the CFSR data in all four seasons. Partly due to the small sample size, the RMSE improvement is only statistically significant (at 90% confidence level) in the winter season.

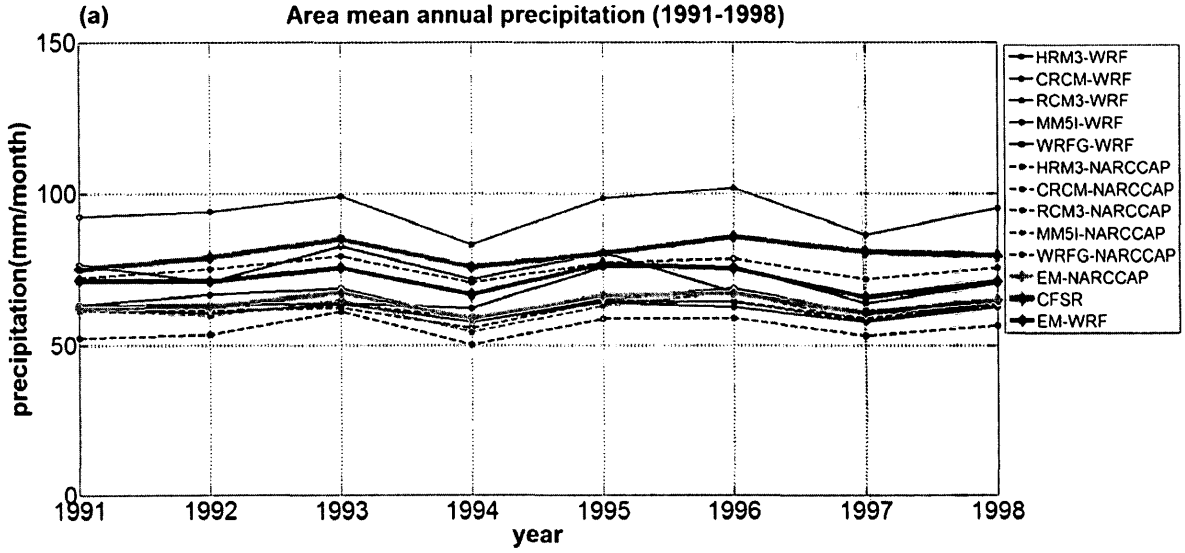
(a)
Area mean annual precipitation (1991-1998)
precipitation(mm/month)
150
100
50
0
1991
1992
1993
1994
1995
1996
1997
1998
year
HRM3-WRF
CRCM-WRF
RCM3-WRF
MM5I-WRF
WRFG-WRF
HRM3-NARCCAP
CRCM-NARCCAP
RCM3-NARCCAP
MM5I-NARCCAP
WRFG-NARCCAP
EM-NARCCAP
CFSR
EM-WRF

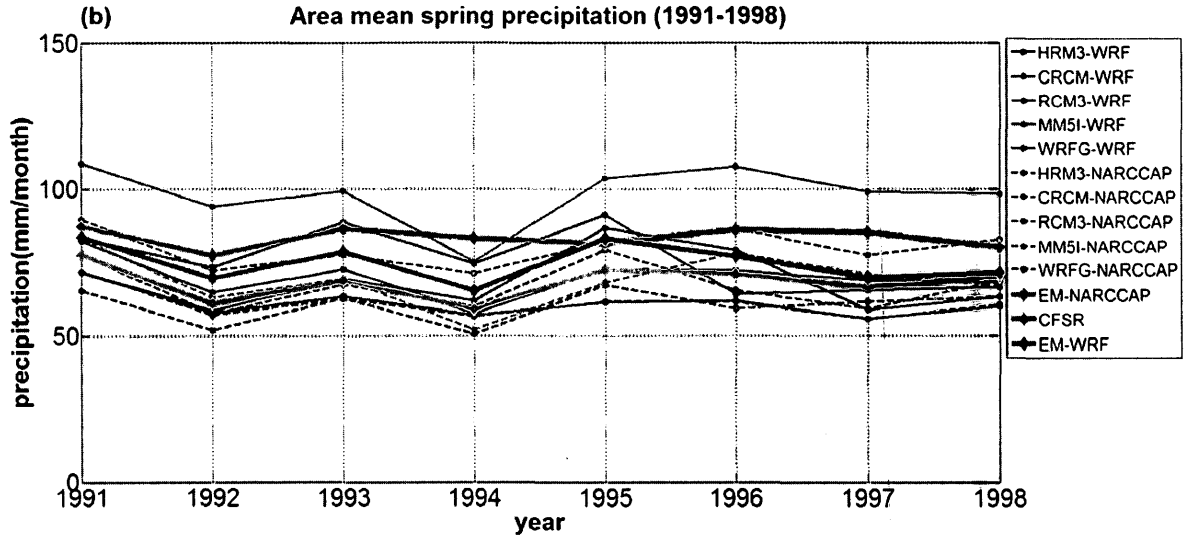
(b)
Area mean spring precipitation (1991-1998)
precipitation(mm/month)
150
100
50
0
1991
1992
1993
1994
1995
1996
1997
1998
year
HRM3-WRF
CRCM-WRF
RCM3-WRF
MM5I-WRF
WRFG-WRF
HRM3-NARCCAP
CRCM-NARCCAP
RCM3-NARCCAP
MM5I-NARCCAP
WRFG-NARCCAP
EM-NARCCAP
CFSR
EM-WRF

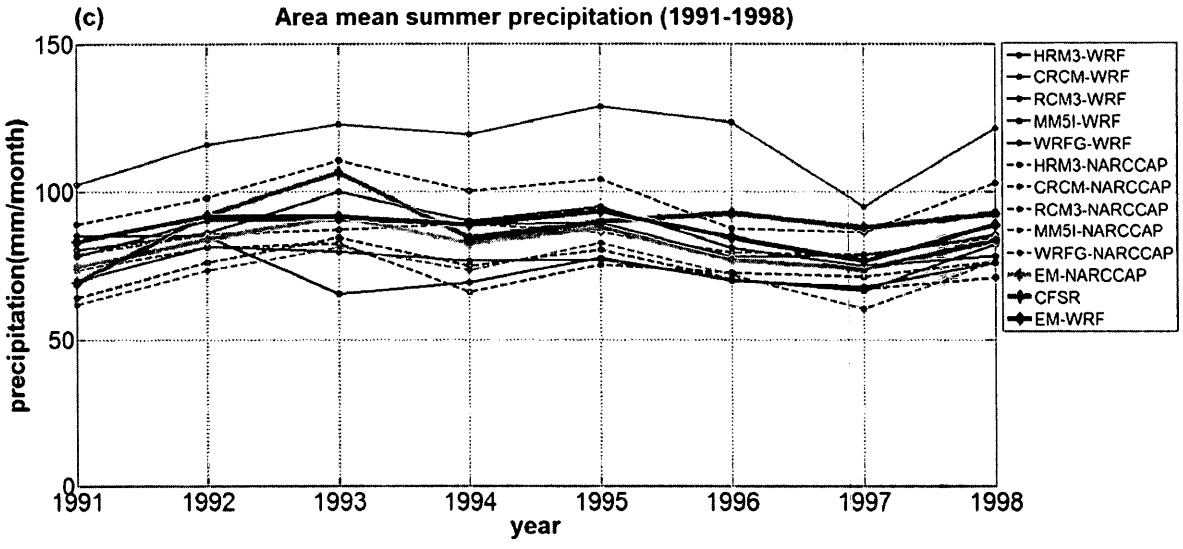
(c)
Area mean summer precipitation (1991-1998)
precipitation(mm/month)
150
100
50
0
1991
1992
1993
1994
1995
1996
1997
1998
year
HRM3-WRF
CRCM-WRF
RCM3-WRF
MM5I-WRF
WRFG-WRF
HRM3-NARCCAP
CRCM-NARCCAP
RCM3-NARCCAP
MM5I-NARCCAP
WRFG-NARCCAP
EM-NARCCAP
CFSR
EM-WRF

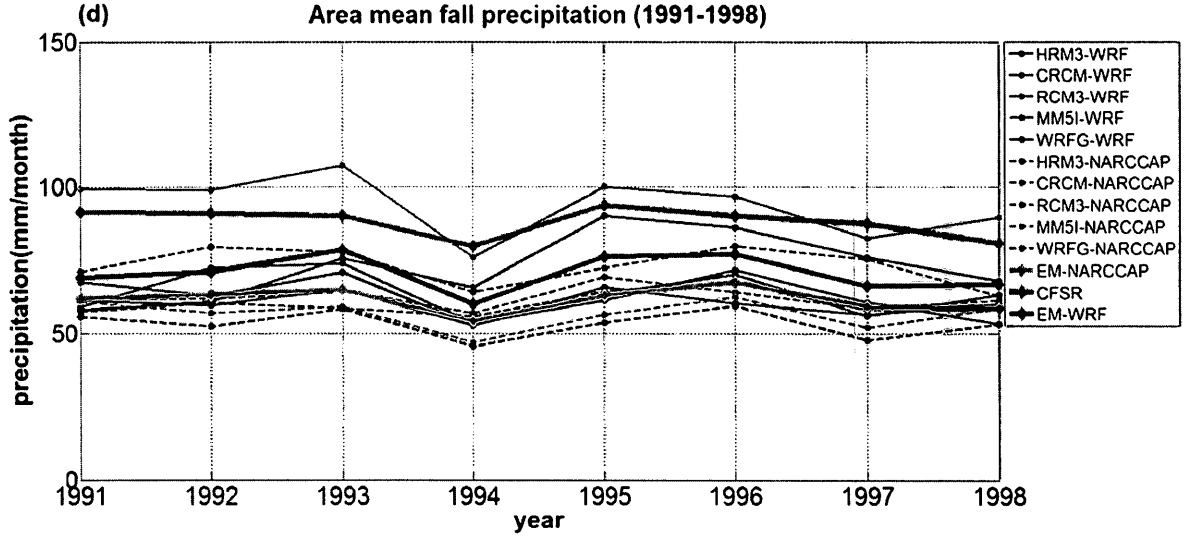
(d)
Area mean fall precipitation (1991-1998)
precipitation(mm/month)
150
100
50
0
1991
1992
1993
1994
1995
1996
1997
1998
year
HRM3-WRF
CRCM-WRF
RCM3-WRF
MM5I-WRF
WRFG-WRF
HRM3-NARCCAP
CRCM-NARCCAP
RCM3-NARCCAP
MM5I-NARCCAP
WRFG-NARCCAP
EM-NARCCAP
CFSR
EM-WRF

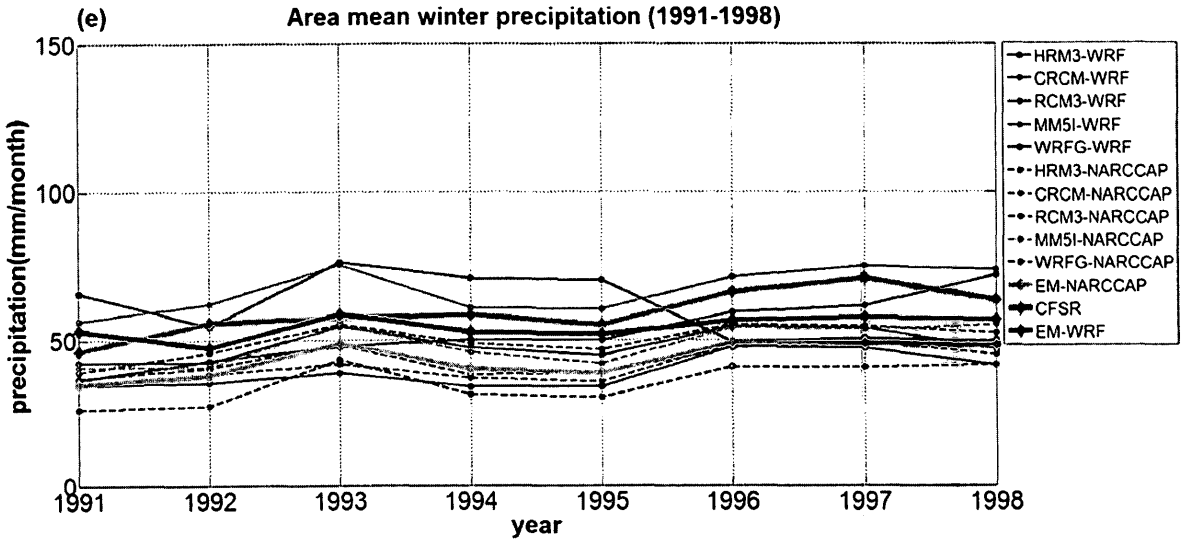

Figure 4. 6: Area mean precipitation. (a) Annual precipitation, (b) spring precipitation, (c) summer precipitation, (d) fall precipitation, (e) winter precipitation. Unit: mm month^{-1}.

Table 4. 9: Annual mean precipitation of different models between 1991 and 1998

	Mean (mm month^{-1})	
	NARCCAP	WRF
HRM3	61.52	67.36
CRCM	62.21	61.46
RCM3	75.14	64.34
MM5I	61.70	93.88
WRFG	55.60	71.80
ENSEMBLE MEAN	63.85	71.77
CFSR	80.19	

Table 4. 10: Spring area mean precipitation of different models between 1991 and 1998

	Mean (mm month^{-1})	
	NARCCAP	WRF
HRM3	66.80	68.55
CRCM	60.79	61.03
RCM3	79.88	69.77
MM5I	68.86	98.16
WRFG	60.15	75.77
ENSEMBLE MEAN	68.07	74.65
CFSR	83.28	

Table 4. 11: Summer area mean precipitation of different models between 1991 and 1998

	Mean (mm month^{-1})	
	NARCCAP	WRF
HRM3	75.01	74.66
CRCM	83.84	85.03
RCM3	97.44	75.61
MM5I	72.77	116.28
WRFG	73.67	85.81
ENSEMBLE MEAN	81.98	87.48
CFSR	89.57	

Table 4. 12: Fall area mean precipitation of different models between 1991 and 1998

	Mean (mm month^{-1})	
	NARCCAP	WRF
HRM3	60.28	72.68
CRCM	62.45	60.33
RCM3	72.96	63.32
MM5I	56.80	93.92
WRFG	53.44	63.52
ENSEMBLE MEAN	61.75	70.76
CFSR	88.16	

Table 4. 13: Winter area mean precipitation of different models between 1991 and 1998

	Mean (mm month^{-1})	
	NARCCAP	WRF
HRM3	43.75	52.52
CRCM	41.51	39.22
RCM3	49.79	48.28
MM5I	48.47	66.92
WRFG	35.28	60.92
ENSEMBLE MEAN	43.41	54.34
CFSR	59.20	

Table 4. 14: Correlation (COR) coefficient and RMSE (units: mm month^{-1}) between CFSR and simulated seasonal precipitation by WRF.

		Spring	Summer	Fall	Winter	Annual
Correlation	NARCCAP ENSEMBLE MEAN	0.49	0.70	0.76	0.83	0.68
	WRF ENSEMBLE MEAN	0.67	0.72	0.79	0.80	0.75
RMSE	NARCCAP ENSEMBLE MEAN	16.00	10.28	26.56	16.27	15.23
	WRF ENSEMBLE MEAN	10.00	9.11	17.81	7.12	10.72

It is noticed that in the previous chapter, the CFSR mean precipitation interpolated onto the selected 8 stations is higher than the mean observed precipitation. Thus, it is not clear whether the WRF ensemble mean being closer to CFSR indeed improves the precipitation simulations. Therefore, we compared the WRF simulations interpolated onto the 8 stations and the observed values.

The annual, summer and winter Ontario 8-station mean precipitations are calculated, and the comparisons with the observations are shown in Fig. 4.7. The annual, summer and winter mean precipitations of the WRF ensemble mean are all smaller than those of the NARCCAP ensemble mean. Both the ensemble means have discrepancies comparing to the observations. The two ensemble means of the annual precipitation show the same peaks in 1993, 1996 and 1998 and the same valleys in 1994 and 1997. However, the observations and CFSR show different summits in 1992 and 1996. The valleys and peaks of the four curves are also different in summer and winter. But the two ensemble means always share their peaks and valleys in the same year. Some are

different from the observations and CFSR, and some are not. Moreover, the annual curve shows that the two ensemble means have a significant increase from 1997 to 1998, which does not occur in the observations and CFSR data. The two ensembles show a more significant upwards tendency in the last two years in summer and a less obvious decreasing trend in the last two years in winter.

Table 4.15 reveals the 8-year mean precipitations, the RMSEs and correlations between the observations and either the CFSR or the ensemble means. The WRF ensemble mean is the one closest to the observations. The correlation of the precipitation between the observations and the ensemble means is much smaller than that of the temperature, which indicates that the precipitation is relatively more difficult to be simulated well. Most of the correlations are significant at 90% level, except the correlations between the observations and the two ensemble means in summer. It is expected that the summer precipitation cannot be simulated well. Nevertheless, the reduced RMSE suggests the WRF ensemble mean performs better than the coarser-resolution NARCCAP RCM ensemble mean.

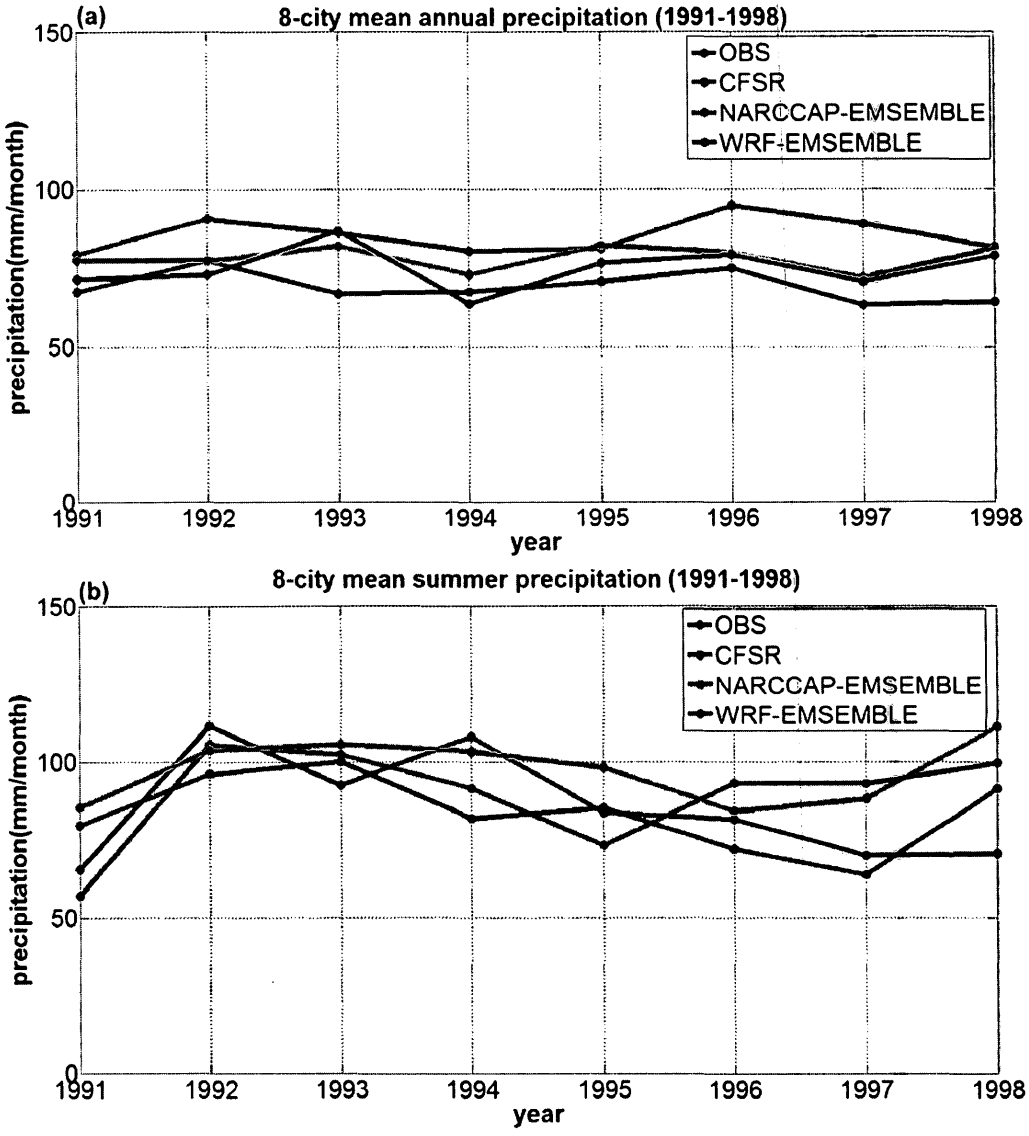
(a)
8-city mean annual precipitation (1991-1998)
OBS
CFSR
NARCCAP-EMSEMBLE
WRF-EMSEMBLE
precipitation(mm/month)
year
(b)
8-city mean summer precipitation (1991-1998)
OBS
CFSR
NARCCAP-EMSEMBLE
WRF-EMSEMBLE
precipitation(mm/month)
year

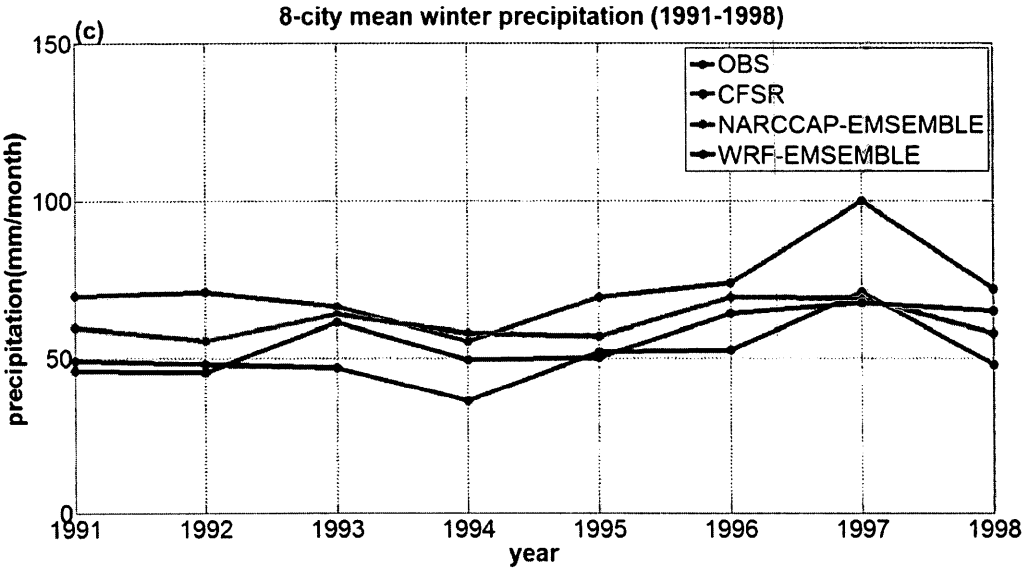

Figure 4. 7: 8-station mean precipitation time series between 1991 and 1998. (a) Annual precipitation, (b) summer precipitation, (c) winter precipitation. Unit: mm month^{-1}.

Table 4. 15: The annual, summer, winter precipitation rate of CFSR data, NARCCAP ensemble mean and WRF ensemble mean and their correlation and RMSE with the observations.

		OBS	CFSR	NARCCAP-ENSEMBLE MEAN	WRF-ENSEMBLE MEAN
Annual mean	Precipitation	69.11 mm month^{-1}	85.45 mm month^{-1}	78.22 mm month^{-1}	74.13 mm month^{-1}
	RMSE with OBS		17.07 mm month^{-1}	10.52 mm month^{-1}	9.83 mm month^{-1}
	Correlation with OBS		0.61	0.55	0.54
Summer mean	Precipitation	85.40 mm month^{-1}	89.34 mm month^{-1}	97.42 mm month^{-1}	83.77 mm month^{-1}
	RMSE with OBS		16.11 mm month^{-1}	18.80 mm month^{-1}	14.73 mm month^{-1}
	Correlation with OBS		0.61	0.46	0.49
Winter mean	Precipitation	50.48 mm month^{-1}	72.22 mm month^{-1}	61.29 mm month^{-1}	56.11 mm month^{-1}
	RMSE with OBS		21.98	12.95	10.23
	Correlation with OBS		0.97	0.64	0.66

4.2.2 Horizontal precipitation distributions

The precipitation patterns in the WRF model domain from five WRF simulations, the CFSR precipitation and the two ensemble means are shown in Fig. 4.8. As shown in section 4.2.1, MM5I-WRF generates the greatest amount of precipitation among all the 5 WRF simulations, while CRCM-WRF generates the least. All five models have the largest precipitation amount in the east and southeast of the domain.

Within Ontario, the precipitation decreases from southeast to northwest. All models describe this distribution properly. Both the NARCCAP ensemble mean and the WRF ensemble mean have a dry bias in the northwest part of the domain. The WRF ensemble mean produces a wet bias in the southeast, and the NARCCAP ensemble mean agrees with CFSR quite well. The high precipitation amount on the southeast boundaries of the domain in the WRF ensemble mean is mainly contributed by the MM5I and HRM3 simulations. The WRF ensemble mean shows some precipitation differences from the NARCCAP ensemble mean, since it has a higher resolution. For example, in the southeast part of the domain, the NARCCAP ensemble mean does not show a very high precipitation near the coastline, but the WRF ensemble mean does. The precipitation over the Great Lakes is also higher in the WRF ensemble mean than in the NARCCAP ensemble mean. Interestingly, the WRF ensemble mean shows high precipitation bands in the top right corner of the domain, which is the northeast part of the Labrador Peninsula stretched into the Labrador Sea. Although the relatively high precipitation can also be seen in the NARCCAP ensemble mean and CFSR precipitation, the WRF ensemble mean depicts a finer and more concentrated linear structure. Further analyses (figures not shown) suggest that the enhanced

precipitation over the Labrador Peninsula is induced by the moist air from the Hudson Strait being forced to ascend along the Torngat Mountains. The lake effect also plays important role in enhancing the precipitation downstream of the Great Lakes and southern Hudson Bay along their east shorelines. Overall, both the ensembles showed good agreements with the CFSR data in the horizontal distribution of precipitation. The 5-member WRF ensemble mean will be discussed further in the next chapter.

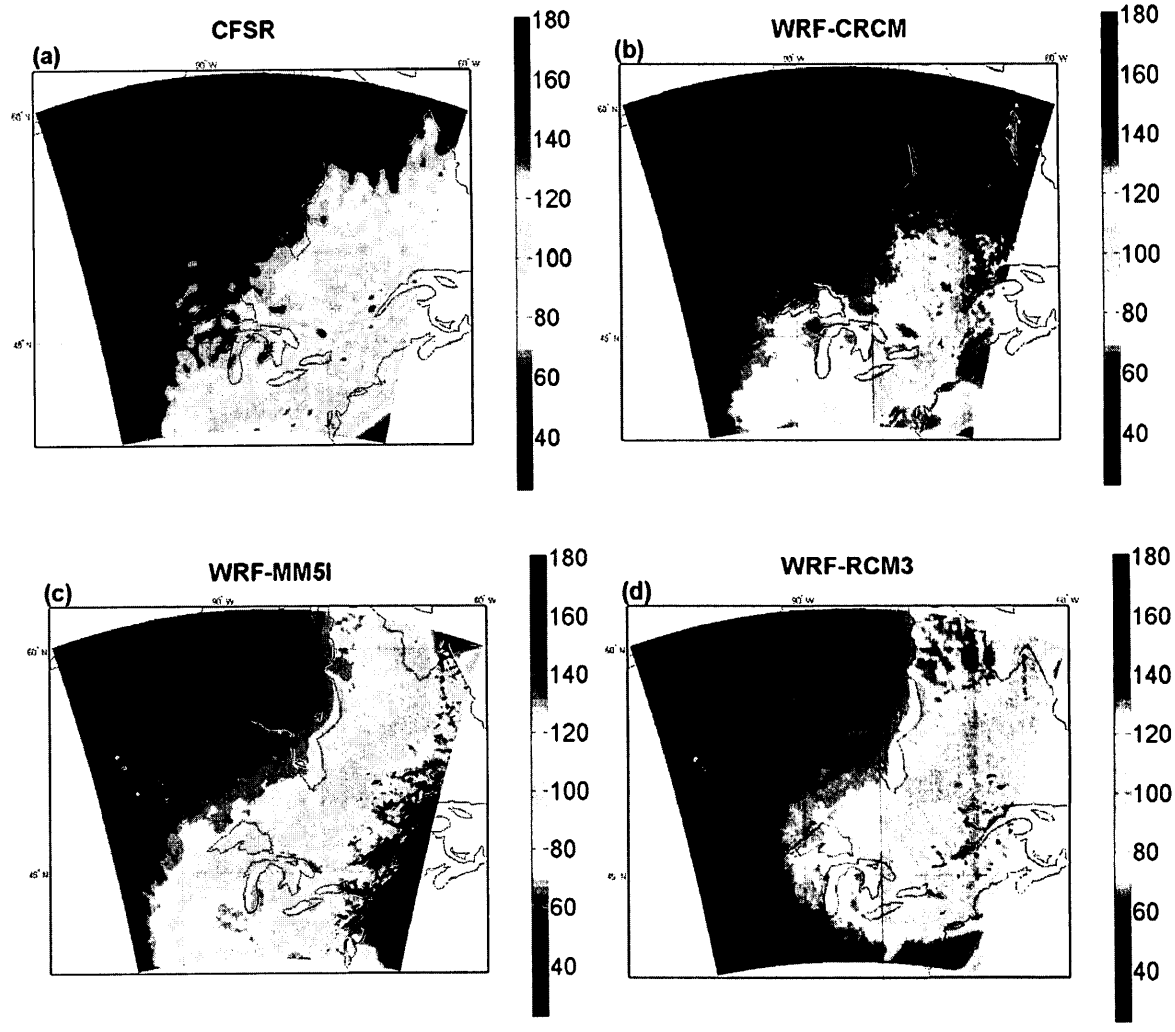

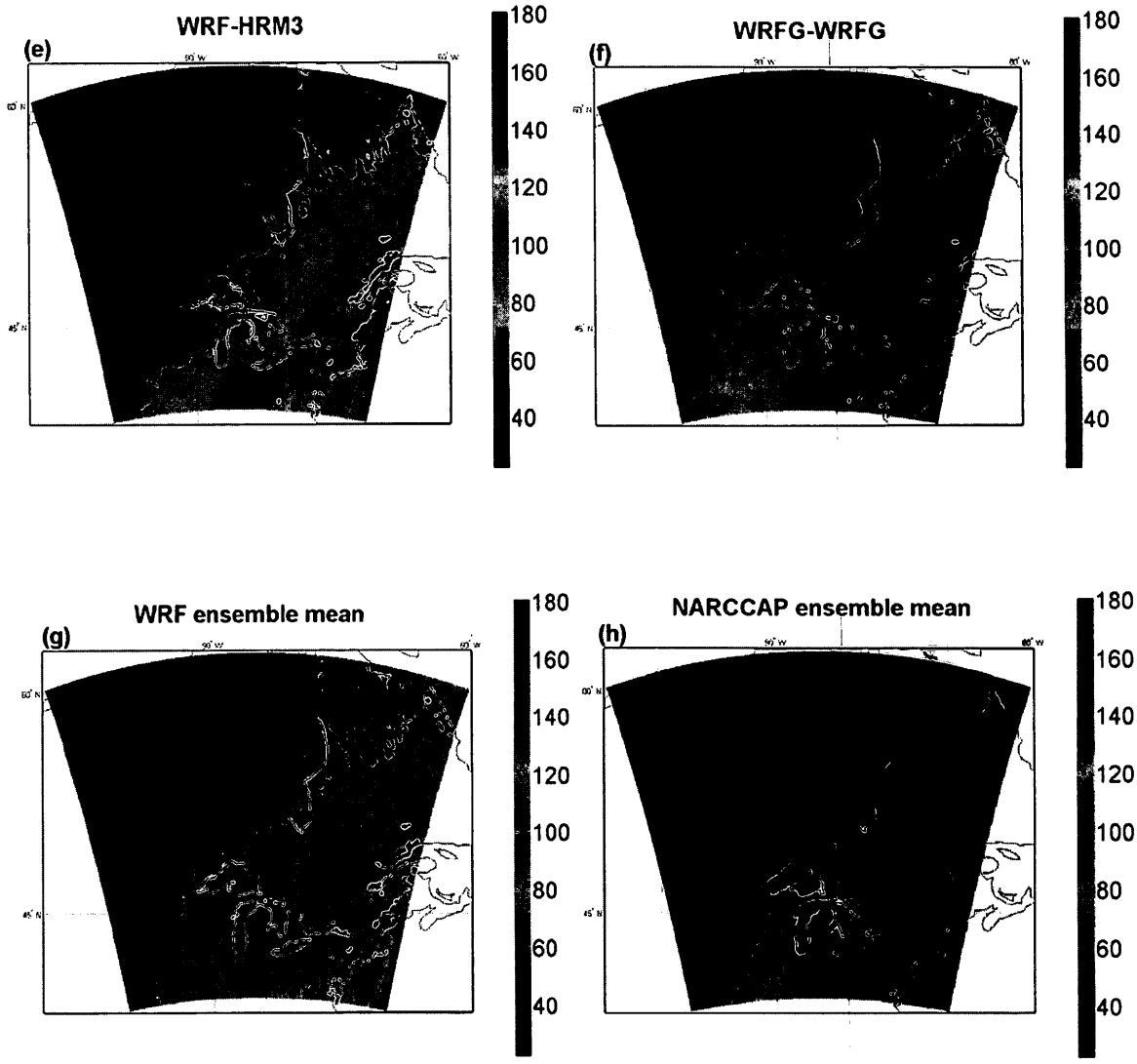

Figure 4. 8: Time mean (1991-1998) precipitation patterns in (a) CFSR, (b) CRCM, (c) MM5I, (d) RCM3, (e) HRM3, (f) WRFG, (g) WRF ensemble mean, (h): NARCCAP ensemble mean. Unit: mm month^{-1}.

Chapter 5 Analysis of stochastic ensemble simulations

Although WRF downscaling is promising in improving the climate simulation, the ensemble size of five is too small to address the climate uncertainties. As stated in Chapter 2, the stochastic kinetic energy backscatter (SKEB) scheme was used to create more ensemble members (Frederiksen and Davies 1997; Shutts 2005; Berner et al. 2009, 2011). The SKEB scheme represents model uncertainties resulting from unresolved scales of motions by adding small random perturbations in wind components and potential temperature at every time step during the simulation. The perturbations may accumulate and grow non-linearly, which lead to different atmospheric states. The SKEB scheme has been shown to improve the probabilistic weather forecast skills (Tennant et. al., 2011). Berner et al. (2011) demonstrated that the ensemble forecast with SKEB schemes outperformed the multi-physics ensemble in weather forecast. There is little work has been done in using SKEB scheme in regional climate simulations. Here we would like to explore whether the advantages of SKEB in ensemble weather forecast can be extended to climate scales.

The simulations with the SKEB scheme started from 30th November 1996, and ran until the last day of 1998. The simulation results can also be used to study the mechanisms of the significant warming as shown in Chapter 3. The WRF restart files on 30th November 1996 of the 5-member WRF simulations discussed in Chapter 4 were resumed but with the SKEB scheme turned on. By assigning different random seeds, the SKEB scheme can generate different perturbations. The WRF simulations driven by WRFG, RCM3, HRM3, CRCM BC's were perturbed twice with different random seeds, while the simulation driven by MM5I BC's was perturbed once. Thus, altogether there were 9 members in this stochastic ensemble experiment. Together with the

previous WRF simulations for the last two years, a 14-member ensemble was built up and was studied in this chapter.

5.1 Temperature analysis

Figures 5.1 to 5.4 depict the winter and summer mean temperature in 1997 and 1998. According to Fig. 5.1 (winter 1997) and 5.2 (winter 1998), the 0 °C isotherm in the 5-member ensemble mean, 14-member ensemble mean and the CFSR data all move northwards (Fig. 5.1-a, c, e and Fig. 5.2-a, c, e), which indicates that the temperature is rising from winter 1997 to winter 1998. In winter 1997, the 0°C isotherm is located at the bottom of the domain, south to the Great Lakes, while it crosses the Great Lakes in winter 1998. The 14-member ensemble mean shows the northernmost location of the 0°C isotherm. When compared with CFSR, both ensemble means perform similarly. In both winters, the ensemble means have a cold bias over large areas compared with the CFSR. The simulations do not perform well over the north part of the domain, especially over the Hudson Bay and its surroundings.

In winter 1997, 0°C temperature difference between ensemble means and CFSR is located at the southern part of the domain. Figures 5.1 b and d show the differences between both ensemble means and CFSR range from 0°C to -10 °C over Ontario. The difference between the two ensemble means was also plotted in Fig. 5.1f. The 14-member ensemble mean is about 0.5°C colder over the Great Lakes and more than 2°C warmer in the surrounding areas of the Hudson Bay. In Ontario, the 14-member ensemble mean shows a 1-2°C warmer than the 5-member ensemble mean. In winter 1998, as seen in Fig. 5.2 b and d, the temperature differences between

the ensemble means and the CFSR become smaller, in particular the 14-member ensemble mean, although the patterns of the differences between the two WRF ensemble means in winter 1998 are similar to that in winter 1997.

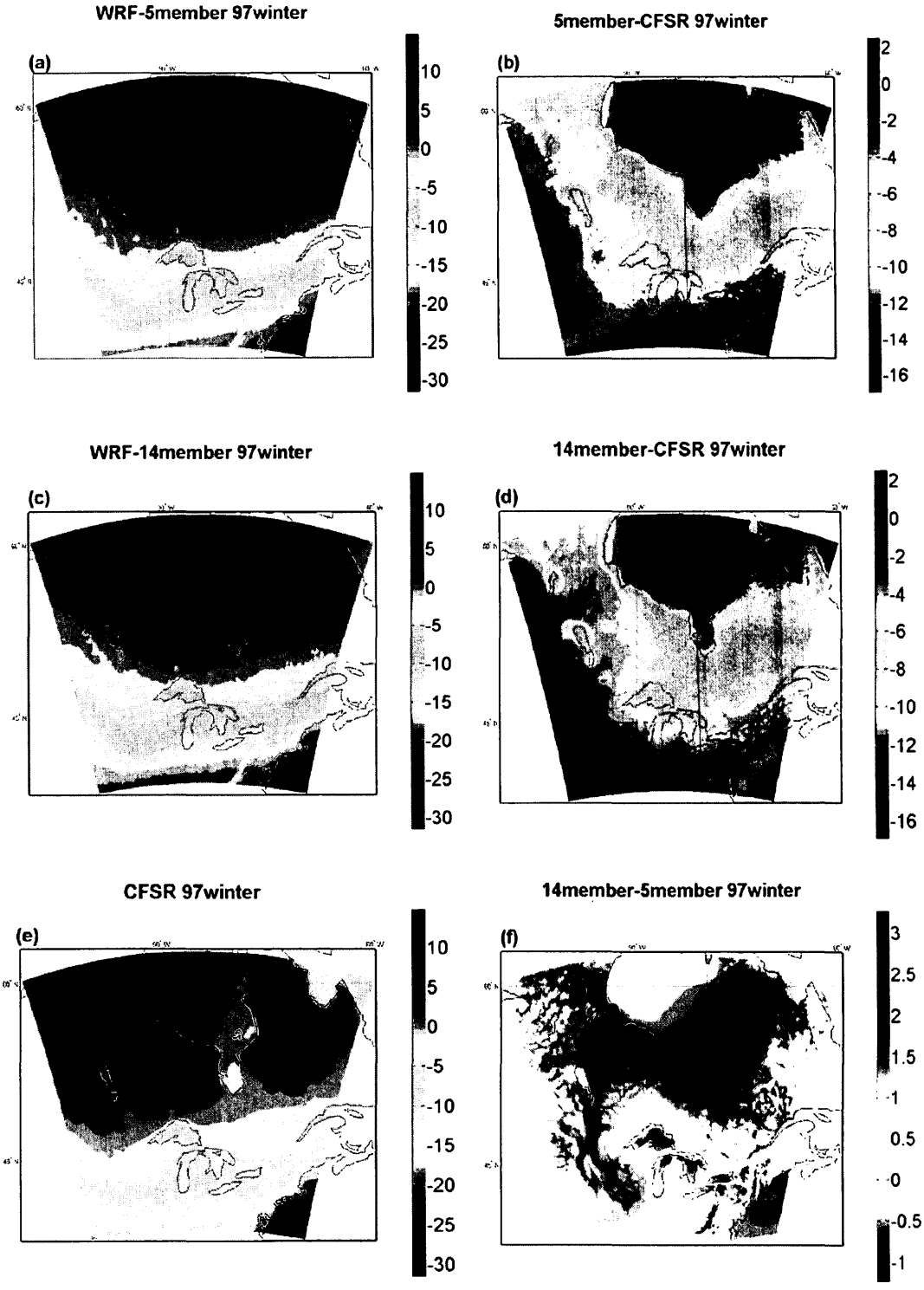

Figure 5. 1: 1997 winter mean temperature (T2, unit: °C). (a) WRF 5member ensemble mean, (b) WRF 5member ensemble mean – CFSR, (c) WRF 14member ensemble mean, (d) WRF 14member ensemble mean – CFSR, (e) CFSR data, (f) WRF 14member ensemble mean – WRF 5member ensemble mean.

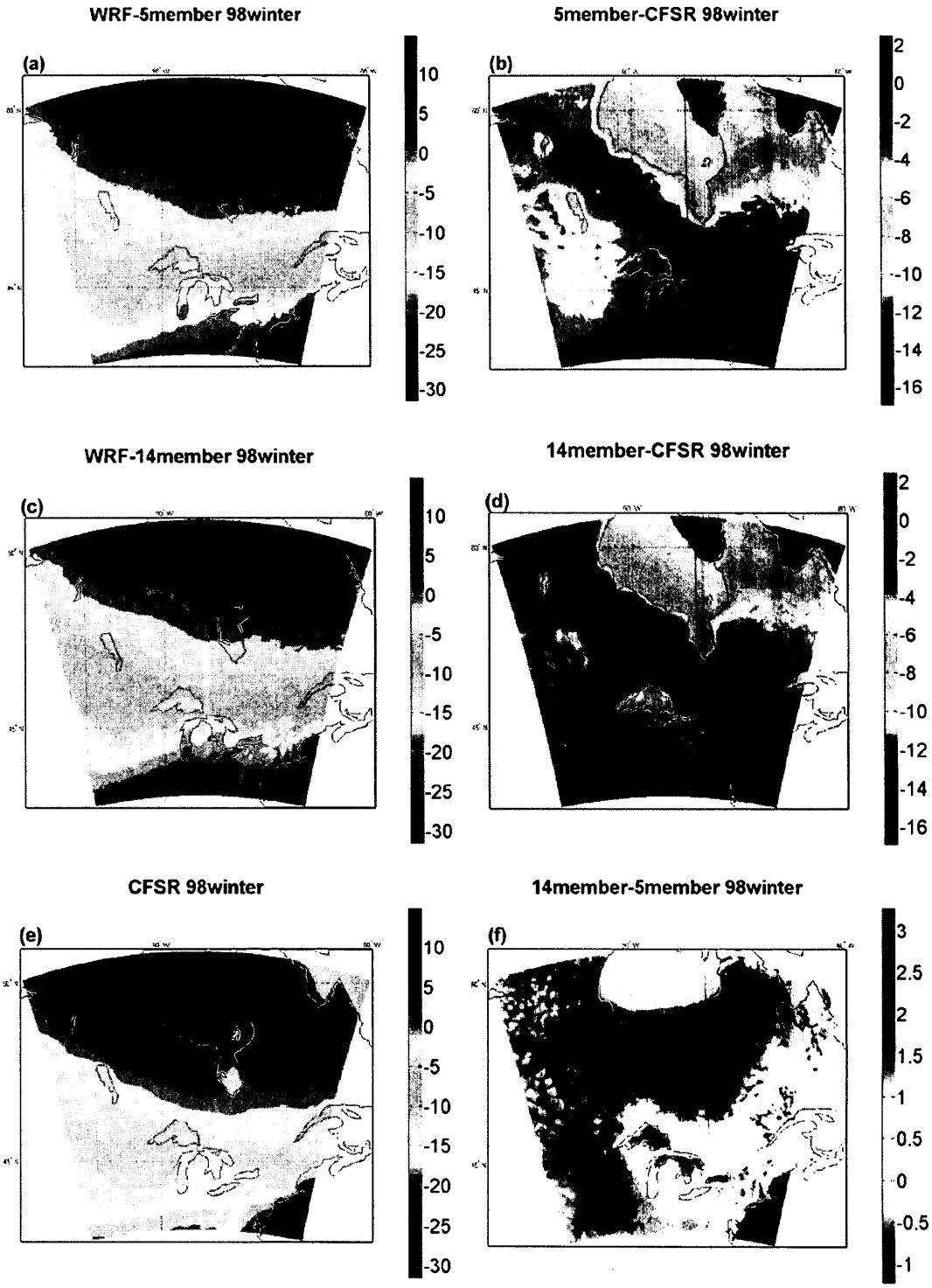

Figure 5. 2: 1998 winter mean temperature (T2, unit: °C). (a) WRF 5member ensemble mean, (b) WRF 5member ensemble mean – CFSR, (c) WRF 14member ensemble mean, (d) WRF 14member ensemble mean – CFSR, (e) CFSR data, (f) WRF 14member ensemble mean – WRF 5member ensemble mean.

In summers of 1997 and 1998, the difference between the 14-member ensemble mean and the 5-member ensemble mean becomes smaller than that in winter. Both ensemble means are approximately 1°C warmer than the CFSR over Ontario in 1997 and 1998 (Fig. 5.3 and 5.4). In the northwest region of Ontario, the difference is larger than the southern region. For the rest of the domain, the differences between the ensembles and the CFSR vary from 2°C to 4°C. The greatest temperature differences are located in the area west to the Hudson Bay (around 8°C). The model generates stronger temperature gradient along the west coast of the Hudson Bay than CFSR. It also produces colder surface temperature along the Appalachian Mountains. Comparing the two ensemble means (Fig. 5.3f and Fig. 5.4f), the temperature differences vary between -1.5°C to 1.5°C, which is milder than the differences in winters. In summer, the 14-member ensemble mean is warmer in the vicinity of the Hudson Bay.

To evaluate the performance of each ensemble mean, the monthly mean domain-averaged temperature were computed, and the correlations and RMSEs between each ensemble mean and the CFSR averaged temperature were calculated. Table 5.1 shows the correlations and the RMSEs between the ensemble means and the CFSR data in different seasons. From this table, it can be seen that, the 14-member ensemble mean generally has smaller RMSEs and higher correlations than the 5-member ensemble mean. The exceptions are summer RMSE and the fall correlation, but the differences are small.

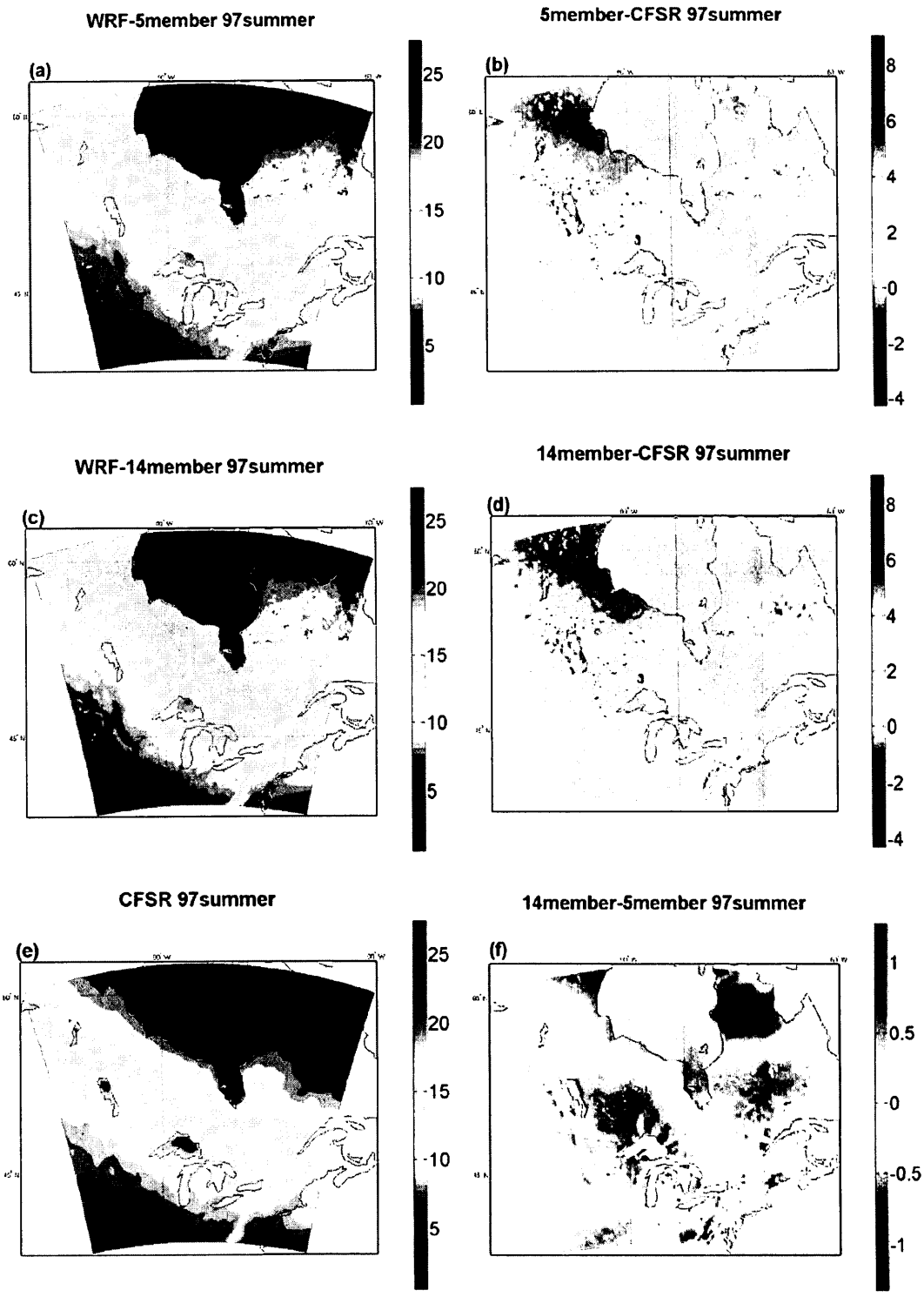

Figure 5. 3: 1998 summer mean temperature (T2, unit: °C). (a) WRF 5member ensemble mean, (b) WRF 5member ensemble mean – CFSR (c) WRF 14member ensemble mean, (d) WRF 14member ensemble mean – CFSR, (e) CFSR data, (f) WRF 14member ensemble mean – WRF 5member ensemble mean.

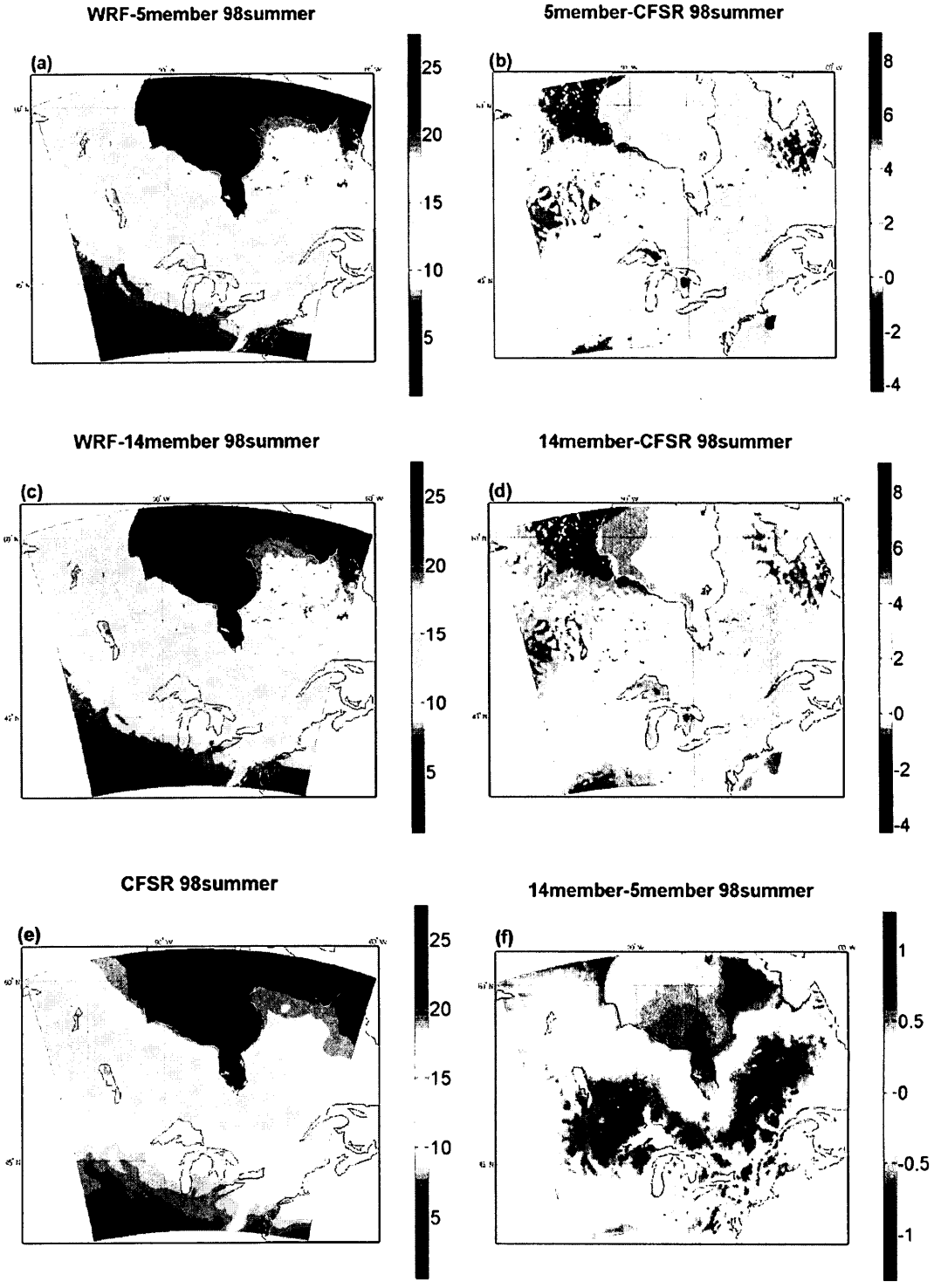

Figure 5. 4: 1998 summer mean temperature (T2, unit: °C). (a) WRF 5member ensemble mean, (b) WRF 5member ensemble mean – CFSR, (c) WRF 14member ensemble mean, (d) WRF 14member ensemble mean – CFSR, (e) CFSR data, (f) WRF 14member ensemble mean – WRF 5member ensemble mean.

Table 5. 1: Correlation (COR) coefficient and root mean square error (RMSE) (units: °C) between CFSR and simulated seasonal temperature using WRF for 1997 and 1998.

	Spring	Summer	Fall	Winter	Annual
COR-5member	0.82	0.88	0.85	0.82	0.84
COR-14member	0.84	0.89	0.84	0.83	0.86
RMSE-5member	2.58	1.66	4.67	3.36	3.51
RMSE-14member	2.01	1.70	4.22	2.86	3.01

5.2 Maximum and minimum temperature

The 14-member ensemble mean maximum and minimum temperatures are interpolated onto the 8 stations first. The 8-station mean values in winter and summer are plotted as dashed red lines in Fig. 5.5. Note that Fig. 5.5 is the same as Fig. 4.5 except the 14-member ensemble mean (only covers 1997 and 1998) is added.

As discussed in the previous chapter, the 5-member WRF ensemble mean is too warm in the summer and too cold in the winter (c.f. Figs. 4.4 and 4.5). The 14-member WRF ensemble is able to dramatically reduce the summer maximum temperature and increase the winter minimum temperature by about 3°C. In fact, the improvements of the maximum and minimum temperatures in both winter and summer can be seen. They are much closer to the observations. It suggests the 14-member ensemble mean can represent well the diurnal variability of the temperature.

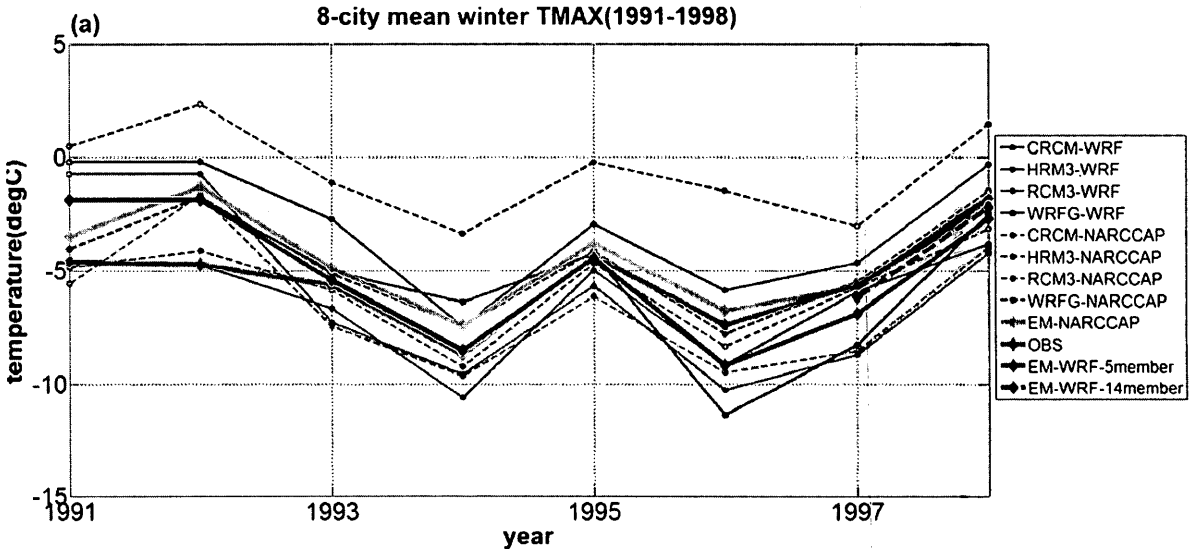
(a)
8-city mean winter TMAX(1991-1998)
temperature(degC)
year
5
0
-5
-10
-15
1991
1993
1995
1997
CRCM-WRF
HRM3-WRF
RCM3-WRF
WRFG-WRF
CRCM-NARCCAP
HRM3-NARCCAP
RCM3-NARCCAP
WRFG-NARCCAP
EM-NARCCAP
OBS
EM-WRF-5member
EM-WRF-14member

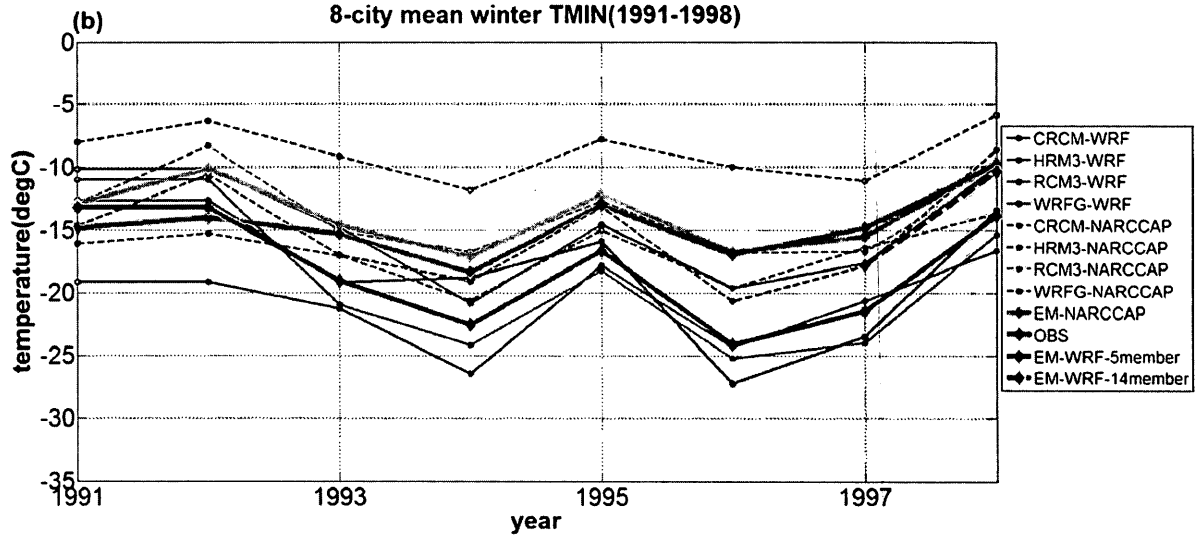
(b)
8-city mean winter TMIN(1991-1998)
temperature(degC)
year
0
-5
-10
-15
-20
-25
-30
-35
1991
1993
1995
1997
CRCM-WRF
HRM3-WRF
RCM3-WRF
WRFG-WRF
CRCM-NARCCAP
HRM3-NARCCAP
RCM3-NARCCAP
WRFG-NARCCAP
EM-NARCCAP
OBS
EM-WRF-5member
EM-WRF-14member

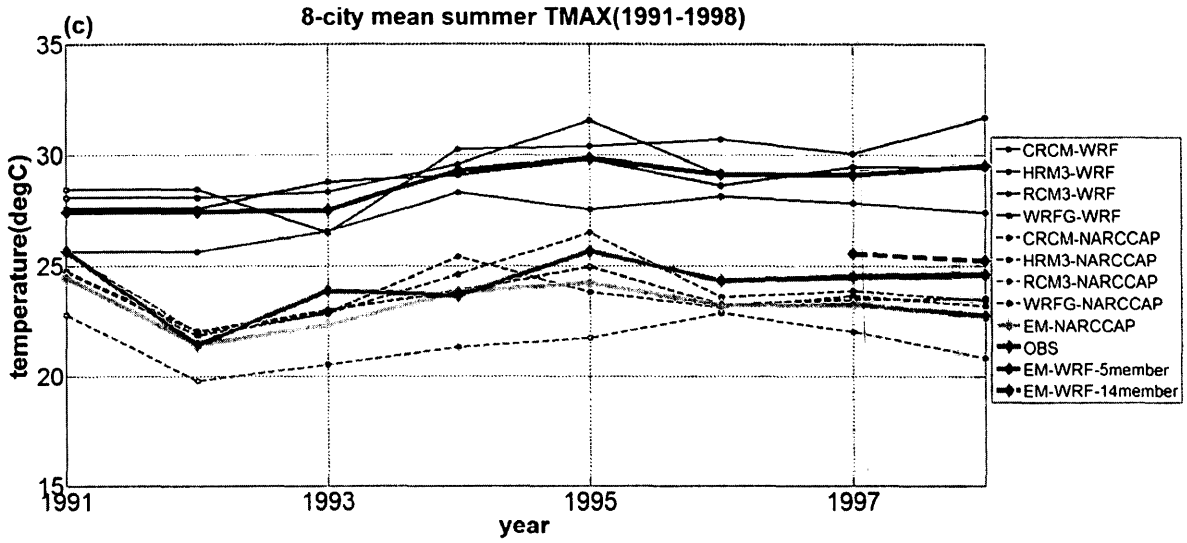

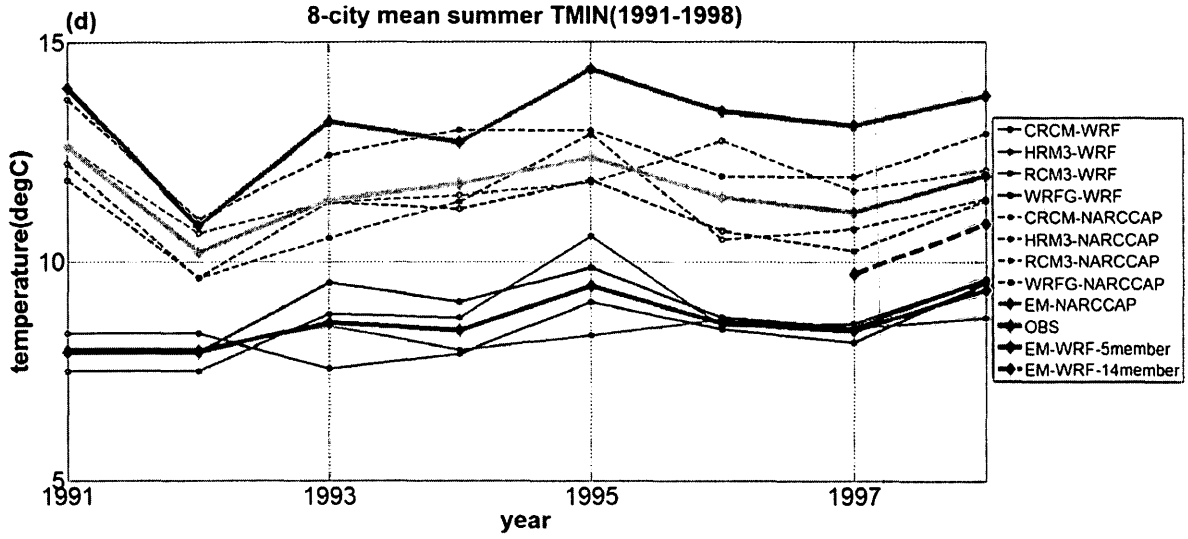

Figure 5. 5: The 8-station mean maximum and minimum temperature (seasonal mean) of the observations, simulations and the ensemble means from 1991 to 1998. (a) Maximum temperature in winter,(b) minimum temperature in winter,(c) maximum temperature in summer,(d) minimum temperature in summer.

5.3 precipitation analysis

In winter, the precipitation of CFSR aggregates in the southeast part of the domain (Figs. 5.6 e, 5.7 e). The precipitation in Ontario varies from 70 mm month^{-1} in the northwest to 250 mm month^{-1} in the southeast. The winter precipitation in 1998 is obviously smaller than that in 1997. In summer, the large precipitation shifts northward to east Canada, while a secondary high precipitation band emerges in the west of the Great Lakes (Figs. 5.8 e and 5.9 e). Two ensemble means show similar precipitation distribution patterns to the CFSR data. The improvement in 14-member ensemble can be seen in both summer and winter seasons. For example, both ensemble means are drier than CFSR in winter 1997, yet, the 14-member ensemble mean produces more precipitation (Fig. 5.6). In winter 1998, the 5-member ensemble mean over-predicts the precipitation in a wide area from the west of Great Lakes to east Canada as well as along the east coast, while the 14-member ensemble mean is able to reduce such excessive precipitation (Fig. 5.7). Altough both ensembles are good at resolving summer precipitations, in particular in the west part of the domain over the continent, they both correctly capture the northward shift of the large precipitation band in east Canada (Figs. 5.8, 5.9).

Table 5.2 summarizes the domain averaged precipitation amount in winter and summer of 1997 and 1998. The averaged CFSR precipitation is 63.22 mm month^{-1} in winter 1997. The 14-member ensemble mean generates 63.22 mm month^{-1}, while the 5-member ensemble mean only produces 57.66 mm month^{-1}. which indicates that it is closer to the CFSR (domain averaged 76.18 mm month^{-1}) than the 5-member ensemble mean (domain averaged 57.66 mm month^{-1}) (Fig. 5.6 a, c). The similar trend in differences has been observed for ensemble means and the

CFSR (Fig. 5.6 b and d). In 1998, the ensemble means and the CFSR indicate a decreasing trend of monthly precipitation compared to winter 1997, as shown in Fig. 5.7 a, c and e. The high precipitation center is right in the southeast region of the domain. The precipitation in Ontario drops to a very low level in 1998. According to Fig. 5.7 b and d, the difference between the 14-member ensemble mean (domain averaged 62.03 mm $month^{-1}$) and the CFSR (domain averaged 63.29 mm $month^{-1}$) is apparently smaller than the difference between the 5-member ensemble mean (domain averaged 56.71 mm $month^{-1}$) and CFSR.

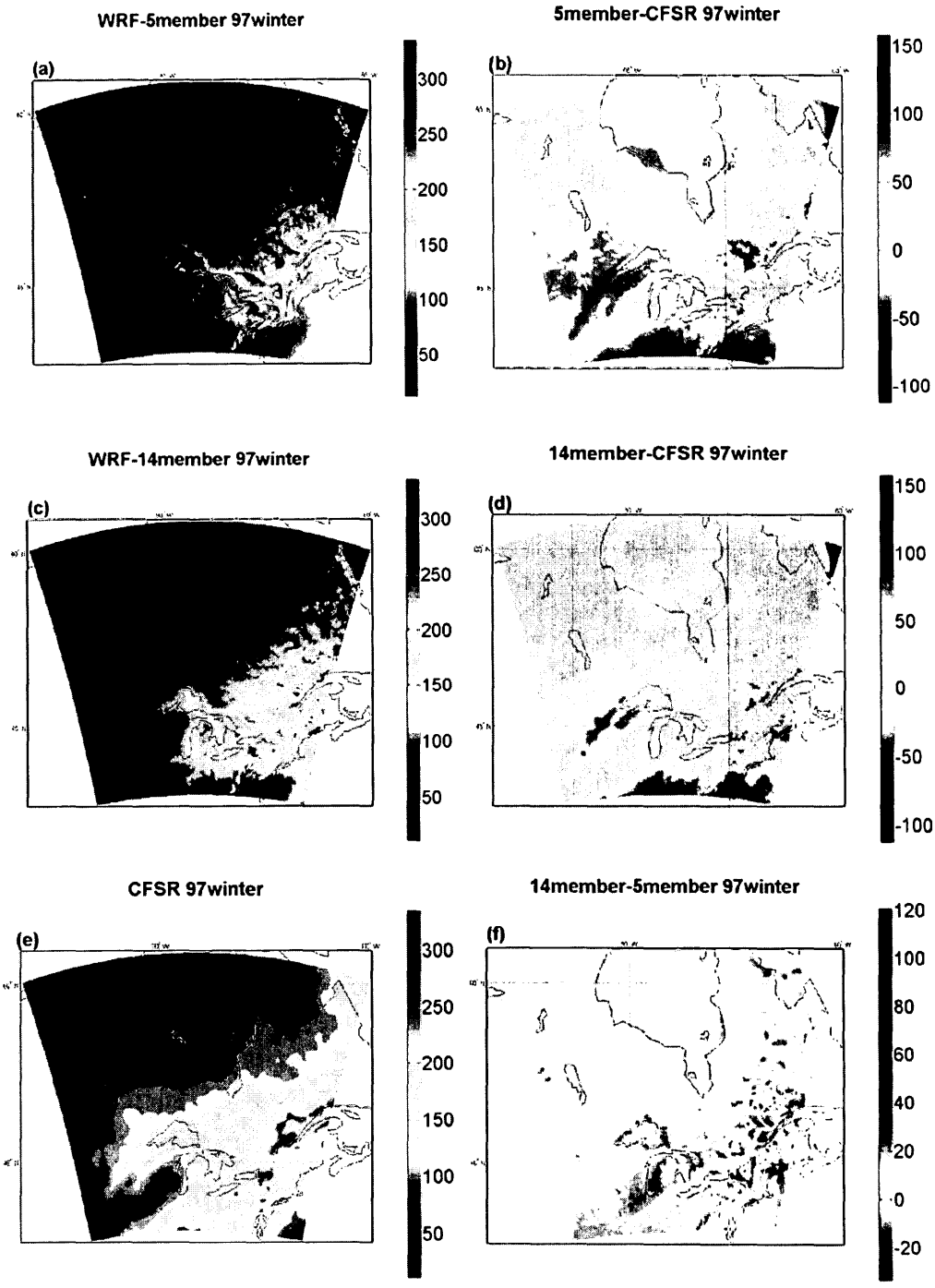

Figure 5. 6: 1997 winter mean monthly precipitation (unit: mm month^{-1}). (a) WRF 5member ensemble mean, (b) WRF 5member ensemble mean – CFSR (c) WRF 14member ensemble mean, (d) WRF 14member ensemble mean – CFSR, (e) CFSR data, (f) WRF 14member ensemble mean – WRF 5member ensemble mean.

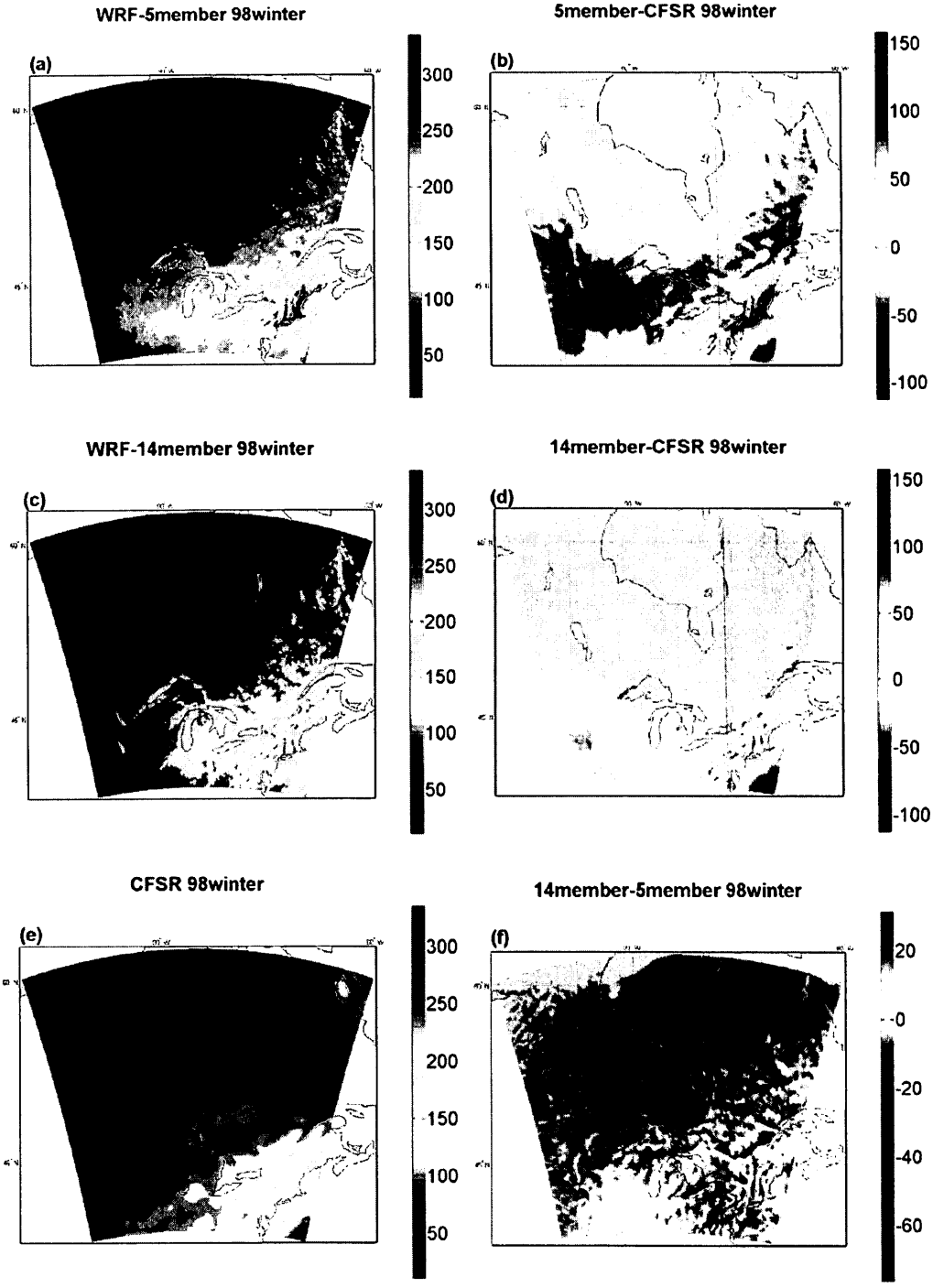

Figure 5. 7: 1998 winter mean monthly precipitation (unit: mm month^{-1}). (a) WRF 5member ensemble mean, (b) WRF 5member ensemble mean – CFSR (c) WRF 14member ensemble mean, (d) WRF 14member ensemble mean – CFSR, (e) CFSR data, (f) WRF 14member ensemble mean – WRF 5member ensemble mean.

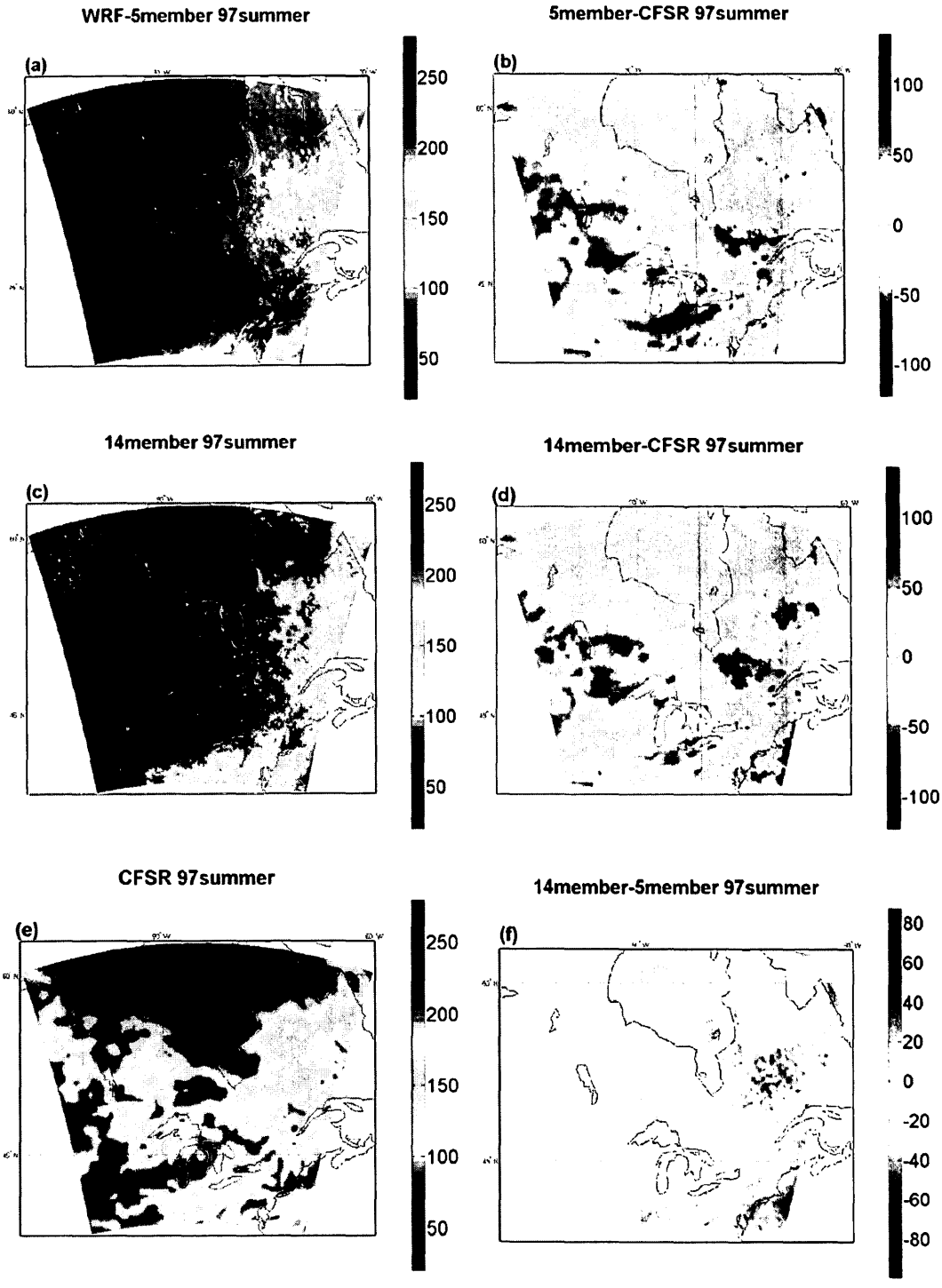

Figure 5. 8: 1997 summer mean monthly precipitation (unit: mm month^{-1}). (a) WRF 5member ensemble mean, (b) WRF 5member ensemble mean – CFSR (c) WRF 14member ensemble mean, (d) WRF 14member ensemble mean – CFSR, (e) CFSR data, (f) WRF 14member ensemble mean – WRF 5member ensemble mean.

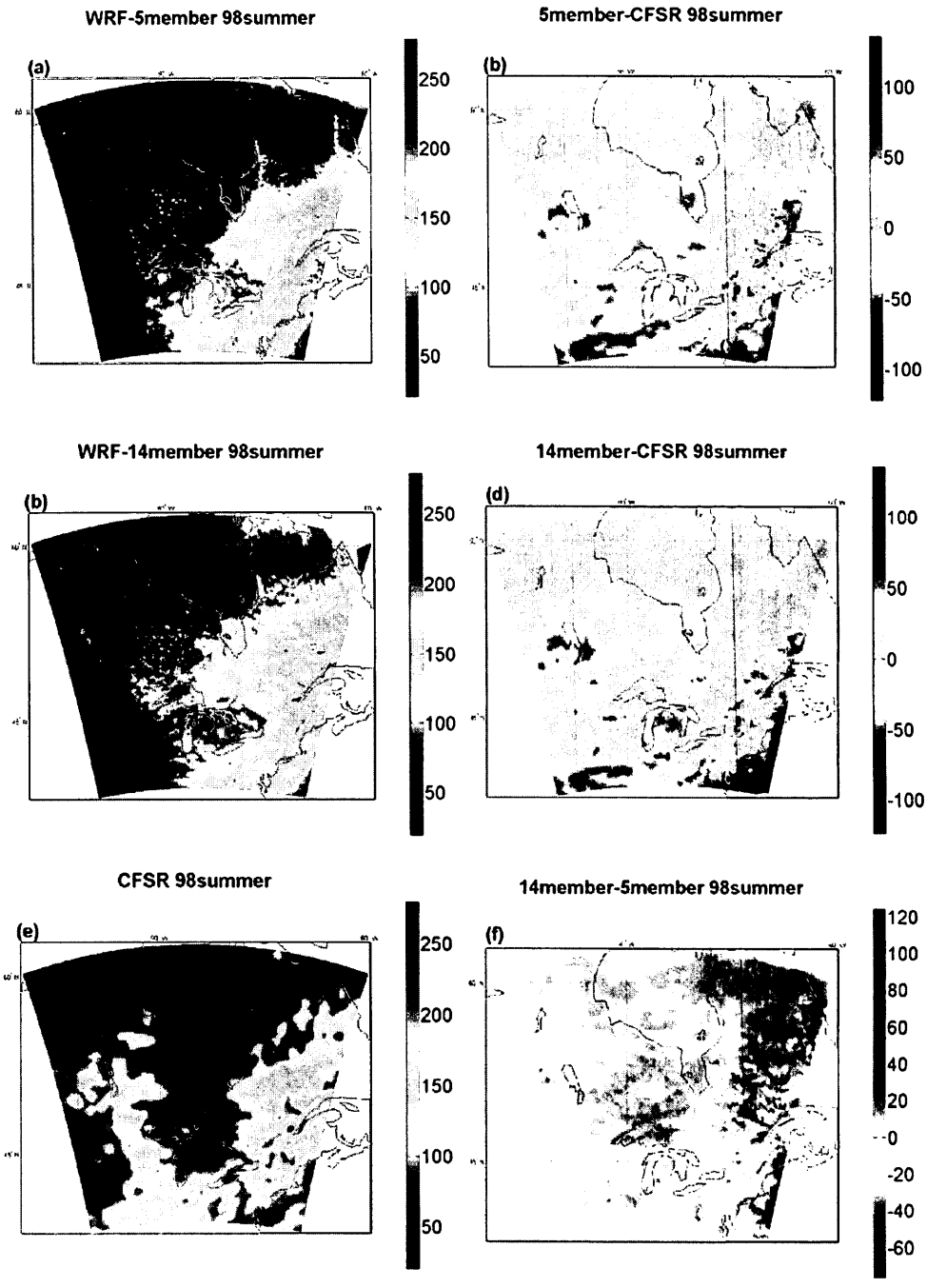

Figure 5. 9: 1998 summer mean monthly precipitation (unit: mm month^{-1}). (a) WRF 5member ensemble mean, (b) WRF 5member ensemble mean – CFSR (c) WRF 14member ensemble mean, (d) WRF 14member ensemble mean – CFSR, (e) CFSR data, (f) WRF 14member ensemble mean – WRF 5member ensemble mean.

Table 5.2 summarizes the domain averaged precipitation amount in winter and summer of 1997 and 1998. The 14-member ensemble mean always reduce the differences between the model and the CFSR values. The improvements are more significant in the winter seasons as expected.

Table 5. 2: domain averaged precipitation (mm month^{-1}) in winter and summer of 1997 and 1998 (brackets show the difference between ensemble means and the CFSR)

	CFSR	5-member ensemble mean	14-member ensemble mean
Winter 1997	76.18	57.66 (-18.52)	63.22 (-12.96)
Winter 1998	63.29	56.71 (-6.58)	62.03 (-1.26)
Summer 1997	89.49	76.68 (-12.81)	77.68 (-11.81)
Summer 1998	89.71	87.55 (-2.16)	90.12 (0.41)

Table 5.3 compares the correlations and the RMSEs of the seasonal domain-averaged precipitation rate with the CFSR data. The precipitation correlations are not as high as the temperature correlations. Only one value is greater or equal to 0.7. Compared to the CFSR precipitation, there are moderate improvements of 14-member ensemble mean over 5-member ensemble mean. The 14-member ensemble RMSE has a larger RMSE in fall, which is the only worse RMSE in the four seasons. The differences are also small, which is similar to the temperature differences.

Table 5. 3: Correlation (COR) coefficient and RMSE (Units: mm month^{-1}) between CFSR and simulated seasonal precipitation rate using WRF for 1997 and 1998.

	Spring	Summer	Fall	Winter	Annual
COR-5member	0.67	0.65	0.61	0.60	0.63
COR-14member	0.70	0.68	0.65	0.66	0.68
RMSE-5member	16.74	17.86	16.88	15.24	16.80
RMSE-14member	15.25	17.12	17.01	15.20	16.21

5.4 The spread of the WRF ensembles

Previous analyses have shown one main advantage of using the ensemble technique in regional climate simulations, that is the ensemble mean is very likely closer to the true atmospheric state. Another major advantage of the ensemble method is that the ensemble spread can be utilized to infer climate uncertainties. The ensemble spread represented by the sample standard deviation (Std) is to measure the differences among the ensemble members. In this section, we only briefly discuss the ensemble spread obtained in our simulations and their possible relationship with the uncertainty.

Figures 5.10 and 5.11 portray the ensemble spreads of the 2-m temperature, while Figs. 5.12 and 5.13 depict the ensemble spreads of the precipitation. Overall, increasing ensemble size by 9 does not change the spread patterns. The horizontal distributions of the ensemble spread in temperature vary from one season to another.

In winter, the ensemble spread of temperature is significantly larger in the northern part of the domain than in the southern part. In summer, the ensemble spread pattern shows that the maximum spread is now located along the west to southwest of the domain. We suspect that the large ensemble spread is caused partly by the spread in the driving NARCCAP models and partly by the model physics in the interior domain. The maximum ensemble spread corresponds to strong temperature gradient in the ensemble mean field (c.f. Figs. 5.1 – 5.4). In these regions, any deviation in wind or temperature field will result in larger uncertainties. It can also be noted

that the spread over the open water (Atlantic Ocean and the Hudson Bay in summer) is small owing to its large heat capacity and stable sea surface temperature which modulate the near surface air temperature.

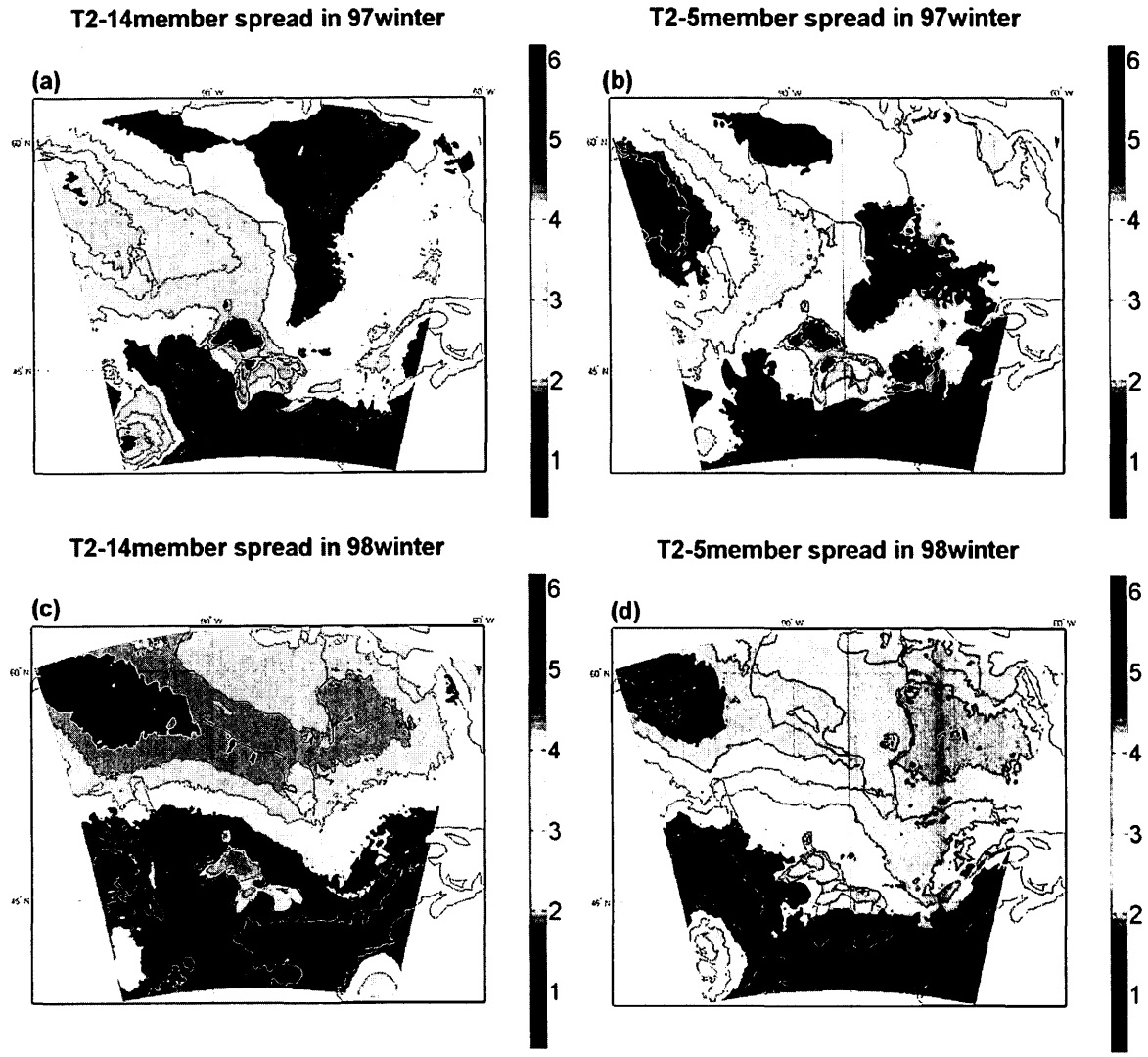

Figure 5. 10: The T2 ensemble spreads of 14-member and 5-member ensemble mean in winter. (a) 14-member spread in 1997, (b) 5-member spread in 1997, (c) 14-member spread in 1998, (d) 5-member spread in 1998 (unit: °C).

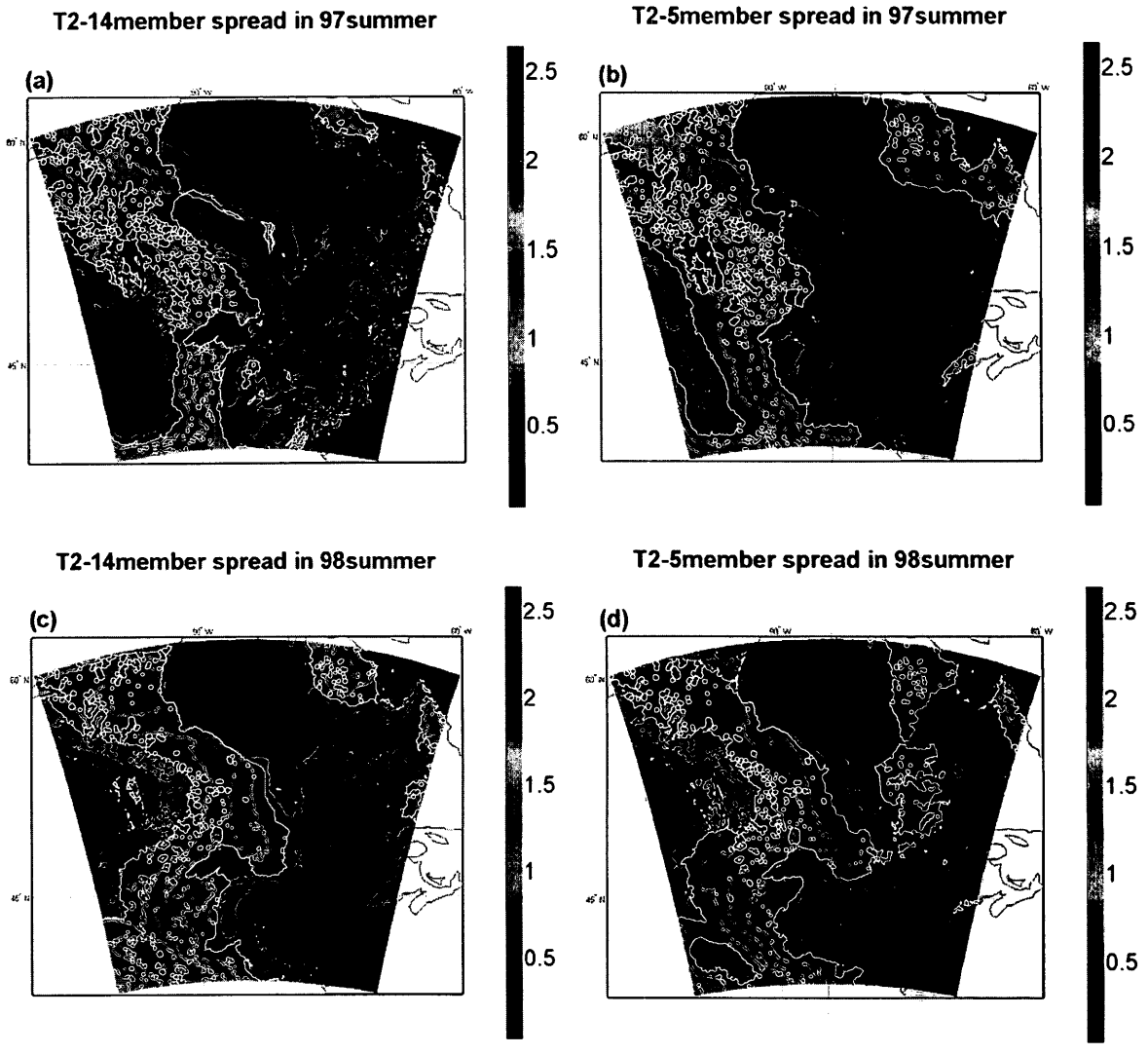

Figure 5. 11: The T2 ensemble spreads of 14-member and 5-member ensemble mean in summer. (a) 14-member spread in 1997, (b) 5-member spread in 1997, (c) 14-member spread in 1998, (d) 5-member spread in 1998 (unit: °C)

The ensemble spread of precipitation has less organized patterns in the interior domain (Figs. 5.12, 5.13). The largest spread are all located along the east boundary, close to regions of the maximum ensemble mean precipitation. The summer precipitation ensemble spread is larger than the winter one once again indicates large uncertainties in predicting summer convections.

Interestingly, adding random perturbations in the model fields by the SKEB scheme does not increase the spread of the precipitation in the interior domain, instead the spread is reduced. Another noticable feature is the large spread southwest of the Great Lakes which is corresponding to the large precipiation band in the summer mean precipitation. It indicates the model, at least some ensemble members, is able to capture the precipitable processes in that region. Using the ensemble members, we will be able to identify the physical processes leading to that precipitation band.

Based on the ensemble spreads of temperature and precipitation, we can quantify the reliability of the regional climate predictions depicted by the ensemble mean. Smaller (larger) ensemble spread represents smaller (larger) model errors and smaller (larger) uncertainties, which indicates that the ensemble results are more (less) reliable. For example, the winter temperature prediction in southeast Ontario is more reliable than that in the northwest due to not only its smaller errors (c.f. Fig. 5.1 d), but also smaller ensemble spread (c.f. Fig. 5.10 a). Using the ensemble products to study climate uncertainty will be a subject for the future study.

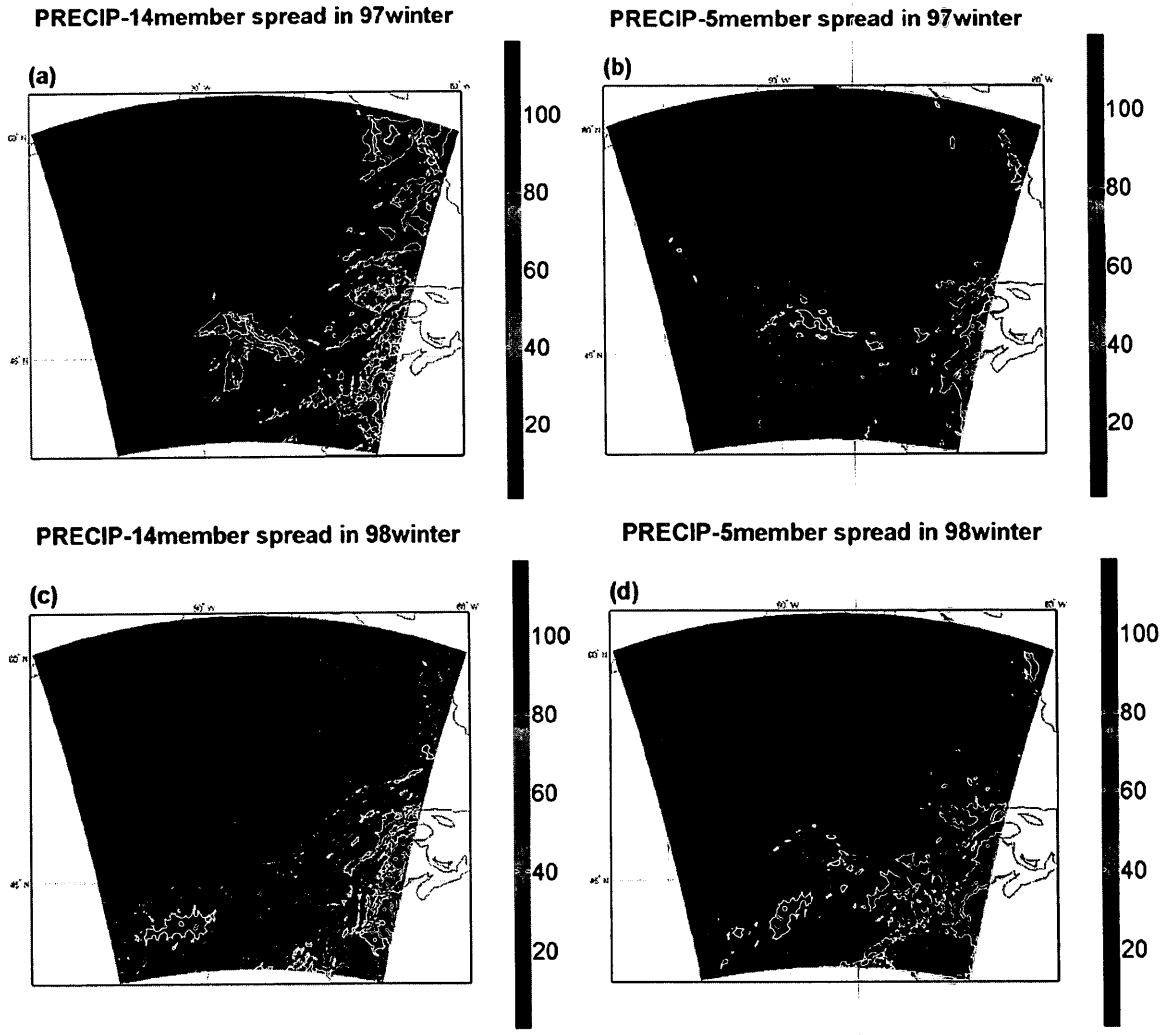

Figure 5. 12: The monthly precipitation ensemble spreads of 14-member and 5-member ensemble mean in winter. (a) 14-member spread in 1997, (b) 5-member spread in 1997, (c) 14-member spread in 1998, (d) 5-member spread in 1998 (unit: mm month^{-1})

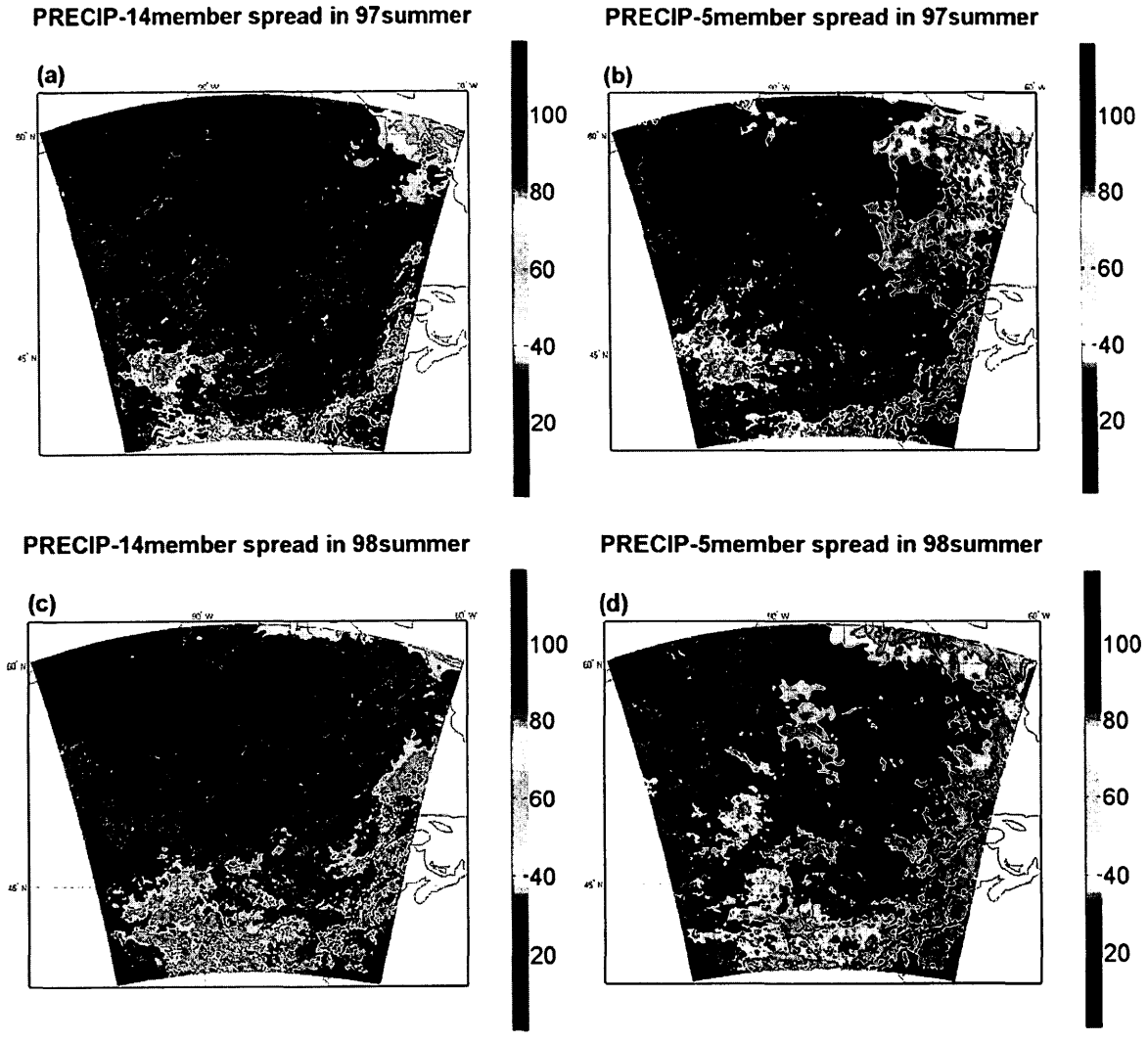

Figure 5. 13: The monthly precipitation ensemble spreads of 14-member and 5-member ensemble mean in summer. (a) 14-member spread in 1997, (b) 5-member spread in 1997, (c) 14-member spread in 1998, (d) 5-member spread in 1998 (unit: mm month^{-1})

Chapter 6 Discussions and Conclusions

This chapter provides a synopsis of the objectives of this thesis and summarizes the major conclusions from the results and findings obtained from the research.

6.1 Review of the thesis and objectives

This thesis set out a number of objectives related to regional climate simulations over Ontario. Chapter 1 introduced the climate changes during recent decades. It explained how the regional climate models worked and developed, and how ensemble simulations may help to improve the regional climate simulations. Chapter 2 discussed the methodologies used in this thesis, including some statistical methods, the WRF model downscaling and the SKEB scheme for generating ensembles. The studied domain was centered in Ontario and covered its surrounding area, including the Great Lakes, the Hudson Bay, and some adjacent provinces in Canada and states in the United States. Chapter 3 analyzed the climate data provided by NARCCAP from 1979 to 2004, for both temperature and precipitation. The possible reasons why the extremely warm, cold, dry and wet seasons form were discussed in Appendix A and B. Chapter 4 discussed the results of the WRF downscaling simulations driven by five NARCCAP regional climate model data. Chapter 5 presented the results of the perturbed ensemble simulations using the SKEB scheme in 1997 and 1998.

6.2 Research outcomes and conclusions

In this study, the NARCCAP regional climate simulations and the observations were analyzed and compared. The ensemble regional climate downscaling simulation over Ontario using the WRF model was the most predominant part of this thesis. The results were evaluated against station observations and NCEP CFSR reanalysis data. The benefits of using the ensemble mean to represent climatological mean state were revealed using 3 sets of ensembles. The potential advantages of using the ensemble spread to study climate uncertainties were also suggested.

6.2.1 The analysis of the observations and NARCCAP temperature and precipitation data

An assessment of the 8-station observations and seven NARCCAP model data was conducted. All the models follow the observed patterns reasonable well. Some models have constantly high biases (HRM3 and ECPC) and others have low biases (RCM3 and CRCM). The high and low biases also appear accordingly in the annual or seasonal mean daily maximum and minimum temperatures. The observed annual area mean temperature has a remarkable rising trend in the late 1990s, which is mainly due to the significant rises of the spring and winter area mean temperatures. All seven NARCCAP model simulations show this trend.

Annual average and winter average temperature variation over Ontario both have two significant periods: 3.7 years (the most significant period) and 13 years (the second most significant), while summer average temperature has 3.7-year (the most significant) and 6.5-year (the second most

significant) periods. CRCM, ECP2, ECPC, WRFG and HRM3 indicate the same periods as the observations, while the variation periods in MM5I and RCM3 are different.

The EOF analysis shows that the dominant temperature variation modes, depicted by the first EOF mode accounting for more than 80% of the total variance, has a good spatial accordance over Ontario. The time coefficient of the first EOF mode in all the NARCCAP models reveal the same remarkable rising trend at the end of the 20^{th} century.

The observed annual area mean precipitation stays nearly steady during 1979-2004. The NARCCAP model simulations show large discrepancies both in amount and trend. The variation in the precipitation observations revealed by the spectral analysis show the most significant oscillation periods are 2.1-year and 4.3-year. Fewer NARCCAP models share the same significant modes, but most of them show peaks in other frequencies. It also suggests that the precipitation is less predictable than the temperature in climate simulations, partly due to the unresolved warm season convections.

6.2.2 The analysis of the WRF simulations driven by the NARCCAP data

Five NARCCAP RCM model results (MM5I, RCM3, HRM3, CRCM and WRFG) from 1991 to 1998 were used to provide initial and boundary conditions for the downscaling simulations using the WRF model. The WRF model domain has 300×300 horizontal grid points with a 10-km grid resolution centered in Ontario. The results showed that improving the representations of surface

topography, land use, convections, and other local physical processes via high resolutions has great impact on the climate simulations.

All the five WRF simulations with different NARCCAP initial and boundary conditions show colder temperatures than their corresponding NARCCAP model simulations. From 1991 to 1998, the domain averaged temperature in the NCEP CFSR data lies mostly between the 7-member NARCCAP ensemble mean temperature and the 5-member WRF ensemble mean temperature. When interpolated onto the 8 stations in Ontario and compared to the station observations, the WRF ensemble mean outperforms the NARCCAP ensemble mean. But the range of the temperature extreme, measured by the maximum and minimum temperatures, in this 5-member WRF ensemble mean appears larger than in the observations or in the NARCCAP ensemble mean.

Increasing resolutions do not always increase the domain-averaged precipitation amount. Among the five downscaling simulations, the annual mean precipitation is enhanced only in HRM3, WRFG, and in particular MM5I driven WRF simulations. Both the NARCCAP ensemble mean and the WRF ensemble mean produce less precipitation than the CFSR data. The WRF ensemble mean precipitation is closer to not only the CFSR precipitation data but also the station observations.

For the time mean horizontal temperature and precipitation over the entire period, the high resolution WRF ensemble mean shows some finer-scale details which otherwise cannot be resolved by the NARCCAP ensemble mean. In particular, the cold temperature related to small

lakes and enhanced precipitation bands related to water body and mountains are captured in the high-resolution WRF ensemble mean.

6.2.3 The analysis of the stochastic WRF ensemble simulations

In the last chapter, the SKEB scheme was used to generate more ensemble members by adding small perturbations to the model fields at every time step. Nine SKEB scheme members were combined with the five WRF simulations to form a 14-member ensemble. The results showed that the new ensemble mean performs better than the original 5 WRF model ensemble mean in temperature and precipitation simulation. The new ensemble also dramatically reduced the excessive temperature extremes, i.e., the maximum and minimum temperatures. The simulations of temperature all show the temperature rise from 1997 to 1998. The 14-member ensemble mean has smaller spreads in most part of the domain.

Based on the ensemble spreads of temperature and precipitation, the reliability of the regional climate predictions depicted by the ensemble mean can be quantified. Using the ensemble products to study climate uncertainty will be a subject for the future study.

6.3 Limitations

It is worth noting that the periods for the WRF simulation (1991 -1998) and the stochastic ensembles (1997-1998) are very short. The ensemble size is also too small in the practical standard in the weather and climate modeling community. The improvements in climate

simulations using the ensemble downscaling method are noticeable, but they are often not very statistically significant. This research serves as our first attempt in this relatively new field. Based on the experiences gained, a better ensemble RCM system will be designed and longer simulations will be conducted for both the current and future climate.

Appendices

Appendix A: Circulations in extremely cold and warm winters

Using the NCEP-DOE reanalysis II data, several factors contributing to the extremely cold and warm winters were discussed here. Figure A.1 shows the sea level pressure averaged over all winter seasons from 1979 to 2004. It is noticeable that a high centre is located over the continent of North America. This prominent high pressure system can drive cold air mass southward from the Arctic region into the mid-latitude region. Over the Atlantic Ocean, Icelandic Low and Azores High are stronger in winter than in summer.

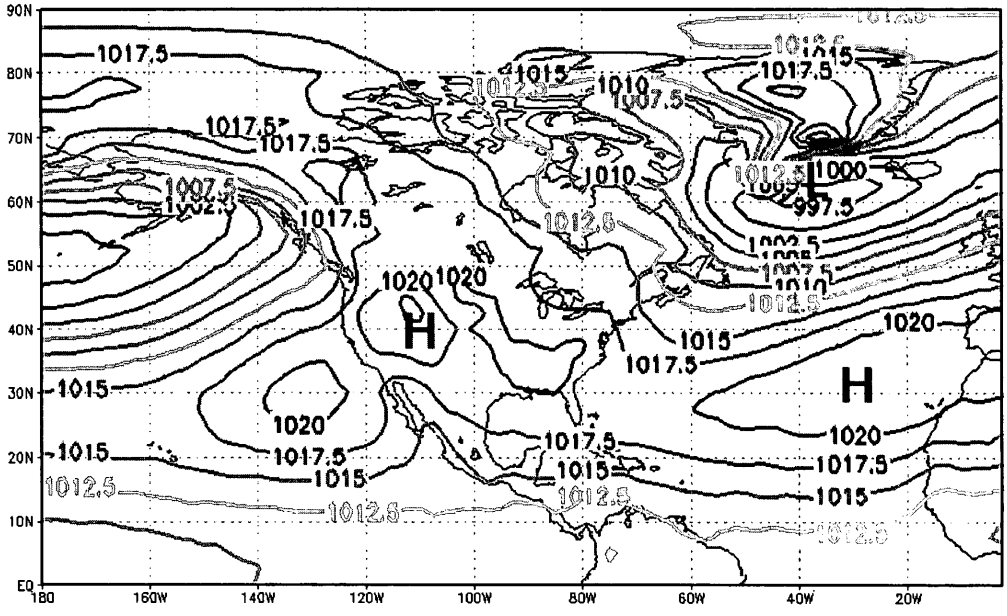

Figure A. 1: Average winter sea level pressure (unit: hPa) from 1979 to 2004.

In extremely cold winters, the North American High is stronger than the average by 1~2hPa (Fig. A.2-a). Stronger southward winds over Ontario and regions to its north advect more cold air southward, leading to the low temperature in Ontario. In the warm winters, the North American High is weaker than average by 2~3hPa (Fig. A.2-b). The surface temperature advection fields clearly demonstrated the consequence the North American High being stronger or weaker. In cold winters, Ontario and its surrounding area are dominated by the cold air advection (Fig. A.3-a). The magnitude can exceed -3×10^{-5} °C s^{-1} (-2.6 °C per day) in most areas of Ontario. Considering the wind and temperature fields can be separated into an average state and an anomaly part, the temperature advection ($-\vec{V} \cdot \nabla T$) can also be decomposed into 4 parts, i.e., the mean temperature advection ($-\bar{\vec{V}} \cdot \nabla \bar{T}$), two first order terms ($-\bar{\vec{V}} \cdot \nabla T'$) and ($-\vec{V}' \cdot \nabla \bar{T}$), and one second order term ($-\vec{V}' \cdot \nabla T'$). The magnitude of the mean advection term is in the order of 10^{-5} °C s^{-1}. The magnitudes of the two first order terms are both 10^{-6} °C s^{-1}, but their total is in the same order of the mean. This indicates that the mean advection and the first order terms are both very important to the temperature change. Therefore, the wind and temperature anomalies associated with the sea-level pressure anomaly in the North American High contribute significantly to the cold or warm winter temperatures. In warm winters, the northerly wind anomaly is not obvious. The temperature advection is positive over most areas of Ontario (Fig. A.3-b).

The cross sections of the horizontal wind speed across Ontario (280° longitude) in extremely cold and warm winters are plotted in Fig. A.4. Both cross sections show jets reach their highest wind speed at 200hPa (a little lower in warm winters). But the jet core in the warm winters is weaker, it is also shifted several degrees northward. The location and the strength of the jet

stream may control the occurrence of the baroclinic weather systems, which in turn influences the temperature variation in winter seasons over Ontario.

To accurately diagnose the temperature change, we will also need to consider adiabatic and diabatic heatings, which are not discussed in this thesis.

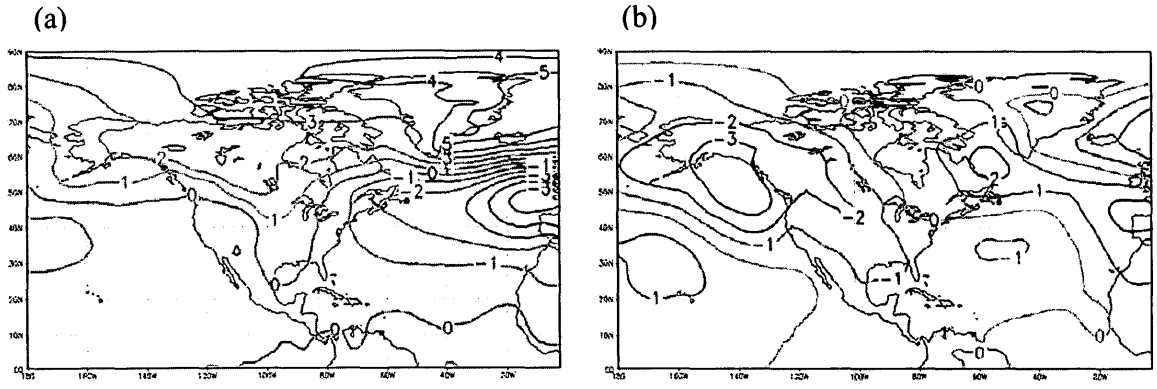

Figure A. 2: Anomaly fields of sea level pressure (unit:hPa) of (a) 3 coldest winters and (b) 4 warmest winters in Ontario.

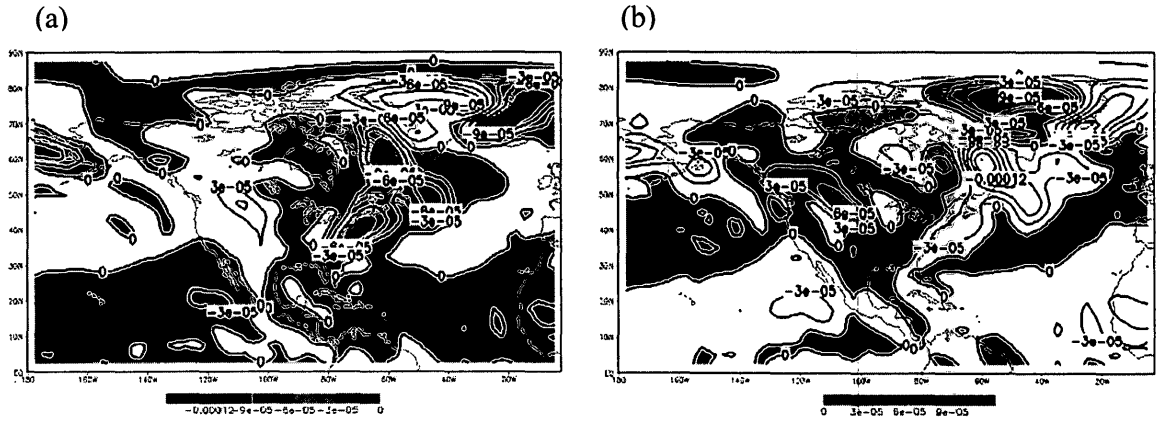

Figure A. 3: Surface temperature advection (unit: °C s^{-1}) in (a) 3 coldest winters and (b) 4 warmest winters in Ontario.

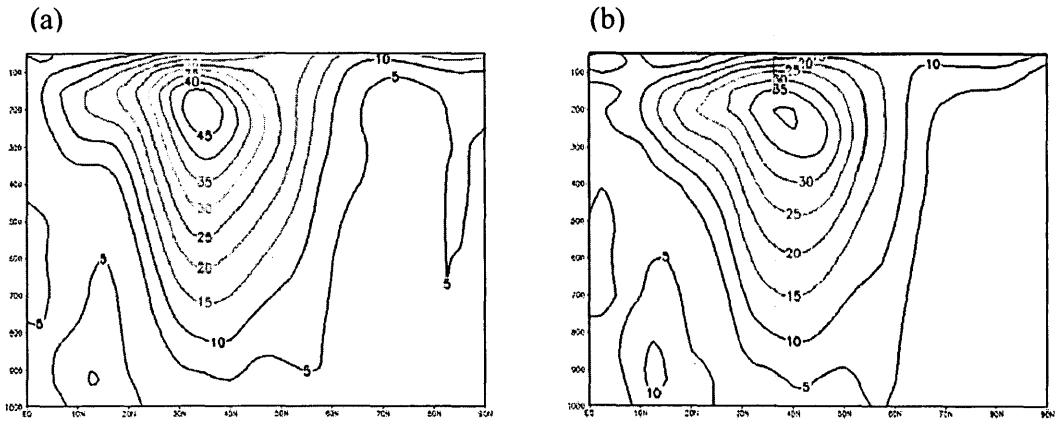

Figure A. 4: cross sections of composite wind (unit: m s^{-1}) at 280° longitude of (a) 3 coldest winters and (b) 4 warmest winters in Ontario.

Appendix B: Circulations in extremely dry and wet winters

As shown in Fig. A.1, the North American High at the sea level controls a large area over North America. Another system at the sea level that can affect Ontario is the low pressure center over the North Atlantic Ocean. Between these two big systems, cold and dry northerly wind is relatively easy to reach to Ontario in winter. Thus, winter does not have as much precipitation as the other three seasons.

When Ontario has positive precipitation anomaly, North American High has a negative anomaly centre (-2hPa), while there is a positive pressure anomaly center over West Atlantic. This pressure anomaly gyre switches signs when Ontario is drier than average (Fig. B.1).

According to geostrophic balance theory, the pressure anomaly gyre is associated with northerly and southerly wind anomalies in the drier and wetter winters, respectively. The wind anomalies can be also seen on 850hPa (Fig. B.2). In dry winters, the northeasterly to northerly wind anomalies tend to bring cold and dry air to Ontario (Fig. B.2-a). The wind anomalies also diverge over Ontario. In the wet winters, both the facts that the the 850hPa wind anomalies reverse in the their directions to southwesterly and the wind anomalies converge especially in east Ontario are all favourable for more precipitation over Ontario.

Meanwhile, Fig. B.3 indicates that for dry winters, the North American trough is deeper than average (-40gpm). Deep North American trough brings more cold air southward to Ontario. But for wet winters, the trough is weaker by 20gpm than average and a negative geopotential height anomaly occurs at high-latitude (not shown). Such distributions of the geopotential height

correspond to the fact that Ontario or even east of North America has an anomalous northward wind component in the mid-level, as well as in the low-level (850hPa).

Moreover, the North American high level jet stream is stronger than average when in dry winters, while weaker jet in wet winters (Fig. B.4).

The necessary conditions for winter stratiform precipitation contain intersections of the cold and warm air, the large-scale ascent and sufficient moisture. Figure B.5 portrays the vertical-latitudinal cross sections of the mean specific humidity anomaly between 270°E and 290°E. Ontario is between 41°N and 57°N. It is noticeable that in wet winters, the corresponding specific humidity field has a large-scale positive anomaly from the surface to around 400hPa, while there is a wide range of dry anomaly in the dry winter. Moreover, the upward motion over Ontario in wet winters is significant. Although there is also upward motion in dry winters, it is much weaker.

Figure B.6 depicts the vertically integrated horizontal water vapor flux anomaly and its divergence. Although the magnitude of moisture flux anomaly in Ontario is comparatively smaller than those in the low-latitude region, it can be clearly seen that in wet winter (Fig. B.6-b), the moisture flux anomaly in Ontario maintains a direction from southwest to northeast, with a negative moisture flux divergence, which means that moisture is converging in this area and may lead to more precipitation. The main moisture source is the Gulf of Mexico and the Atlantic Ocean. When a negative precipitation anomaly occurs, anomalous moisture fluxes point to southwest and diverge in Ontario.

In total, the favorable conditions to form a wet winter include anomalous southerly wind, excessive low-level moisture and large-scale upward motions lifting moisture to high levels.

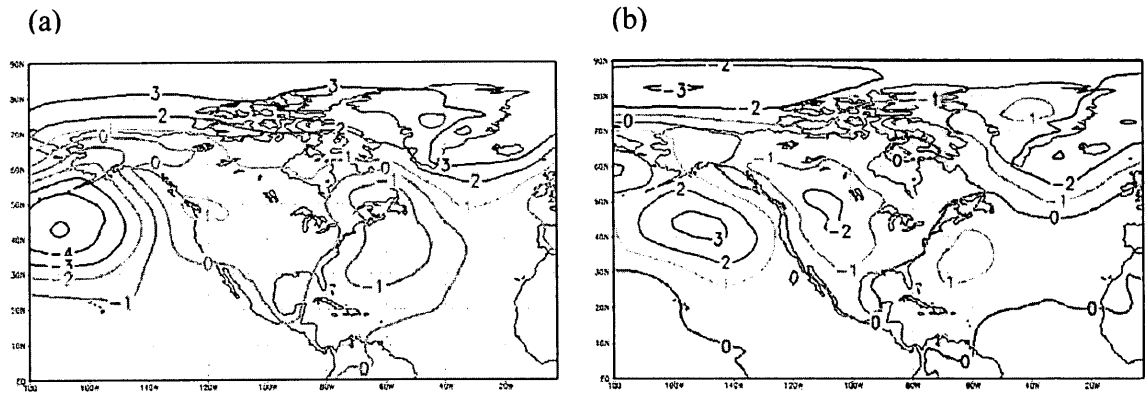

Figure B. 1: Anomaly fields of sea level pressure (unit:hPa) of (a) 2 driest winters and (b) 2 wettest winters in Ontario.

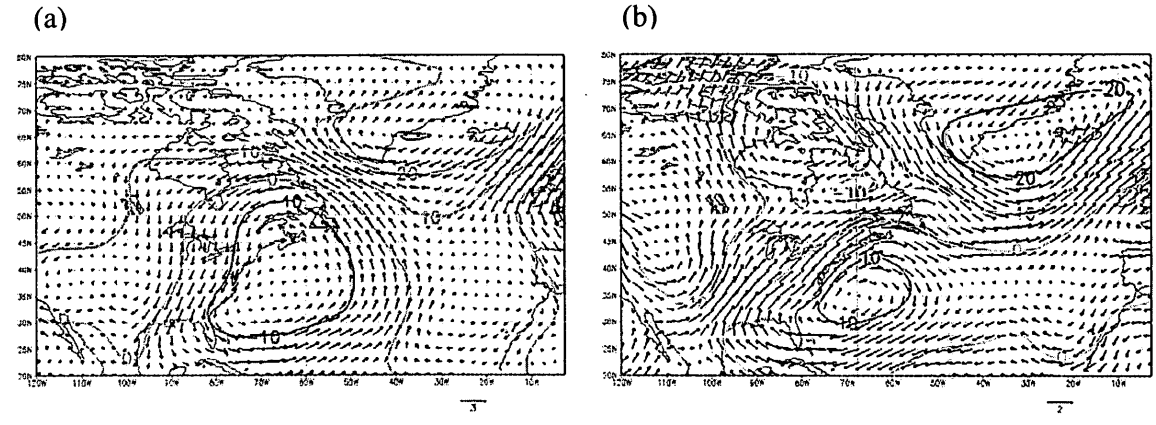

Figure B. 2: Anomaly fields of 850hPa horizontal winds (vectors, m s^{-1}) and geopotential heights (gpm) of (a) 2 driest winters and (b) 2 wettest winters in Ontario.

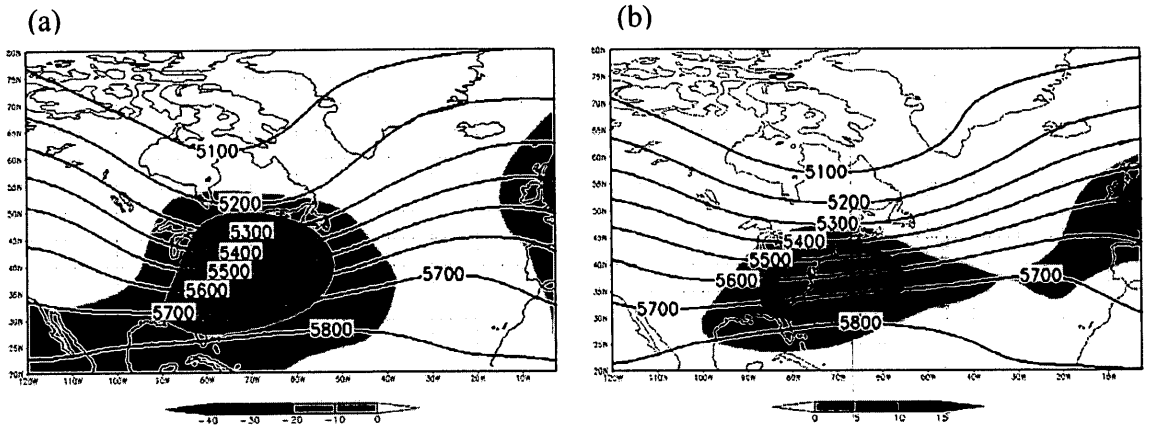

Figure B. 3: Anomaly fields of 500hPa geopotential heights (gpm) of (a) 2 driest winters and (b) 2 wettest winters in Ontario.

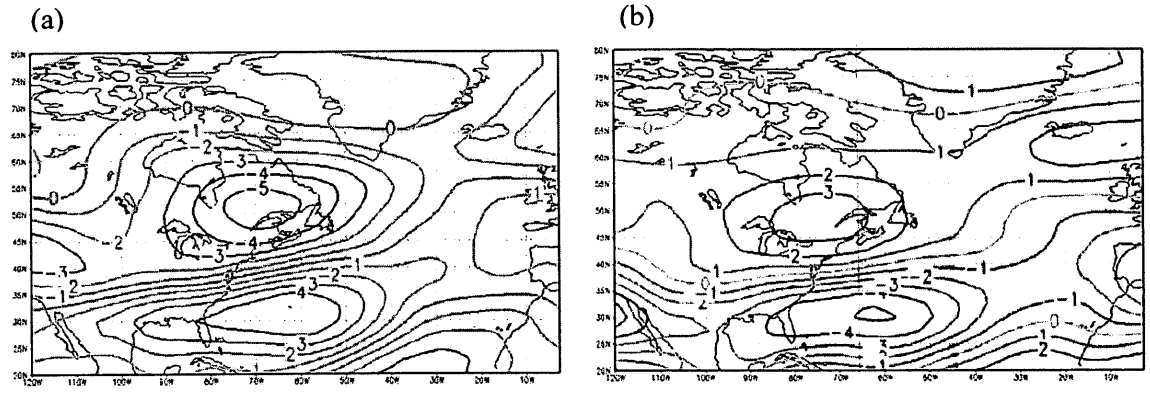

Figure B. 4: Anomaly field of 200hPa jet stream (m s^{-1}) of (a) 2 driest winters and (b) 2 wettest winters in Ontario.

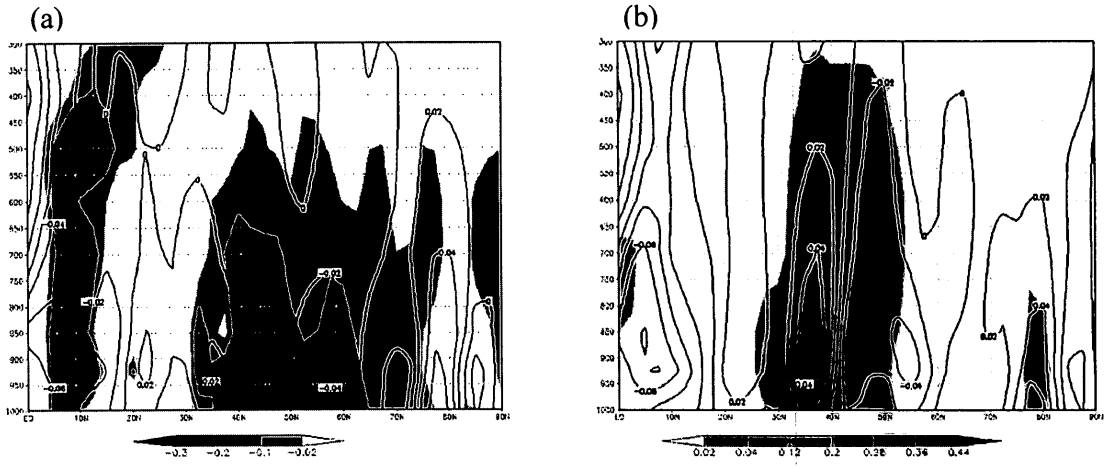

Figure B. 5: Vertical and latitudinal cross sections (averaged between 270°E and 290°E) of the vertical velocity (contours, unit:Pa s^{-1}) and specific humidity (SH) anomalies (shaded, unit:g kg^{-1}) in (a) the driest winters and (b) the wettest winters (shading : left: SH negative anomaly smaller than -0.02g kg^{-1}, right: SH positive anomaly greater than 0.02g kg^{-1}).

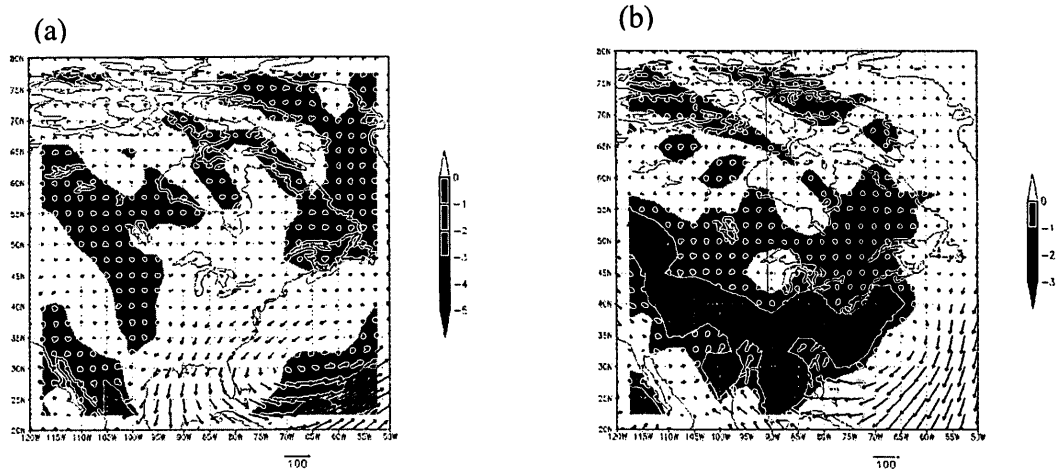

Figure B. 6: Vertically integrated anomaly moisture flux (vectors, kg $(m \cdot s)^{-1}$) and anomaly moisture flux divergence (shaded parts, 10^{-6} g $(cm^2 \cdot hPa \cdot s)^{-1}$) from 1000 hPa to 300 hPa for (a) rain-abundant and (b) rain-scarce winters in Ontario.

Reference

[1]Alexandru, A., R. de Elia, and R. Laprise, 2007: Internal variability in regional climate downscaling at the seasonal scale. Mon. Wea. Rev., **135**, 3221–3238.

[2]Barker, T.W., 1991: The relationship between spread and forecast error in extended-range forecasts. J. Climate, **4**, 733–742.

[3]Berner, J., S.Y. Ha, J.P. Hacker, A. Fournier and C. Snyder, 2011: Model Uncertainty in a Mesoscale Ensemble Prediction System: Stochastic versus Multiphysics Representations. Mon. Wea. Rev., **139**, 1972–1995.doi: http://dx.doi.org/10.1175/2010MWR3595.1

[4]Bourdages, L. and D. Huard, 2010: Climate Change Scenario over Ontario Based on the Canadian Regional Climate Model (CRCM4.2), OURANOS. Retrieved June 29, 2013, from http://www.ouranos.ca/Ontario/Results_html/Rapport.pdf.

[5]Bowden, J.H., T.L. Otte, C.G.Nolte and M.J.Otte, 2012: Examining Interior Grid Nudging Techniques Using Two-Way Nesting in the WRF Model for Regional Climate Modeling. J. Climate, **25**, 2805–2823.doi: http://dx.doi.org/10.1175/JCLI-D-11-00167.1

[6]Buizza, R., 1997: Potential forecast skill of ensemble prediction and spread and skill distributions of the ECMWF ensemble prediction system. Mon. Wea. Rev., **125**, 99–119.

[7]Bukovsky, M.S. and D.J. Karoly, 2009: Precipitation Simulations Using WRF as a Nested Regional Climate Model. J. Appl. Meteor. Climatol., **48**, 2152–2159.

[8]Cao, Z. and J. Ma, 2009: Summer severe-Rainfall frequency trend and variability over Ontario, Canada. J. Climate Appl. Meteor., **48**, 1955-1960.

[9]Charron, M., G. Pellerin, L. Spacek, P. L. Houtekamer, N. Gagnon, H. L. Mitchell, and L. Michelin, 2010: Toward random sampling of model error in the Canadian Ensemble Prediction System. Mon. Wea. Rev., 138, 1877–1901.

[10]Chien, F.C., Y.C. Liu, and B.J.D. Jou (2006), MM5 ensemble mean forecasts in the Taiwan area for the 2003 Mei-yu season, Weather Forecast., **21**, 1006–1023

[11]Chu, G., Q. Sun, X. Wang, and J. Sun, 2008: Snow anomaly events from historical documents in eastern China during the past two millennia and implication for low-frequency variability of AO/NAO and PDO. Geophys. Res. Lett., **35**, L14806.

[12]Collins, W.D., P.J. Rasch, B.A. Boville, J,J, Hack, J.R. McCaa, D.L. Williamson, J.T. Kiehl, B. Briegleb, C. Bitz, S-J. Lin, M. Zhang, Y. Dai, 2004: Description of the NCAR community atmosphericmodel (CAM 3.0). NCAR Tech. Note, NCAR/TN-464+STR, 226.

[13]Collins, W.G., 1983: Vertical Interpolation of Heights and Temperatures for Model Input/output. Retrieved 25th July, 2013 from http://www.ncep.noaa.gov/officenotes/NOAA-NPM-NCEPON-0004/014083F2.pdf.

[14]Doblas-Reyes, F.J. M. Déqué, and J-P. Piedelievre, 2000: Multi-model spread and probabilistic forecasts in PROVOST. Quart. J. Roy. Meteor. Soc., **126**,2069–2087.

[15]Environment Canada, 2013: National Inventory Report.

[16]Forest, C. E., P. H. Stone, A. P. Sokolov, M. R. Allen, and M. D. Webster, 2002: Quantifying uncertainties in climate system properties with the use of recent climate observations.Science, **295**, 113–117.

[17]Frederiksen, J. S., and A. G. Davies, 1997: Eddy viscosity and stochastic backscatter parameterizations on the sphere for atmospheric circulation models. J. Atmos. Sci., 54, 2475–2492.

[34]Lambert, S.J. and G.J. Boer, 2001: CMIP1 evaluation and intercomparison of coupled climate models., Climate Dyn. **17**, 83-106.

[35]Leung, L. R. and Y. Qian, 2003: The sensitivity of precipitation and snowpack simulations to model resolution via nesting in regions of complex terrain. Journal of Hydrometeorology, **4**, 1025–1043.

[36]Leung, L.R. and Y. Qian, 2009: Atmospheric rivers induced heavy precipitation and flooding in the western U.S. simulated by the WRF regional climate model. Geophys. Res. Lett., **36**, L03820, doi:10.1029/2008GL036445.

[37]Leung, LR, Y.H. Kuo and J. Tribbia, 2006: Research needs and directions of regional climate modeling using WRF and CCSM. B Am Meteorol Soc, **87**, 1747–1751.

[38]Lo, J. C. F., Z. L. Yang, and R. A. Pielke Sr., 2008: Assessment of three dynamical climate downscaling methods using the Weather Research and Forecasting (WRF) model. J. Geophys. Res., **113,** D09112. doi:10.1029/2007JD009216.

[39]Mann, M. E., J. Park, and R. S. Bradley, 1995: Global interdecadal and century-scale climate oscillations during the past five centuries, Nature, **378**, 266– 270.

[40]McCarthy, M.P., C.Harpham, C.M.Goodess and P.D.Jones, 2011: Simulating climate change in UK cities using a regional climate model, HadRM3. Int. J. Climatol., **32**, 1875-1888. doi: 10.1002/joc.2402.

[41]Meehl, G. A., C. Covey, T. Delworth, M. Latif, B. McAvaney,J. F. B. Mitchell, R. J. Stouffer, and K. E. Taylor, 2007: TheWCRP CMIP3 multimodel dataset: A new era in climate change research. Bull. Amer. Meteor. Soc., **88**, 1383–1394.

[42]Mobley, C. D. and R. W. Preisendorfer, 1985: Statistical Analysis of historical climate data sets. J. Climate Appl. Meteor., **24**, 555-567.

[43]Munich Re, 2002: Topics, an annual review of natural catastrophes. Munich Reinsurance Company Publications, Munich, 49 pp.

[44]Murphy, J. M., 1988: The impact of ensemble forecasts on predictability. Quart. J. Roy. Meteor. Soc., **114**, 463–493.

[45]NARCCAP,2007: http://www.narccap.ucar.edu/.

[46]New, M., M. Todd, M. Hulme and P. Jones, 2001: Precipitation measurements and trends in the twentieth century. Int. J. Climatol., **21**, 1899–1922.

[47]Pal.J, F. Giorgi, X. Bi, N. Elguindi, F. Solmon, S. A. Rauscher, X. Gao, R. Francisco, A. Zakey, J. Winter, M. Ashfaq, F. S. Syed, L. C. Sloan, J. L. Bell, N. S. Diffenbaugh, J. Karmacharya, A. Konaré, D. Martinez, R. P. da Rocha, and A. L. Steiner, 2007: Regional climate modeling for the developing world: The ICTP RegCM3 and RegCNET. Bull. Amer. Meteor. Soc., **88**, 1395-1409.

[48]Patz, J.A., D. Campbell-Lendrum, T. Holloway and J.A. Foley, 2005: Impact of regional climate change on human health. Nature, **438**, 310-317.

[49]Qian, Y., S.J. Ghan, and L. R. Leung, 2010:Downscaling hydroclimatic changes over the Western US based on CAM subgrid scheme and WRF regional climate simulations. Int. J. Climatol., **30**, 675-693.

[50]Qian, Y. and L. R. Leung, 2007: A long-term regional simulation and observations of the hydroclimate in China. J. Geophys. Res., **112**, D14104, doi:10.1029/2006JD008134.

[51]Randel, W. J. and D. L. Williamson, 1990: A comparison of the climate simulated by the NCAR community climate model (CCM1:R15) with ECMWF analyses, J. Cliamte, **3**, 608-633.

[52]Roads, J. 2004. Experimental weekly to seasonal U.S. forecasts with the regional spectral model. Bull. Amer. Meteor. Soc. **85**, 1887–1902.

[53]Rougier, J., D. M. H. Sexton, J. M. Murphy and D. Stainforth, 2009: Analyzing the climate sensitivity of the HadSM3 climate model using ensembles from different but related experiments. J. Climate, **22**, 3540-3557.

[54]Shutts, G. J., 2005: A kinetic energy backscatter algorithm for use in ensemble prediction systems. Quart. J. Roy. Meteor. Soc., **131**, 3079–3102.

[55]Stahl, K., L. M. Tallaksen, L. Gudmundsson and J. H. Christensen, 2011: Streamflow data from small basins: A challenging test to high-resolution regional climate modeling, J. Hydrometeor, **12**, 900-912.

[56]Stensrud, D. J., J. W. Bao and T. T. Warner, 2000: Using initial condition and model physics perturbations in short-range ensemble simulations of mesoscale convective systems. Mon. Wea. Rev., **128**, 2077–2107.

[57]Storch, H.V. and F. W. Zwiers: Statistical analysis in climate research, Cambridge University Press, 2002.

[58]Tennant, Warren J., Glenn J. Shutts, Alberto Arribas, Simon A. Thompson, 2011: Using a Stochastic Kinetic Energy Backscatter Scheme to Improve MOGREPS Probabilistic Forecast Skill. Mon. Wea. Rev., **139**, 1190–1206.

[59]Torrence, C. and C.P. Gilbert, 1998: A practical guide to wavelet analysis. Bull. Amer. Meteor. Soc., **79**, 61-78.

[60]Vincent, L. A. and E. Mekis, 2006: Changes in daily and extreme temperature and precipitation indices for Canada over the twentieth century. Atmos. -Ocean, **44**, 177-193.

[61] Wei, F.Y., 1999: Modern Climatic Statistical Diagnosis and Forecasting Technology (Beijing: China Meteorological Press) pp77-88 (in Chinese).

[62]Whitaker, J.S. and A.F.Loughe, 1998: The Relationship between Ensemble Spread and Ensemble Mean Skill. Mon. Wea. Rev., **126**, 3292–3302.doi: http://dx.doi.org/10.1175/1520-0493(1998)126<3292:TRBESA>2.0.CO;2.

[63]Wild, M., A. Ohmura, 2005: RSRN longwave downward radiation measurements combined with GCMs show promise for greenhouse detection studies. GEWEX Newsletter, **14 (4),** 9-10.

[64]Williams, P. D., T. W. N. Haine and P. L. Read, 2004: Stochastic resonance in a nonlinear model of a rotating stratified shear flow, with a simple stochastic, inertia–gravity wave parametrization. Nonlinear Processes Geophys., **11,** 127–135.

[65]Qiu, X. and H. Zhu, 2012: MOE Grant Project: Developing High Resolution (45km x 45km) Probabilistic Climate Projections over Ontario from Multiple Global and Regional Climate Models. Retrieved on 6th Aug 2013 from http://jllmoe.dyndns.org:88/reports/2010-11-YorkU-Prob-s.pdf.

[66]Zeng, G., S. Lian, X. Cheng, Z. Hua and Y. Qi, 2006: EOF analysis of intra-seasonal variabilities of SST in the East China Sea and Yellow Sea. Adv. Mar. Sci., **24**, 146-155.

[67]Zhang, X., L. A. Vincent, W.D. Hogg and A. Niitsoo, 2000: Temperature and precipitation trends in Canada during the 20th century. Atmos. -Ocean, **38**, 395-429.

[68]Zhang, Y., B. Duliere, Philip W. Mote and Eric P. Salathe Jr., 2009: Evaluation of WRF and HadRM mesoscale climate simulation over the U.S. Pacific Northwest. J. Climate, **22**, 5511-5526.

[69]Zhang, Z., D. Gong, D. Guo, X. He and Y. Lei, 2008: Anomalous winter temperature and precipitation events in southern China. Acta. Meteor. Sinica, **63**, 899-912.